NASA CONTRACTOR REPORT

PERFORMANCE AND NOISE GENERATION STUDIES OF SUPERSONIC AIR EJECTORS

by P. S. Barna

Prepared by
OLD DOMINION UNIVERSITY
Norfolk, Va. 23508
for Langley Research Center

NATIONAL AERONAUTICS AND SPACE ADMINISTRATION • WASHINGTON, D. C. • JUNE 1972

1. Report No.	2. Government Accession No.	3. Recipient's Catalog No.
NASA CR-2056		

4. Title and Subtitle	5. Report Date
PERFORMANCE AND NOISE GENERATION STUDIES OF SUPERSONIC AIR EJECTORS	June 1972
	6. Performing Organization Code
7. Author(s)	8. Performing Organization Report No.
P. S. Barna	
	10. Work Unit No.
9. Performing Organization Name and Address	11. Contract or Grant No.
Old Dominion University Research Foundation P. O. Box 6173 Norfolk, VA 23508	NAS1-9635
	13. Type of Report and Period Covered
12. Sponsoring Agency Name and Address	Contractor Report
National Aeronautics and Space Administration Washington, D. C. 20546	14. Sponsoring Agency Code

15. Supplementary Notes

16. Abstract

Experimental investigations were conducted to determine the aerodynamic performance and noise generation characteristics of five ejectors having subsonic secondary flow. Primary nozzles with equal exit area for Mach numbers 1, 1.5, 2, 2.5, and 3 produced a variety of noise and pumping effects. The pumping capacity, specific power and noise generation of the Mach 1 nozzle was the highest and its mass augmentation was the lowest among the nozzles tested. The Mach 3 nozzle was found superior in mass augmentation and it also produced the lowest noise, however its pumping capacity and specific power was the lowest.

17. Key Words (Suggested by Author(s))	18. Distribution Statement
Ejectors - performance and noise generation Ejectors - supersonic primary nozzles Ejectors - subsonic secondary flow	Unclassified - Unlimited

19. Security Classif. (of this report)	20. Security Classif. (of this page)	21. No. of Pages	22. Price*
Unclassified	Unclassified	80	$3.00

*For sale by the National Technical Information Service, Springfield, Virginia 22151

PERFORMANCE AND NOISE GENERATION

STUDIES OF SUPERSONIC AIR EJECTORS

P. S. Barna
Professor of Engineering
Old Dominion University

SUMMARY

Experimental investigations were conducted on air ejectors to determine their aerodynamic performance and noise generation characteristics. Five different primary nozzles, all having the same exit area, were designed for Mach numbers 1, 1.5, 2, 2.5 and 3. The secondary flow was subsonic in all experiments. Each of these nozzles was tested, in turn, with constant stagnation pressure which was increased by equal increments of 20, starting with 20 p.s.i.g. and concluding with 100 p.s.i.g. While the pressure was kept constant during each test, observations were made for a number of different secondary flow rates.

The tests show that the nozzles produced a variety of sound and pumping effects. The pumping capacity, specific power and noise generation of the Mach 1 nozzle was the highest and its mass augmentation was the lowest among the nozzles tested. The Mach 3 nozzle was found superior in mass augmentation and it also produced the lowest noise; however, its pumping capacity and specific power was the lowest.

The experiments were conducted at NASA Langley Research Center.

INTRODUCTION

Ejectors have been known to be capable of boosting the mass flow rate of a particular fluid in motion and pumping both fluids against a resistance. For some period of time their application was limited to oil and gas burners and similar devices in which the motion of fluids was relatively slow. More recently, however, their application was extended to meet higher performance requirements and it became necessary for the primary booster fluid, and possibly for the induced secondary flow, to attain velocities equal or exceeding the speed of sound. While these ejectors proved capable of moving large masses, they were found to be excessively noisy.

Theory and the fluid dynamic performance characteristic of various ejector types has been widely studied by numerous investigators (Ref. 1-10). However, these simple theories prove chiefly applicable to "matching expansion", that is to a condition under which the ejector operates with "correct" back pressure. Most ejectors, however, are found to operate satisfactorily even with incorrect back pressure. The preduction of such "off-design" operation entails more

complex calculation and their reliability becomes limited because of the variety of shockwaves that accompany nozzles operating with incorrect back pressure.

The noise generation of ejectors, which has also been the subject of some studies (Ref. 11, 12) appears to be closely linked with fluid-dynamic performance. In ejectors where the co-flowing secondary air envelops the centrally located primary jet, an interaction between the two fluid streams occurs. Since any variation of the secondary flow rate changes the effectiveness of the acoustic impedance of the air layer surrounding the primary jet, a variance in noise emittance may be anticipated. It is reasonable to assume, therefore, that the noise generation of the ejector ultimately depends on the nature of jet interaction, which may be controlled by ejector geometry and operating pressures.

The purpose of the present investigation was to make a comprehensive study by further exploring the aerodynamic performance and noise generation of ejectors operating mainly under off-design conditions. While the mixing tube and diffuser geometry remained essentially unchanged during the tests; variation of the overall ejector geometry was in fact attained by employing different primary nozzles. Accordingly, five nozzles of equal exit area and with passage contours designed to attain Mach numbers 1, 1.5, 2, 2.5 and 3, respectively, were selected and were tested in turn. With exit area so fixed, changes in ejector geometry were produced by the variation of the ratio of mixing tube to nozzle throat area, (A_t/A_{th}). During the tests, the mass flow rate, the mass augmentation, the pressure distribution along the flow and the noise generation was studied under a range of primary pressures similar for each nozzle. Testing of the nozzles under correct back pressure was considered of minor importance.

Ultimately, it was intended to establish similarities between the ejectors and compare performance on the basis of a specified constant exit area.

SYMBOLS

$\bar{a}$	average room coefficient, Sabine
A	area of resistance package open to air flow, ft^2
A_{th}	primary nozzle throat area, in^2
A_t	sectional area of mixing tube, in^2
c_d	discharge coefficient of Venturi tube
c	speed of sound, ft/s
d_{min}	minimum cross section diameter of Venturi tube, ft
d_{in}	diameter of Venturi intake, ft

dt	mixing tube diameter, in
dB	decibel
f	frequency, Hz
F	thrust (drag) force of air passing through resistance, lb
g	gravitational acceleration, ft/s^2
G	combined mass flowrate denoted as pumping capacity of ejector, lb/s
G'	primary mass flowrate, lb/s
G''	secondary mass flowrate, lb/s
LPW	sound power level, re 10^{-12} Watts
m	mass augmentation ratio defined as G''/G'
M	Mach number at exit from primary nozzle
p	static pressure measured along mixing tube and diffuser, in. Hg
ΔP_V	pressure differential between inlet and min, cross section of Venturi tube, lb/ft^2
ΔP_{Rev}	pressure differential between reverberation chamber and ambient air, psi
P_{at}	atmospheric pressure, psi
p'_{NE}	static pressure at primary nozzle exit, psi
p''_{NE}	static pressure at secondary nozzle exit, psi
P_o	stagnation pressure of secondary air in plenum chamber, psi
P_1	stagnation pressure of primary air, psi
P_m	mechanical power of the combined flow, Watts/s
Q	volumetric flowrate, ft^3/s
R	gas constant, ft-lbf/lbm-^oR
SPL	sound pressure level, re 0.0002 microbar
T_a	atmospheric temperature, ^oR
T_1	stagnation temperature of primary air, ^oR

v velocity, ft/s

V volume of reverberation chamber, ft^3

x distance measured along mixing tube from primary nozzle exit, in.

ρ density of fluid, lb/ft^3

DESCRIPTION OF TEST FACILITY

For the purpose of studying the combined effects of aerodynamic performance and noise generation, a scale model ejector was constructed. The apparatus, fig. 1, was designed to incorporate all the salient features of a typical ejector and was provided with some flexibility featuring both interchangeable primary nozzles and mixing tubes. The essential design features of the ejector and details of various components will be described in turn.

Essential Design Features of the Ejector

The ejector essentially consisted of a primary nozzle, a secondary nozzle, a cylindrical mixing tube and a diffuser. The primary nozzle was located "centrally" inside the secondary nozzle and both nozzles aligned coaxially with the mixing tube. The high pressure air expanded inside the primary nozzle and after leaving the nozzle the high velocity jet passed through the mixing tube where it combined with the slower moving secondary air. The exit area of the primary nozzle was aligned with the inlet section of the mixing tube; hence, a "constant-area mixing process", was insured throughout the tests. The mixed airstreams were discharged through a diffuser into a reverberation chamber, from which the air entered a passage provided with acoustic baffles and was finally exhausted into the atmosphere through a variable resistance.

The high pressure air to the primary nozzle was supplied from the main distribution system available in the laboratory. The pressure was carefully monitored by a control system, consisting of a relief regulator valve, a supply of high pressure nitrogen and a "dome loader" flow valve built into the airline. The relief valve regulated the nitrogen pressure acting on the diaphragm in the dome loader. A safety valve was installed in the line as a precautionary measure against excessive pressure.

The secondary air first passed through a horizontal Venturi tube and subsequently entered a plenum chamber of cylindrical shape. The flow of air then turned upward and, having passed through the secondary nozzle, it finally combined with the primary flow in the mixing tube. For noise measurements a microphone was set up inside the reverberation chamber in a suitable location.

Components of the Apparatus

The primary nozzles.- Five nozzles were employed in turn during the tests, and they were designed for Mach numbers 1, 1.5, 2, 2.5 and 3.0. The nozzles were made of stainless steel and were essentially identical in appearance, fig. 2. They were interchangeable, having identical threaded ends. Each nozzle was provided with a static pressure tapping located near the nozzle exit section which was also identical for all nozzles, 0.5 inch in diameter. The divergent passage of the supersonic nozzles had a 5 degree taper angle.

Secondary air nozzle and plenum chamber.- Air entered the secondary nozzle from the plenum chamber at substantially atmospheric condition. This nozzle was made of aluminum and the air passage was of conical shape with a 30 degree included angle. The nozzle was provided with a rounded entrance and was mounted on top of the plenum chamber. Flow into the secondary nozzle was considered uniform because the plenum chamber was substantially larger than the nozzle.

In order to ensure proper location of the primary nozzle, both centrally and axially, the secondary nozzle was provided with three set screws equally spaced apart around the circumference. The screws extended into the secondary air passage with their pointed ends slightly touching the side of the primary nozzle, as shown in fig. 3. In order to measure the pressure of the secondary airflow the secondary nozzle was provided with a static pressure tapping located in the exit plane of the primary nozzle.

The plenum chamber was cylindrical, 15 inches in diameter 10 inches high, and was fabricated from aluminum. It was provided with a side port, to which the Venturi meter was connected, and with a pressure tapping for measuring the stagnation pressure of secondary air. The circular plywood top, on which the secondary nozzle was mounted, was made removable for inspection purposes. The height of the plenum chamber above ground level was adjustable.

Mixing tube and diffuser.- During the tests, two mixing tubes were employed alternately, one with circular and the other with square cross section. The circular plexiglass tube of 1/8 inch wall thickness had 1.5 inches inside diameter and was employed for all tests involving performance and pressure distribution. The square tube of 1.5 x 1.5 inch internal dimension was solely used for flow visualization experiments. Both tubes were about 15 inches long and were, in turn, mounted on top of the secondary nozzle. Pressure tappings were distributed along the circular mixing tube at spacing shown in fig. 4(a). Of the four sides of the square tube two opposite sides were made of 1/4 inch good quality plate glass and the remaining two sides were 3/8 inch aluminum. Details of the square mixing tube are shown in fig. 4(b).

After leaving the mixing tube the flow entered a diffuser which was made of sheet metal and was provided with static pressure tappings. The diffuser was 14 1/4 inches long with a taper angle 3 1/2 degrees and exit diameter of 3 1/4 inches. Between the exit from the diffuser and cover plate of the reverberation chamber a short length of bellows was inserted which allowed for height adjustment.

Venturi meter.- For metering the secondary airflow a Venturi tube of standard design was employed. The tube was provided with a well rounded entrance and, at the minimum cross section, three static pressure tappings were distributed around the circumference at equal distances. Details of the Venturi are shown in fig. 5.

Reverberant Chamber.- The box shaped reverberant chamber was made of 3/4 inch plywood and was provided on four sides with double walls to improve its reverberation characteristics. Internal dimensions of the chamber were: 16 inches wide, 27 inches long and 24 inches high. The box was externally reinforced by angle iron bars to guard against possible splitting of the wood under excessive pressure. The bottom of the box was provided with a removable 1/2 inch thick aluminum coverplate which was required for inspection purposes. The coverplate was provided with a circular hole to which the bellows, fitted to the exit from the diffuser section of the ejector, was fastened. The microphone was placed into a tube, which was inserted through a hole in the coverplate alongside the diffuser exit, its pickup position being about 6 inches above the plate.

The baffled duct passage was bolted to the side of the reverberation chamber and the air entered into the passage through a 6 inch circular port cut into the side of the chamber. Over this port a 1/2 inch metal circular reflector shield was mounted on the exhaust side, allowing air to pass and at the same time partially reflecting the sound generated in the chamber. The acoustic baffles fitted into the passage were designed to reduce noise generated by the resistance to travel upstream.

A safety device was provided near the exit of the passage to guard against pressure build-ups in excess of 5 p.s.i. inside the reverberation chamber. It consisted of a 35 pound dead weight pressing on a rubber seal placed over a 3 inch opening.

The reverberation box and ducted passage were supported by a solid timber frame.

Variable resistance.- Resistance to the flow was attained by gradually building up the thickness of layers of porous felt. Sheets of felt material were cut into 8 inch diameter discs and layers, of varying thickness, were sandwiched between two wire mesh discs reinforced at their perimeter. This felt "package" was subsequently placed inside a screw press where it was firmly held together by applying moderate pressure on these discs at their line of contact. The press consisted of two cylinders, fig. 6, one sliding inside the other and this cylinder could be moved by a screw arrangement. During the tests the sliding cylinder pressed against the felt package and was withdrawn after each test run when changing thickness of the layers was required.

By building up the felt layer thickness from about 1/16 of an inch to about 2 inches the resistance was varied from low to high. The highest resistance was attained when the pressure in the reverberation chamber was raised to 5 p.s.i. above atmospheric. To attain the highest resistance it was also necessary to restrict the cross sectional area open to flow. To achieve this,

an additional resistance was added to the felt package, which consisted of a wooden disc provided with a centrally located 4 1/2 inch diameter circular opening.

Flow visualization.- To obtain photographic records of flow patterns, flow visualization experiments were conducted employing both Schlieren and shadowgraph techniques. For the former, both long and short (spark) exposure light sources were employed and, for the shadowgraph technique, spark illumination of one milli-second duration was used. The experimental set up for the Schlieren tests in shown in fig. 7.

Instrumentation

Pressure.- For the measurement of primary stagnation pressure a Bourdon type dial guage was used which was calibrated prior to installation. For the measurement of pressures along the mixing tube and diffuser a vertical mercury-in-glass multitube manometer was employed. For the measurements of pressure in the reverberation chamber, water was used as indicating fluid up to 1 p.s.i. pressure; above 1 p.s.i., mercury was used. For the measurement of flow rate of the secondary air an inclined tube manometer, with alcohol as indicating fluid was employed. For low flow rates the angle of incline of the tube could be lowered to 10 degrees, as measured from the horizontal, which considerably increased instrument sensitivity.

Noise.- A commercially available microphone system was employed for the measurements. It consisted of a 1/4 inch condenser microphone (set up inside the reverberation chamber), a one third octave band frequency analyser and graphic level recorder. The system had a useable frequency response range from 5 Hz to 100 kHz with accuracy of $\pm$ 1 dB between 40 Hz and 100 kHz. This system was calibrated with a sine wave at a pressure level of 125 dB.

TEST PROCEDURE

Pumping tests.- Each of the five nozzles was tested in turn and all nozzles were operated under choked flow condition. A test set for a nozzle consisted of keeping the primary pressure constant over a period of time during which observations on the pumping performance of the ejector were made. Resistance to airflow was kept constant during a test run while observations were made; it was subsequently varied stepwise for the next test run, each step leading to an increase in resistance. This procedure was repeated until the highest resistance for the test was attained. A test set normally consisted of about seven tests runs.

Sets of tests were obtained for primary pressures 20, 40, 60, 80, and 100 p.s.i. gauge pressure (except for the M = 1 and 1.5 nozzles for which the air supply system proved inadequate at 100 p.s.i.g.). The pressures registered on the multitube manometer were instantaneously recorded by photographic means while pressures on individual manometers were directly noted.

During the tests a small drift of the primary gauge pressure was generally observed and this was immediately corrected with the fine control of the relief regulator. The prevailing ambient air conditions were under constant surveillance throughout the tests and data were recorded daily.

Noise tests.- Noise tests were performed after the pumping tests were concluded. The experiments were planned to reproduce the same pumping effects of the ejector as previously experienced, however this time the main objective was measurement of noise generation. Overall noise pressure levels were recorded for all test sets and frequency analysis was performed for flow conditions of special interest. During the tests the microphone calibration was checked periodically.

Flow visualization.- Photographic records were obtained for all nozzles when pumping against either the lowest (L) or the highest (H) resistance and during these tests the square mixing tube was employed. For taking the shadowgraph pictures the spark was set up about 5 ft. from the test section and the light rays remained uncollimated. The space surrounding the test section was blacked out for the tests.

PRESENTATION OF RESULTS

Details of calculation of results is given in the Appendix.

Results concerning ejector performance and noise generation are presented in three sets of five graphs, where pumping capacity, G, mass augmentation, m, and sound power levels of the ejector, LPW, respectively, are plotted against specific mechanical power of the ejector, P_M/G.

The term pumping capacity refers to the sum of the primary and secondary flow rate through the ejector

$$G = G' + G''.$$

Since the nozzles were operated under choked flow conditions the flow rate through the nozzles, G', remained constant for a specified primary pressure. The induced secondary flow rate, G'', however, depends a great deal on the air resistance, and therefore varies considerably.

The term "mass ratio" stands for mass augmentation and is expressed as the ratio of secondary to primary flow rate

$$m = \frac{G''}{G'}.$$

The term "specific mechanical power" of the ejector refers to the mechanical power per unit mass flow, which represents an overall pumping effort. This depends primarily on the pressure inside the reverberation chamber.

The term "constant resistance" (denoted R_1 to R_7) refers to a particular set of felt layers which were employed during a test run. (See also fig. 22.) Wherever possible, constant resistance lines are shown on the graphs as dashed lines, while the constant primary pressure lines (P_1) appear as solid lines.

Results on pumping performance.- The first set of graphs (fig. 8) indicate that, for all nozzles tested, the overall pumping performance is remarkably similar. For a specified resistance, both pumping capacity, (G), and specific power, Pm/G, increases with rising primary pressure. Conversely, for a specified constant primary pressure (from 20 to 100), pumping capacity decreases with increasing resistance. All constant pressure curves show a tendency of G to remain constant while resistance is relatively low (R_1 to R_3), but show a gradual decrease in pumping capacity when higher resistances are encountered (R_4 to R_7). The effect of resistance on pumping is more marked while primary pressures are low (20, 40 p.s.i.) and becomes less noticeable when primary pressures are high. In the case of M = 1 and 1.5 nozzles, practically no change in G is experienced when P_1 = 80 and 100 p.s.i. On the other hand, for the higher Mach nozzles, sensitivity to resistance generally increases.

The general impression that may be gained from inspection of the first set of graphs is, that under similar operational conditions, the lower Mach nozzles pump more air and attain higher specific work values than the higher Mach nozzles.

Results on mass augmentation.- The second set of graphs, (fig. 9) indicates that mass augmentation of the various primary nozzles is less consistent than could be expected from the overall pumping performance. However it may be shown that the results obtained are generally consistent with ejector theory.

It appears from the figures that, while specific work increases with increasing primary pressure for low resistances, the mass augmentation substantially decreases. In following a constant pressure line the decrease of m is more marked for lower primary pressures and may become very sensitive to changes in resistance when high Mach nozzles are employed. Constant low pressure curves frequently intersect pressure curves of the higher pressure family signifying that, at the point of intersection, the same mass augmentation and specific power may be attained with different primary pressures. These effects are particularly noticeable with the higher Mach nozzles.

When comparing the mass augmentation of the various nozzles tested the most important result that appears is the improving mass augmentation for higher Mach nozzles. For example, the M = 3 nozzle almost doubles the mass augmentation for P_1 = 20 p.s.i. when P_m/G = 350 (say), as compared with the M = 1 nozzle. The comparison becomes even more favorable for the M = 3 nozzle at P_1 = 40 when it pumps three times more air than the M = 1 at P_m/G = 500 (say).

On the other hand, as compared with the lower, the higher Mach nozzles fall short of pumping efforts against higher resistances. The reason for this

is consistent with supersonic nozzle theory and, under the circumstances, the low Mach number nozzles (1 and 1.5) tend to underexpand at higher pressures and thus carry into the air stream "unspent" energy while the high Mach nozzles tend to overexpand and self adjust the stream pressure to the surroundings at the nozzle exit. The "unspent" energy was subsequently dissipated by shock-waves set up in the mixing tube as shown by the flow visualization experiments.

Results on noise generation.- The third set of graphs (fig. 10) shows results of considerable complexity. For a specified nozzle both primary pressure and resistance affect noise. Nevertheless in the various nozzles employed during the tests the variation in noise generation is significant. For example the difference between noise levels generated by the lowest and highest primary pressure is markedly greater for the M = 1, 1.5 and 2 nozzles and may amount to approximately 14-16 dB; for the M = 2.5 nozzle this difference reduces to about 10 dB and drops to about 2.5 dB for the M = 3 nozzle.

Changes in noise generation with increasing resistance is of particular interest as it may be observed that, depending on nozzle Mach number and primary pressure, noise may either increase, decrease or remain constant.

For convenience, results on noise generation, as a function of resistance, are summarized in Table I.

Pressure distribution along mixing tube and diffuser.- Results of pressure distribution along the mixing tube and diffuser are shown in figs. 11 to 15 where absolute pressure (inches mercury) is plotted against distance along the mixing tube and diffuser. Location of static pressure tappings are shown along the mixing tube marked on the abscissa with encircled station numbers 1 to 7 and along the diffuser with encircled station letters A to F. The position of the secondary nozzle exit is located approximately at the zero mark of the abscissa.

It appears from the graphs that all curves exhibit some common characteristics such as the "humps" and "hollows" in the mixing tube and that they show steady pressure recovery in the diffuser. Generally two "humps" and three "hollows" may be observed in the mixing tube when the ejector pumps against low resistance. However, when pumping against high resistances, pressure recovery commences earlier in the mixing tube and, in this case only, one "hump" and two "hollows" may be observed.

Results on flow visualization.- Shadowgraph pictures are presented in figures 16 - 20 where sets of five pictures are shown, side by side, for each nozzle operating against the lowest (L) or highest (H) resistance respectively. In addition to the pattern issuing from the various nozzles employed during the tests, these pictures also show the effect of the co-flowing secondary air on the wave pattern which may be considered to be of special interest in ejector studies.

All pictures show the familiar periodic or chain-like wave structure which is well known from studies on gaseous jets exhausting into still air. A complete report on the same nozzles which were employed in the present tests was

published in Ref. 13, which discusses the various flow patterns and furnishes detailed explanation of flow characteristics obtained when discharging into still air. While these results are relevant and useful, some differences in the patterns, caused by the moving "boundary" (co-flowing) air, may be anticipated. Indeed some differences may be observed for similar patterns for different resistances. Furthermore, the turbulent "mixing" pattern of the secondary with the primary flow along the mixing tube required consideration and photographic observations were made over a distance of five tube diameters. (on account of space restriction this was reduced to four tube diameters in this report.)

The results of these flow visualization experiments are presented in Table II where the top and second row of figures refer to pressures measured at exit of the primary (p_{NE}") respectively; the third row shows the operating pressure ratio (p_{NE}'/p_1), while the fourth row indicates the particular character of the expansion process observed, the letter "U" referring to under and "O" to over-expansion. The correct or near correct expansion is shown by the letter C. The various flow patterns shown by the shadowgraph pictures are further classified and are divided into six categories each representing a typical pattern which then can be recognized with the aid of fig. 21 where for the sake of clear recognition of the flow pattern shown on the corresponding shadowgraph is represented by a simple line diagram. The patterns are provided with Roman reference numbers I to VI and these appear in the fifth row of Table II. The first column shows the nozzle design Mach numbers, under which the correct pressure ratio is inserted between brackets, and successive columns are headed by the operating

Resistance effects.- The effect of resistance on flow rate for the various layers employed in the test is shown in fig. 22, where pressure in the reverberation chamber is plotted against mass flow. Reference to thickness, noted as R_1, R_2 . . . etc., is shown on the top left corner of the figure. The slope of the curves indicates the flow character 1:1 being laminar and 1:2 being turbulent.

DISCUSSION

It is of interest to first briefly summarize the results and compare the aerodynamic performance of the various nozzles tested to establish a performance rating.

It was observed that for a specific primary pressure, both the overall pumping capacity and the specific power of the ejector decreased for increasing nozzle Mach numbers. The reason for this is due to primary nozzle design which features constant exit area and decreasing throat area with increasing Mach numbers.

Since mass flow rate for a specified pressure and temperature is known to by proportional to the throat area, the drop in overall performance for increasing Mach numbers was primarily caused by the falling mass flow rate of the primary "activating" air. In addition some minor energy changes occurred through formation of shock waves due to incorrect back pressure which also contributes to performance deficiency.

One gains a more favorable impression when studying the results on mass augmentation. It appears that the lower number nozzles suffer from severe limitations in mass augmentation in addition to being rather insensitive to

changes in resistance. The higher number nozzles, on the other hand, appear to be superior and yield figures more than double in mass augmentation in addition to being also reasonably sensitive to changes in resistance.

The presentation of ejector performance, as shown in these diagrams where pumping capacity and mass augmentation are plotted against specific power, may be regarded inadequate for a complete appraisal. Supplementary methods may prove helpful for further illuminating various effects, comparing performance and predicting effectiveness.

For example, specific power may be based on primary mass flow rate (G') rather than on total flow rate (G). Replacing P_m/G by P_m/G' results in (1 + m) times higher specific power, (see Appendix), and since m is greater for the higher Mach number nozzles, their performance figures on this basis may surpass those of the lower Mach number nozzles.

Effectiveness of nozzle performance may also turn in favor for the higher number nozzles by adopting a different nozzle design. The results obtained for overall performance would have been altogether different, had the throat area been kept constant for all nozzles tested. Some minor changes in geometry may also be considered. For example, one may adjust the throat area for the higher number nozzles to yield the same pumping capacity as the M = 1 nozzle. This and other possible "normalizing methods" have not been fully explored at the time of writing this preliminary report.

The results on noise generation may be classified into various categories, major effects being due to pumping and minor effects due to ejector geometry and possibly flow mixing.

Noise due to pumping effects may be related to mass augmentation. When comparing corresponding graphs, one observes that along constant pressure lines no substantial change in noise occurs, while mass augmentation remains unchanged. This appears normally the case in all nozzles for low resistance. For M = 1, 1.5 and 2 nozzles the low resistance limit is reached at R_4 for pressures 20 and 40, while for M = 2.5 and 3 the limit is reached at a somewhat lower resistance, R_3.

With increasing resistance, noise increases substantially when mass augmentation falls off. For the M = 1 nozzle a sharp increase in noise of about 10 dB at P_1 = 40 appears exactly over the same range of P_m/G = 6000-8400 where m falls from 1.6 to 1.1. Again for the same pressure, noise for the M = 1.5 nozzle increases by 5 1/2 dB over P_m/G = 5500-7300, where m falls from 1.75 to 1.45; for the M = 2 nozzle, noise increases by about 10 dB over P_m/G = 1150-5800 where m falls from 2.84 to 1.35.

Similar sharp increases in noise generation appear in the M = 2.5 and 3 nozzles, but the results seem to vary a great deal. In comparing these nozzles, it appears that noise markedly increases with pressure at low resistances for the M = 2.5 nozzle, while the M = 3 nozzle shows hardly any difference. For the M = 2.5 nozzle noise begins to increase at P_m/G = 500 when P_1 = 20 and at P_m/G = 850 when P_1 = 40. Again for P_1 = 60 no change in noise appears until

P_m/G = 2000 and sharp increases are experienced at the end of all constant pressure lines when the highest resistance is attained. Similar results are experienced for the M = 3 nozzle.

When comparing the noise generation curves with mass augmentation, one invariably finds that noise commences to rise at approximately the same P_m/G value where mass augmentation begins to fall. One may therefore conclude that the secondary air flow rate has significant contribution to noise suppression of ejectors. Among the nozzles tested, the M = 3 nozzle generated the lowest noise and produced the highest mass augmentation.

The reason for this characteristic behavior of the experimental ejector may now be readily explained. The noise generated by the ejector results from a combination of the primary and the secondary flow noise. The mass flow rate of the primary nozzle, being proportional to its throat area and primary pressure, contributes to noise power to a larger extent with the lower Mach nozzles and to a smaller extent with the higher Mach nozzles for reasons, that with constant exit area, the lower Mach nozzles having the largest throat produced the highest primary flow rate. Conversely, the higher Mach nozzles having smaller throats produce less primary flow. The proportion of secondary to primary flow, that is mass augmentation, appears to have a major effect on noise generation. Since the mixing of a large proportion of low speed secondary with a small proportion of high speed primary airflow is known to promote noise abatement, the high Mach nozzles produce the more favorable noise attenuation effects.

Furthermore, the noise level of the lower Mach nozzles appears to be proportional to primary pressure, hence noise is largely due to primary flow rate without being markedly affected by the surrounding slow moving secondary airflow (which was found sub-sonic in all experiments). While noise was found to be affected by pressure to some extent in the higher Mach nozzles, the variation was relatively much smaller due to the lower primary and higher secondary mass flow rates.

In addition to major effects on noise generation, there appear minor effects as well. These fall into two categories: first, a gradual rise followed by a gradual decrease in noise level, second, a gradual decrease all the way along with increasing resistance. For example, for the M = 1 nozzle along the 80 p.s.i. line one observes noise to first increase about 2 1/2 dB then to decrease by about the same amount, while along the 60 p.s.i. line one observes a 5 1/2 dB continuous decrease. Similar observations were made on other nozzles, and the rise and fall was even noticeable to observers in the laboratory. At the time of writing this report these phenomena are still being studied.

The operation of incorrectly expanded nozzles needs further consideration. While the effects of friction on the operation of correctly expanded nozzles are considered small, the presence of friction and boundary layers may considerably affect the operation of incorrectly expanded nozzles.

In underexpanded nozzles the flow is known to be controlled by geometry. However, downstream from exit of an underexpanded nozzle the air continues to

expand until equilibrium, by way of pressure equalization with the surrounding co-flowing secondary air, is attained. The primary jet spreads out immediately after leaving the nozzle and so the passage remaining for the secondary air contracts (see figs. 16, 17). This has a marked effect on the secondary flow which accelerates and attains a maximum speed at some section downstream where the passage area attains minimum value. The first "hollow" on pressure distribution curves appears at this section. In going further downstream, the primary stream seems to contract, thereby allowing an increase in the secondary flow passage area. The resulting deceleration is accompanied by a pressure rise and thus the first "hump" in the pressure distribution appears. Both the pressure distribution curve and the shadowgraph picture show that the first hollow is about 0.8 inches and the first hump is about 1.6 inches from the nozzle exit of the M = 1 nozzle. Further downstream, as turbulent mixing begins to take effect, the shock pattern of the primary jet becomes less definite and the shadowgraph only shows high levels of turbulence while the pressure distribution curves indicate non uniform flow along the photographed length of the mixing tube.

In overexpanded nozzles, the flow downstream is known to be controlled by back pressure and its variation results in different patterns. Starting from the case when the nozzle exit pressure is slightly under the value of the correct back pressure, the adjustment of the flow near the wall takes place through an oblique shock. The stream contracts downstream from exit, allowing the secondary air to decrease its speed, thereby recovering pressure. Thus in overexpanded nozzles, first a "hump" appears on the pressure distribution curve which is then followd by a "hollow" further downstream indicating jet spreading and turbulent mixing (see for example M = 2.5, P_1 = 60 p.s.i.). For low resistance (L) the first shock pattern of the multiple shock chain appears outside the nozzle exit, but for high resistance (H) a part of the pattern is inside the nozzle as if it was being "pushed" upstream with the increasing back pressure. The flow generally separates from the wall upstream from the nozzle exit and the darker lines visible on each side of the wave pattern show the separated boundary layer.

There appear a number of different patterns which may be observed on the shadowgraph and their detailed description may be found in reference 14 (see also fig. 21).

The faster moving primary air issuing from higher Mach nozzles enhances the performance of ejectors because of the increased rate of momentum exchange taking place along the mixing tube. Calculations based on measurements of nozzle exit (p'_{NE}) show that if oblique shockwaves appear the stream may remain supersonic over a distance downstream from the exit of an overexpanded nozzle. Employing the photographed wave pattern as guide to estimate shock strength, one finds M = 2.2 at exit of the M = 3 nozzle with primary operating pressure 100 p.s.i.g. This amounts to being able to satisfactorily operate the nozzle at considerably lower pressure ratio than correct expansion would otherwise require.

CONCLUSIONS

Since this report is of preliminary nature, comments are limited to merely summarizing results of observations made on the test ejector. There are several aspects which need further consideration if a fair critical appraisal of performance and noise generation of supersonic ejectors is desired.

Comparing performance on the basis of specified (constant) exit area for all nozzles employed in the ejector, one finds:

1. The M = 1 nozzle produced the largest mass flow rate and the smallest mass augmentation; conversely the M = 3 nozzle produced the smallest mass flow rate and the largest mass augmentation.

2. Noise generated by the ejector was found highest for the M = 1 nozzle and lowest for the M = 3 nozzle.

3. The fact that noise increased with decreasing mass augmentation shown along the constant pressure lines, proves that the noise generated by the ejector resulted from a combination of the primary and the secondary flow noise.

APPENDIX

CALCULATION OF RESULTS FROM OBSERVED DATA

Primary mass flow rate.- Since all nozzles were operated under choked condition throughout the tests, the formula

$$G' = 0.528\, A_{th} \frac{P_1}{\sqrt{T_1}} \quad \text{(lb/sec)}$$

was employed, where values of A_{th} for various nozzles appear in fig. 2. The stagnation pressure P_1 was observed 18 inches upstream from nozzle exit with a static pressure gauge. Correction for frictional losses and a conversion to stagnation pressure was subsequently applied. The increase due to kinetic presure was found to be approximately compensated by a decrease in pressure due to frictional losses, hence the observed P_1 on the gauge was adopted as the true stagnation pressure.

Secondary mass flow rate.- The mass flow rate of the secondary air through the Venturi tube was calculated from

$$G'' = Q\rho$$

where the volumetric flow rate

$$Q = C_d \frac{d^2_{min}\pi}{4} \frac{1}{\sqrt{1 - \left(\frac{dmin}{din}\right)^2}} \sqrt{2g \frac{\Delta p_v}{\rho}}$$

Because of the rounded intake of the tube, the term $(d_{min}/d_{in})^2$ was ignored. The pressure differential between air inlet and minimum cross section was measured by the inclined manometer containing alcohol of specific gravity - SG = 0.8 and the air density was calculated from the equation of state

$$\rho = \frac{P_{at}}{R\ T_{at}}$$

Sound power level.- From measurements of sound pressure level in the reverberation chamber, the sound power level was obtained from Ref. 15. (e.g. 43, p. 919)

$$LPW = SPL + 10 \log V + 10 \log D - 10 \log (\rho c^2) - 2.1\bar{a} + 4.1$$

From measurements made in the reverberation chamber the sound attenuation was established. The following data were employed for the calculation:

Volume of reverberation chamber, V = 6 ft.^{3}

Density of air, $\rho = 1.2$ Kg/m^3.

Speed of sound, c = 343 m/s.

Room constant $\bar{a} = 0.16$.

Sound attenuation, D = 300 dB per sec.

With these values

$$LPW = SPL - 15.45.$$

Specific power.- The mechanical power P_m of the ejector may be obtained from the simple consideration that pressure inside the reverberation chamber exerts a "drag" froce on the resistance against flow. Since the force results from the pressure acting on the resistance area, the "drag-power" of the air resistance, assuming incompressible flow

$$P_m = (F_1 - F_2)\ V$$

where F_1 and F_2 are the forces acting on the upstream and downstream face A respectively of the resistance package and V is the air velocity. In terms of air resistance, that is, pressure difference between the chamber and the atmosphere

$$P_m = AV\ (p_{rev} - p_{at}) = \Delta AV\ p_{rev}$$

Since mass flow through the ejector

$$G = \rho_{rev} AV$$

and from the gas equation

$$\rho_{rev} = \frac{Prev}{R.T} = \frac{P_{at} + \Delta P_{rev}}{RT}$$

Substitution results in

$$\frac{P_m}{G} = RT \frac{P_{rev}}{P_{at} = P_{Rev}}$$

During the experiments an average value of T = 540°R was observed, and with R = 53.3 ft/°R, with conversion factor 1kW = 1.355 HP at with p_{at} = 14.7 p.s.i.a., hence specific power

$$\frac{P_m}{G} = 39068 \frac{\Delta P_{rev}}{14.7 + \Delta P_{rev}}, \text{ WATTS/lb/sec.}$$

Specific power based on primary mass flow G' may be obtained from the identity

$$\frac{P_m}{G} = \frac{P_m}{G' (1 + m)}, \text{ hence } \frac{P_m}{G'} = (1 + m) \frac{P_m}{G}$$

REFERENCES

1. Flügel, G.: Berechnung Von Strahlapparaten, VDI Forschungsheft 395, 1939. (Also available NACA TM 982, 1941.)

2. The M. W. Kellogg Co. Special Products Dept.: The General Case of Entrainment Mixing and Compression of Gases in a Straight Mixing Tube, issued by Republic Aviation, Rept. No. SPD 88, 1947.

3. Laidlaw, W. R.: Ejector Theory and its Application to Induction Type Wind Tunnels. National Research Council of Canada, Rept. No. MA-232, 1950.

4. Lewis, W. G. E.; Drabble, J. S.: Ejector Experiments. National Gas Turbine Establishment, Rept. No. 151, 1954.

5. Deleo, R. V.; Rose, R. E.: An Experimental Investigation of the Use of Supersonic Driving Jets for Ejector Pumps. Wright Air Development Center, Technical Rept. 57-357, 1958.

6. Emmons, H. W., ed.: Fundamentals of Gas Dynamics, High Speed Aerodynamics and Jet Propulsion, Vol. III. Princeton University Press, 1958, pp. 279-287.

7. Fabri, J.; Paulon, J.: Theory and Experiments on Supersonic Air-to-Air Ejectors. NACA TM 1410, 1958.

8. Chisholm, R. G. A.: Design and Calibration of an Air Ejector to Operate Against Various Back Pressures. University of Toronto Institute of Aerophysics, Technical Note No. 39, 1960.

9. Krenkel, A. R.; Lipowsky, H. H.: Design Analysis of Central and Annular Jet Ejectors. Office of Aerospace Research, U.S. Air Force, ARL 66-0210, 1966.

10. Vasilyev, Y. N.: Theory of a Supersonic Gas Ejector with a Cylindrical Mixing Chamber. NASA Technical Translation TT F-11, 554, 1968.

11. Middleton, D.: A Note on the Acoustic Behavior of Ejectors When Used With Corrugated Nozzles. Aeronautical Research Council. ARC 25 187-N.270., 1964.

12. Middleton, D.: The Noise of Ejectors. Aeronautical Research Council. R.&M. No. 3389, Ministry of Aviation, G. B., 1965.

13. Love, E. S.; Grigsby C. E.; et. al.: Experimental and Theoretical Studies of Axisymmetric Free Jets. NASA Technical Rept. R-6, 1956.

14. Emmons, H. W.: Op. cit., pp. 166-169.

15. Young, R. W.: Sabine Reverberation Equation and Sound Power Calculation, Journal of Acoustical Society of America, Vol. 31, No. 7, July 1959, pp. 912-921.

TABLE I

NOISE GENERATION OF EJECTOR AS FUNCTION OF RESISTANCE

Nozzle Number M	Resist-ance	Primary Stagnation Pressure, p.s.i.					Matching Condition
		20	40	60	80	100	
1	Low	slight increase	constant	constant	slight increase	no data	(marked X) -
	High	slight increase	strong increase	decrease all way	slight decrease		
1.5	Low	constant	constant	constant	constant	constant	constant
	High	slight increase	strong increase	decrease & increase	decrease	slight decrease	strong increase
2	Low	constant	constant	constant	constant	constant	
	High	strong increase	strong increase	constant (approx.)	increase min. 5-6K*	decrease all way	
2.5	Low	constant	constant	constant	constant	constant	
	High	strong increase	strong increase	strong increase	strong increase	strong increase	
3.0	Low	slight increase	slight increase	constant	constant	constant	
	High	strong increase	strong increase	strong increase	strong increase	strong increase	

* Min. occurs at $P_m/G = 5500$

TABLE II (continued)

CLASSIFICATION OF FLOW PATTERNS

High Resistance

Nozzle Number M	Nozzle Exit Pressure	Primary Gauge Pressure, P_1, p.s.i.				
		20	40	60	80	100
1 (0.528)*	P_{NE}'	16.3	25.8	34.9	43.6	No
	P_{NE}''	14.7	14.4	13.4	13.8	Data
	P_{NE}'/P_1	0.468	0.467	0.466	0.458	
		U	U	U	U	U
		I	II	III	III	III
1.5 (0.272)	P_{NE}'	11.3	16.5	22.1	27.6	33.0
	P_{NE}''	14.6	14.0	13.8	13.5	13.4
	P_{NE}'/P_1	0.316	0.301	0.296	0.291	0.286
		O	U	U	U	U
		IV	I	II	III	III
2 (0.128)	P_{NE}'	14.1	11.4	10.6	14.1	16.2
	P_{NE}''	14.8	14.3	14.4	14.1	12.9
	P_{NE}'/P_1	0.422	0.214	0.142	0.143	0.141
		O	O	O	C	U
		V	V	IV	IV	IV
2.5 (0.058)	P_{NE}'	14.0	13.1	13.1	13.2	12.8
	P_{NE}''	14.7	14.6	14.6	14.3	14.3
	P_{NE}'/P_1	0.404	0.239	0.176	0.139	0.111
		O	O	O	O	O
		VI	VI	V	V	IV
3 (0.027)	P_{NE}'	14.6	14.5	14.3	13.1	13.8
	P_{NE}''	14.8	14.0	14.8	14.7	14.6
	P_{NE}'/P_1	0.419	0.264	0.191	0.138	0.120
		O	O	O	O	O
		VI	VI	VI	VI	V

*Numerical figures under Mach number show correct pressure ratio.

TABLE II (concluded)

CLASSIFICATION OF FLOW PATTERNS

Low Resistance

Nozzle Number M	Nozzle Exit Pressure	Primary Gauge Pressure, P_1, p.s.i.				
		20	40	60	80	100
1 (0.528)	P_{NE}'	16.6	25.4	34.9	44.1	No
	P_{NE}'	13.4	13.2	13.2	13.3	Data
	P_{NE}'/P_1	0.482	0.462	0.466	0.464	-
		U	U	U	U	U
		I	II	III	III	III
1.5 (0.272)	P_{NE}'	10.9	18.8	22.3	27.5	33.2
	P_{NE}''	8.8	13.6	13.1	13.3	13.4
	P_{NE}'/P_1	0.313	0.344	0.299	0.290	0.287
		U	U	U	U	U
		I	I	II	III	III
2 (0.128)	P_{NE}'	11.4	7.8	10.5	13.1	16.3
	P_{NE}''	13.8	13.5	13.3	13.1	12.8
	P_{NE}'/P_1	0.339	0.145	0.141	0.143	0.142
		O	O	O	C	U
		IV	IV	IV	IV	IV
2.5 (0.058)	P_{NE}'	13.0	11.7	11.3	11.0	10.7
	P_{NE}''	14.1	13.7	13.3	13.0	12.9
	P_{NE}'/P_1	0.375	0.215	0.151	0.116	0.093
		O	O	O	O	O
		VI	VI	V	V	IV
3 (0.027)	P_{NE}'	14.0	13.3	12.9	12.1	11.1
	P_{NE}''	14.5	13.3	13.8	13.5	13.0
	P_{NE}'/P_1	0.402	0.243	0.172	0.129	0.097
		O	O	O	O	O
		VI	VI	VI	V	V

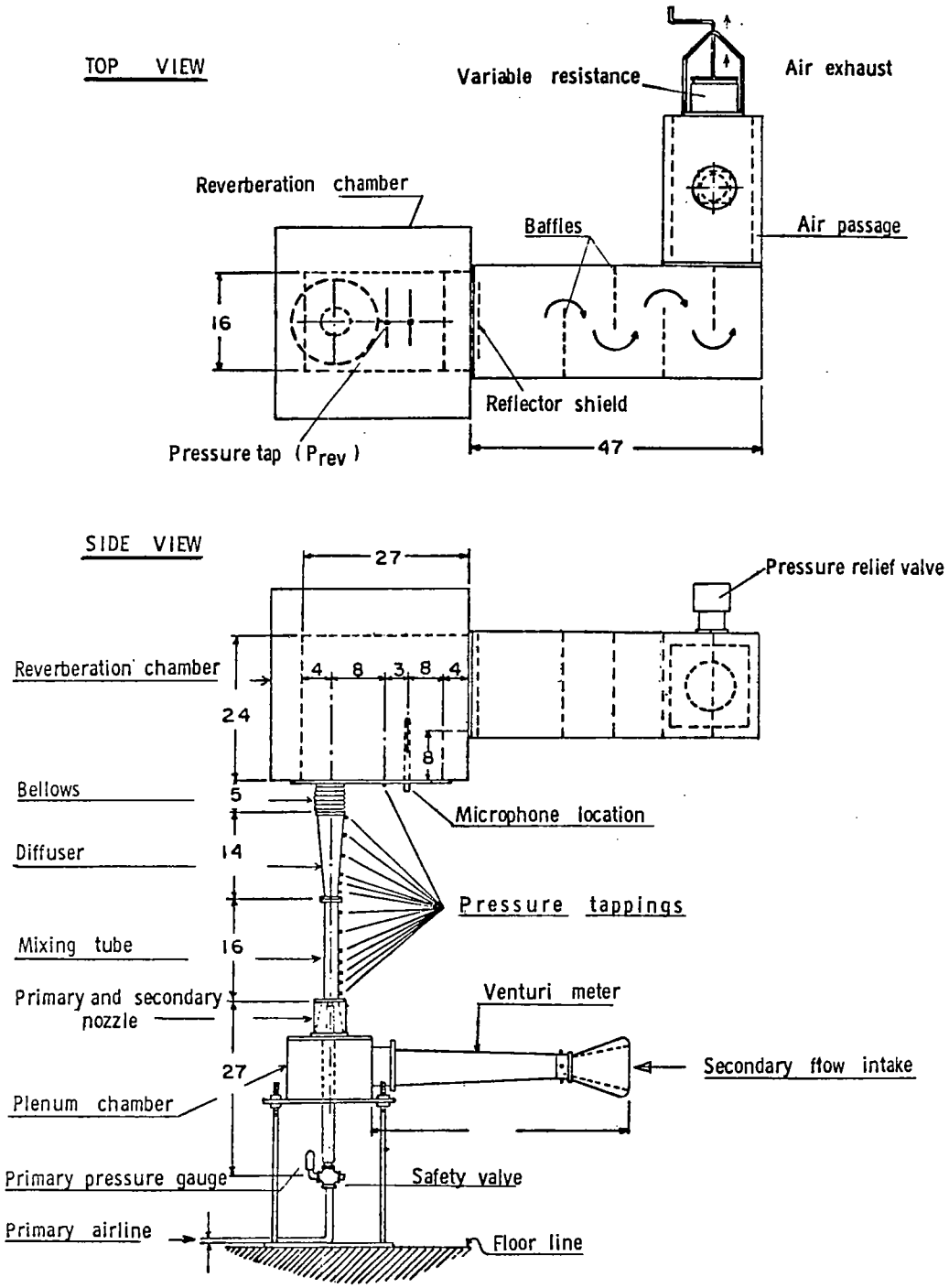

(a) Schematic diagram , top and side elevation . All dimensions are in inches (not to scale).

FIGURE 1 . EXPERIMENTAL APPARATUS (continued)

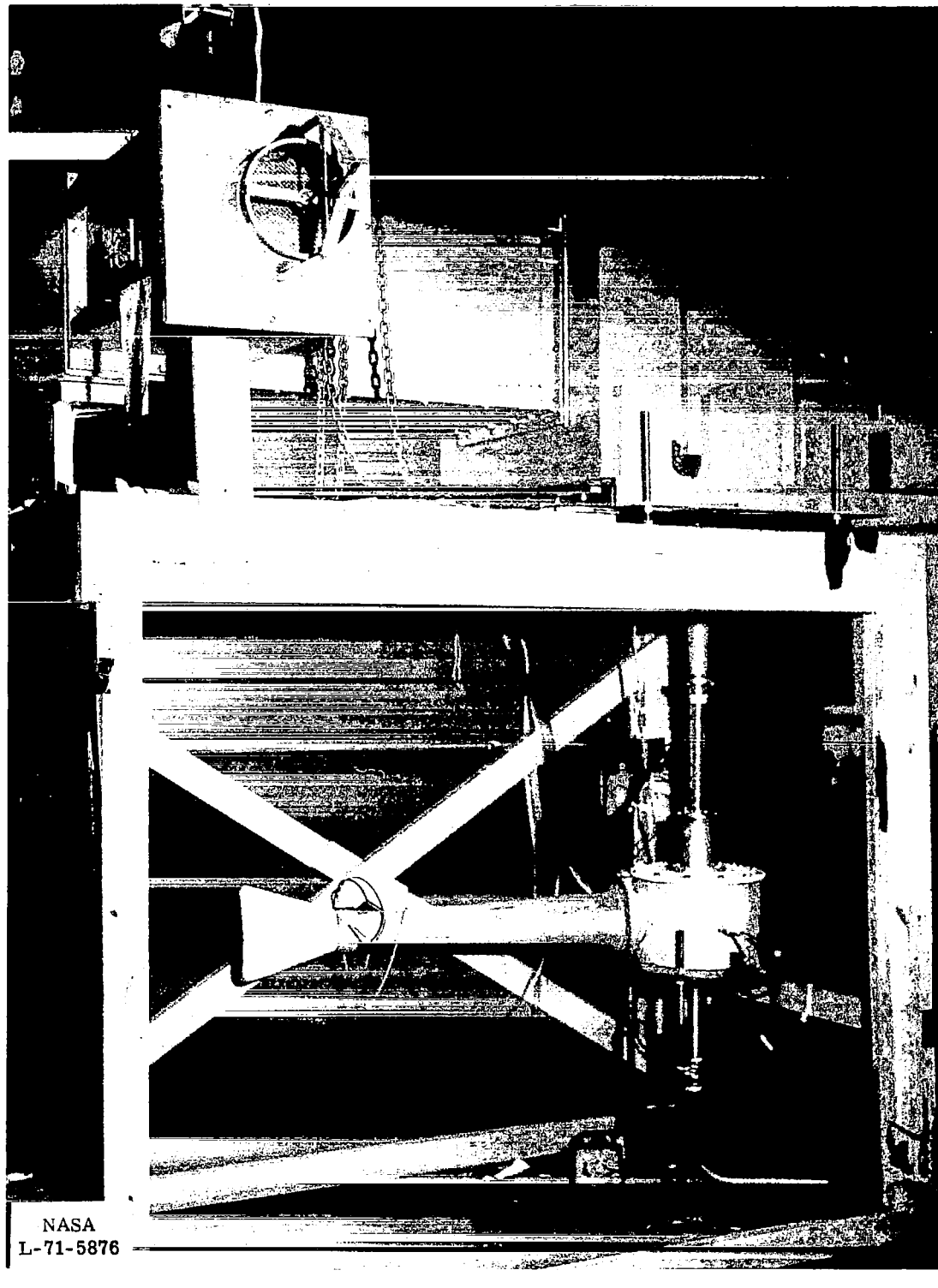

(b) Photographic view

Figure 1. - Concluded.

M	THROAT dia. d_{th}
1	0.4988ins.
1.5	0.4693
2	0.3895
2.5	0.3070
3	0.2460

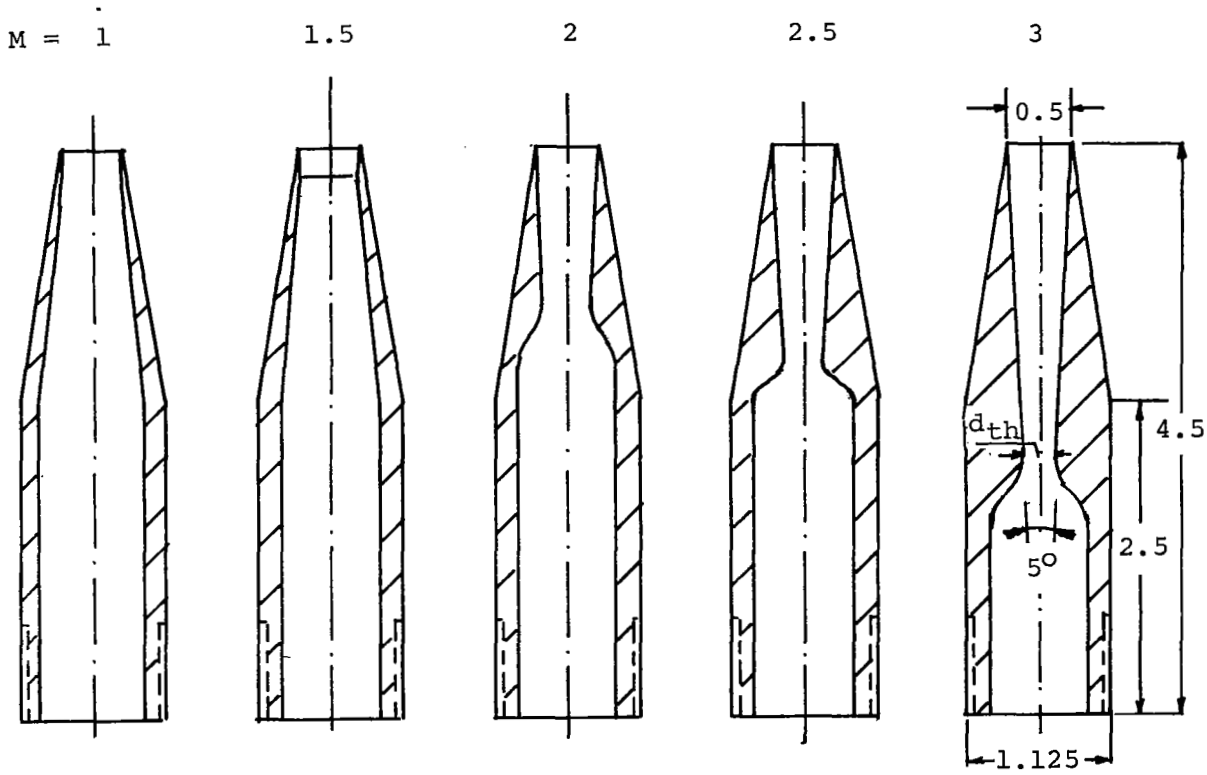

Figure 2.-Sectional View of Test Nozzles.

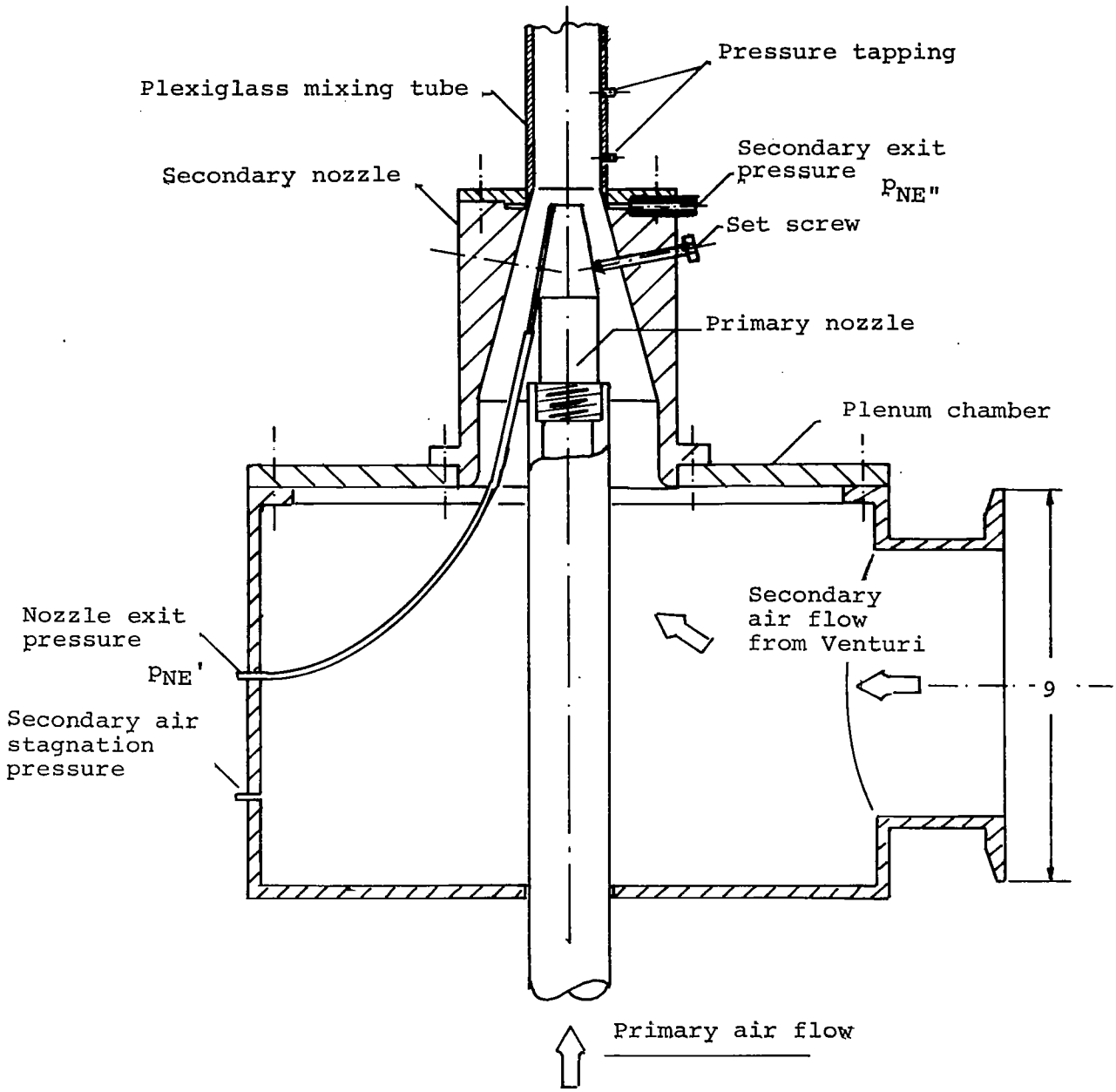

Figure 3.- Sectional View of Primary, Secondary Nozzle and Plenum Chamber.

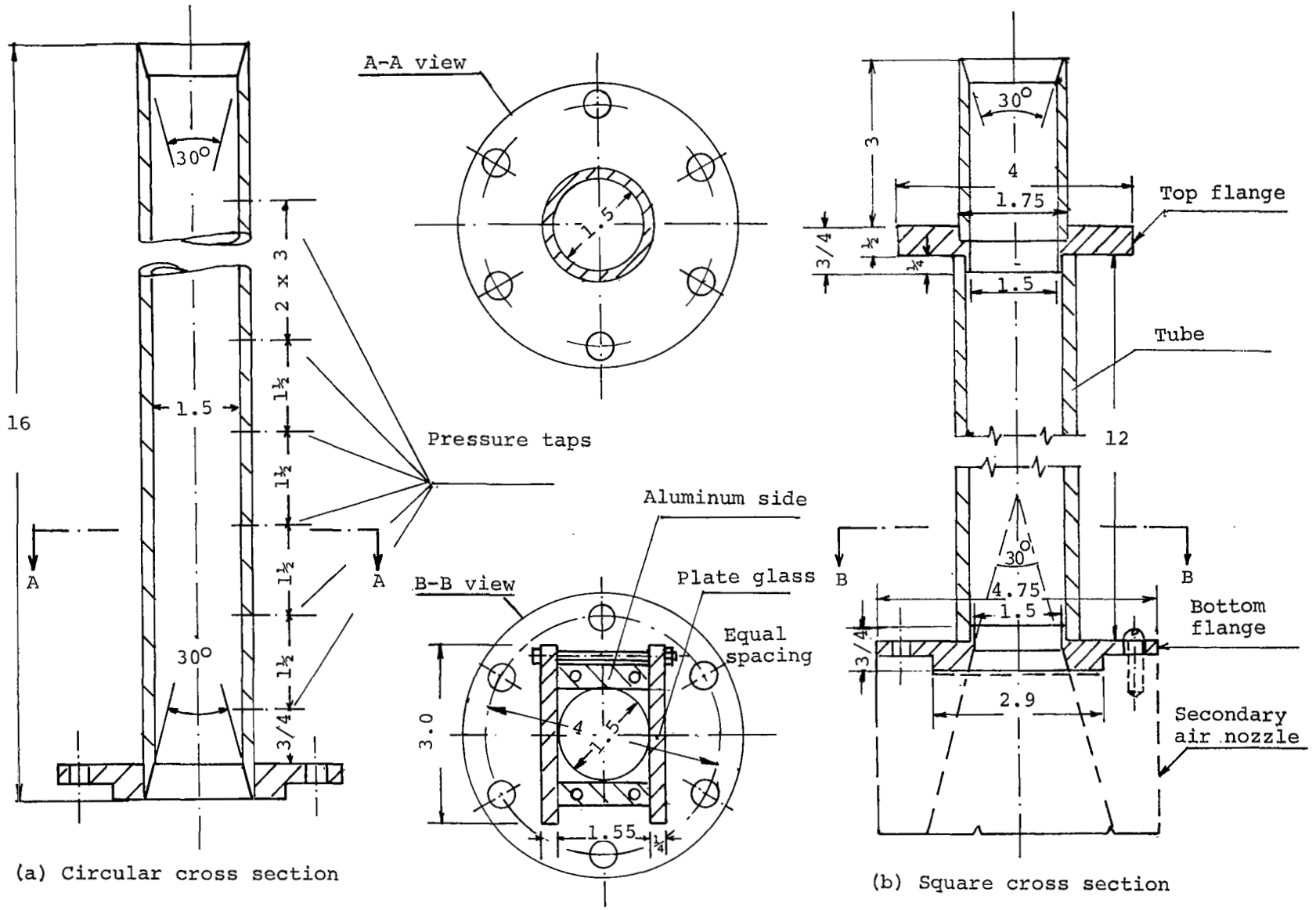

Figure 4.- Sectional Views of Mixing Tubes.

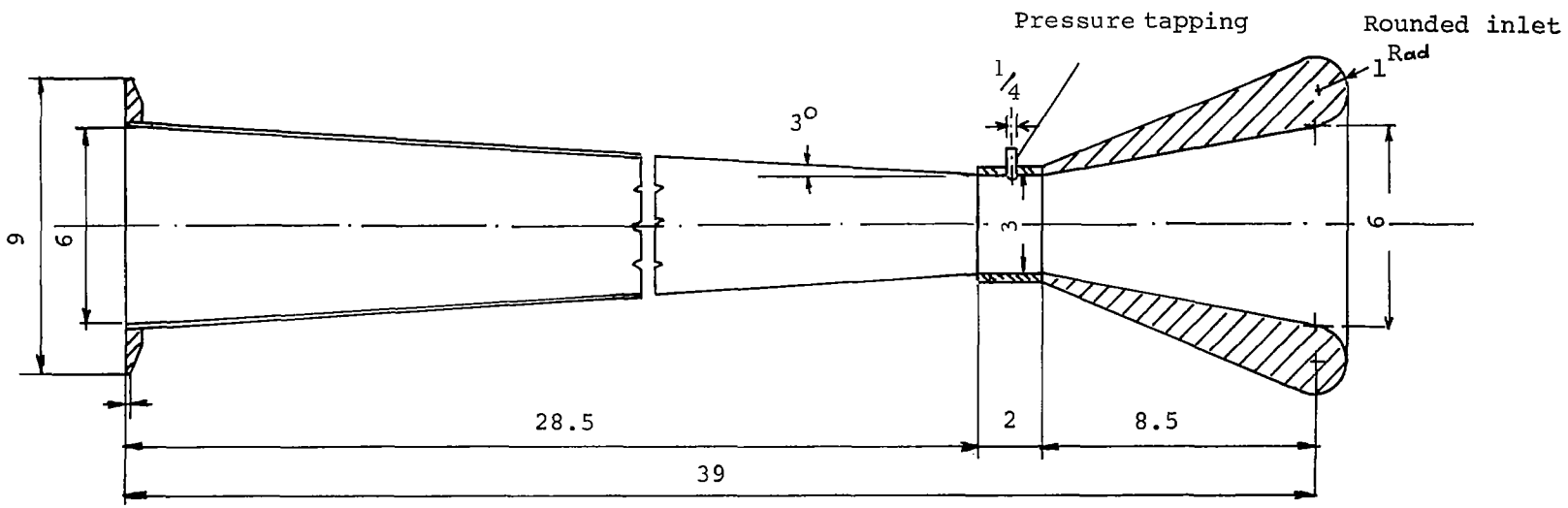

Figure 5.- Sectional View of Venturi Tube.

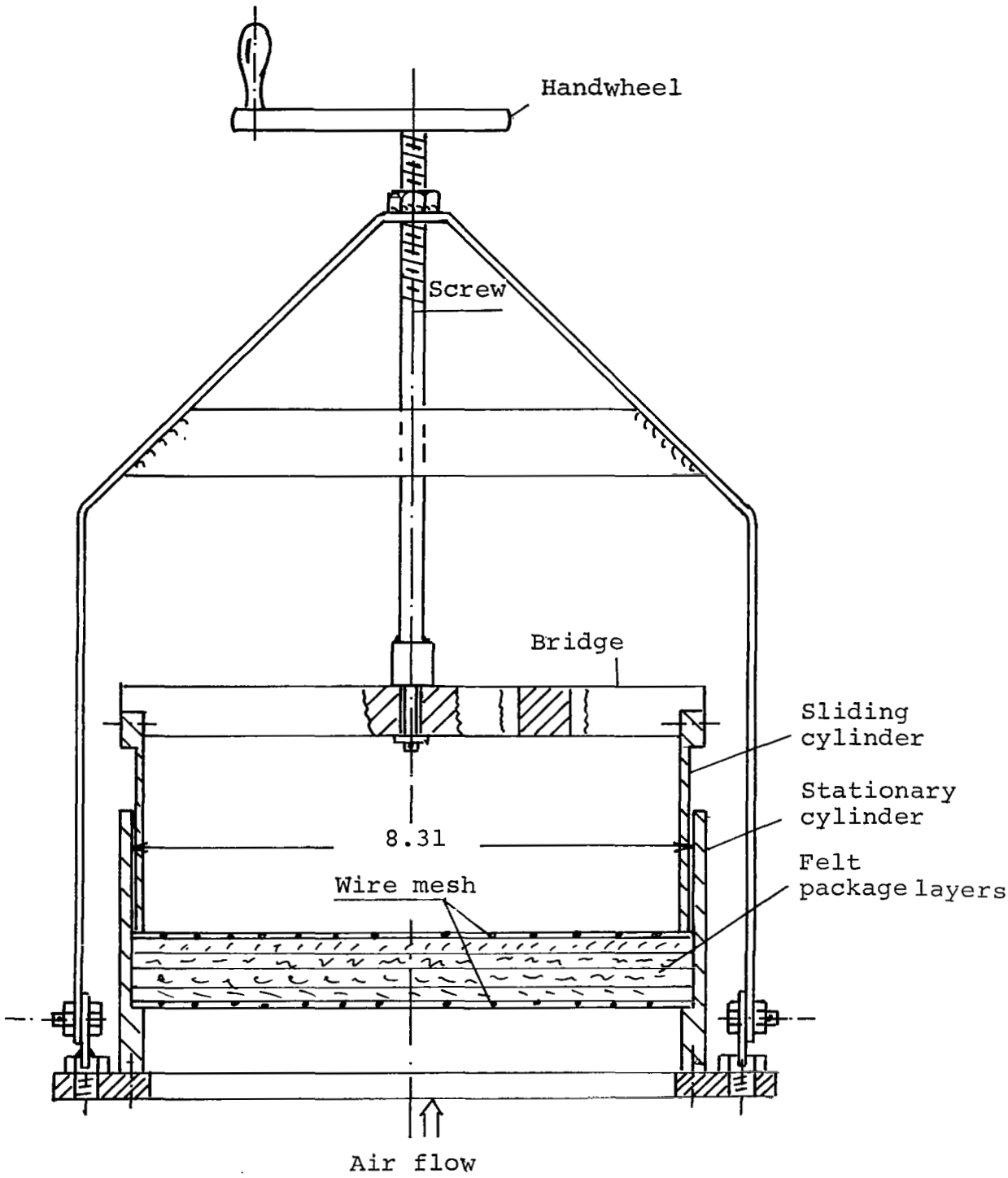

Figure 6.- Sectional View of Air Flow Resistance Apparatus.

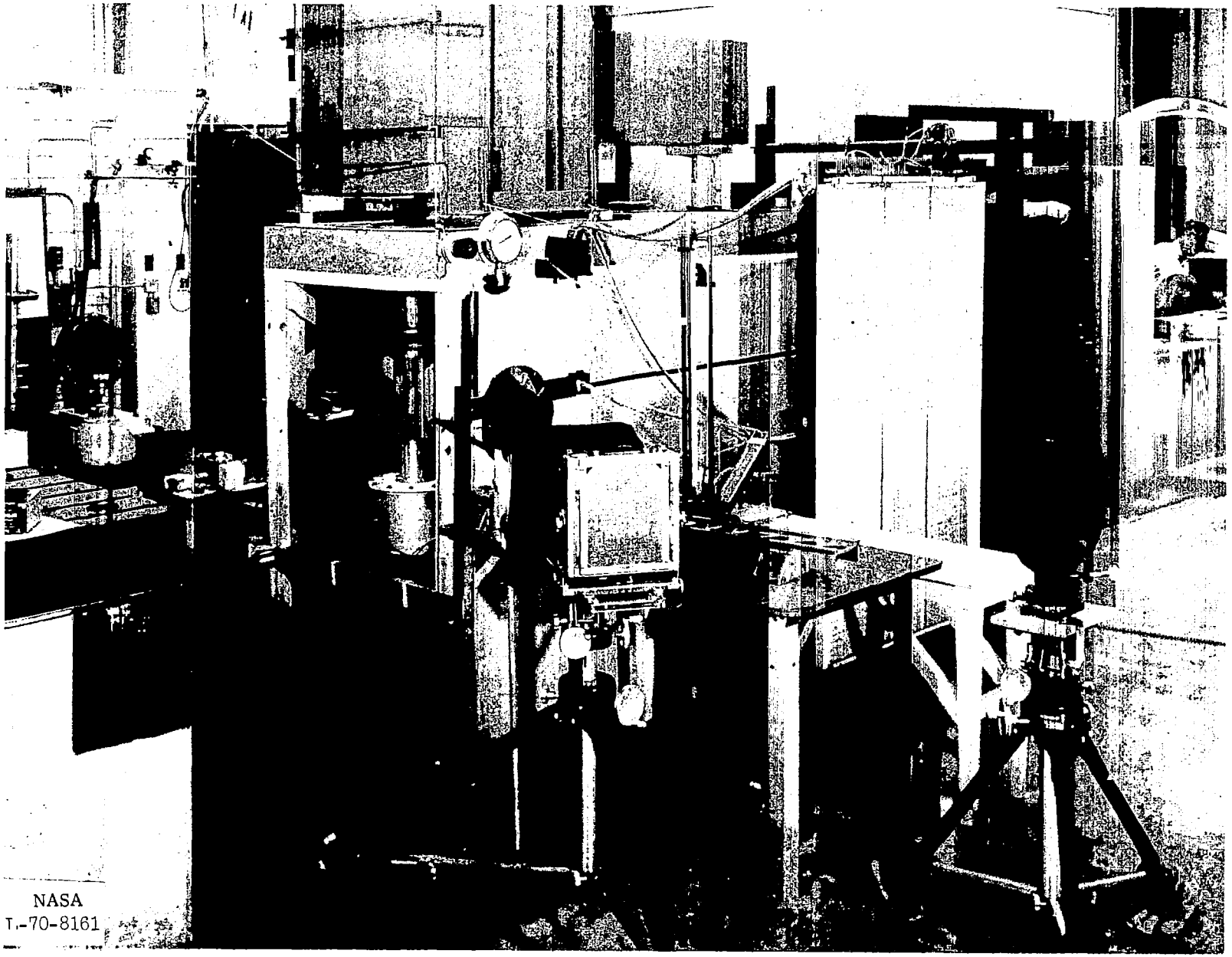

Figure 7. Apparatus set-up for Schlieren photography

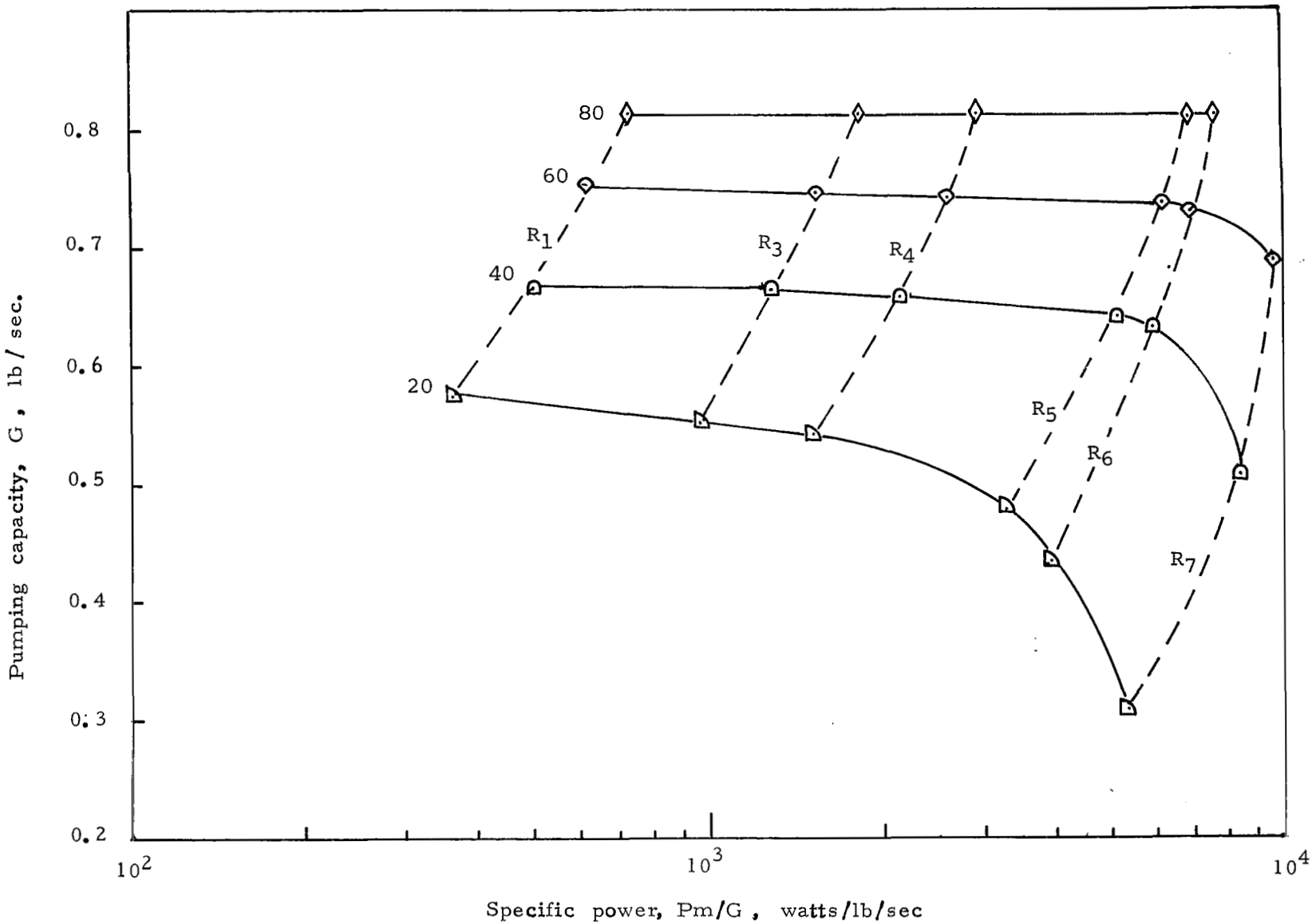

(a) Nozzle Mach number M=1

Figure 8. Pumping performance of ejector

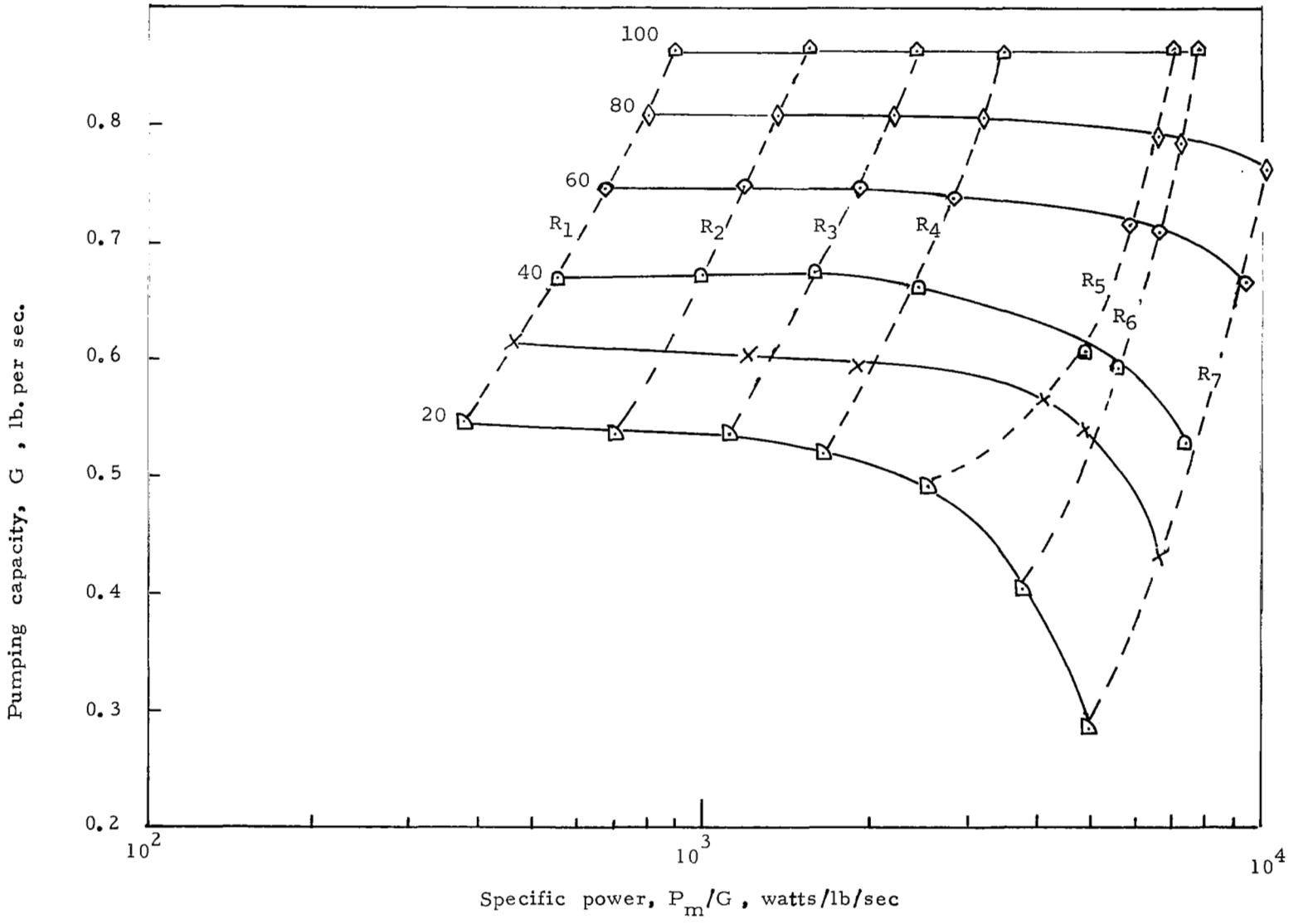

(b) Nozzle Mach number M= 1.5

Figure 8.- Continued

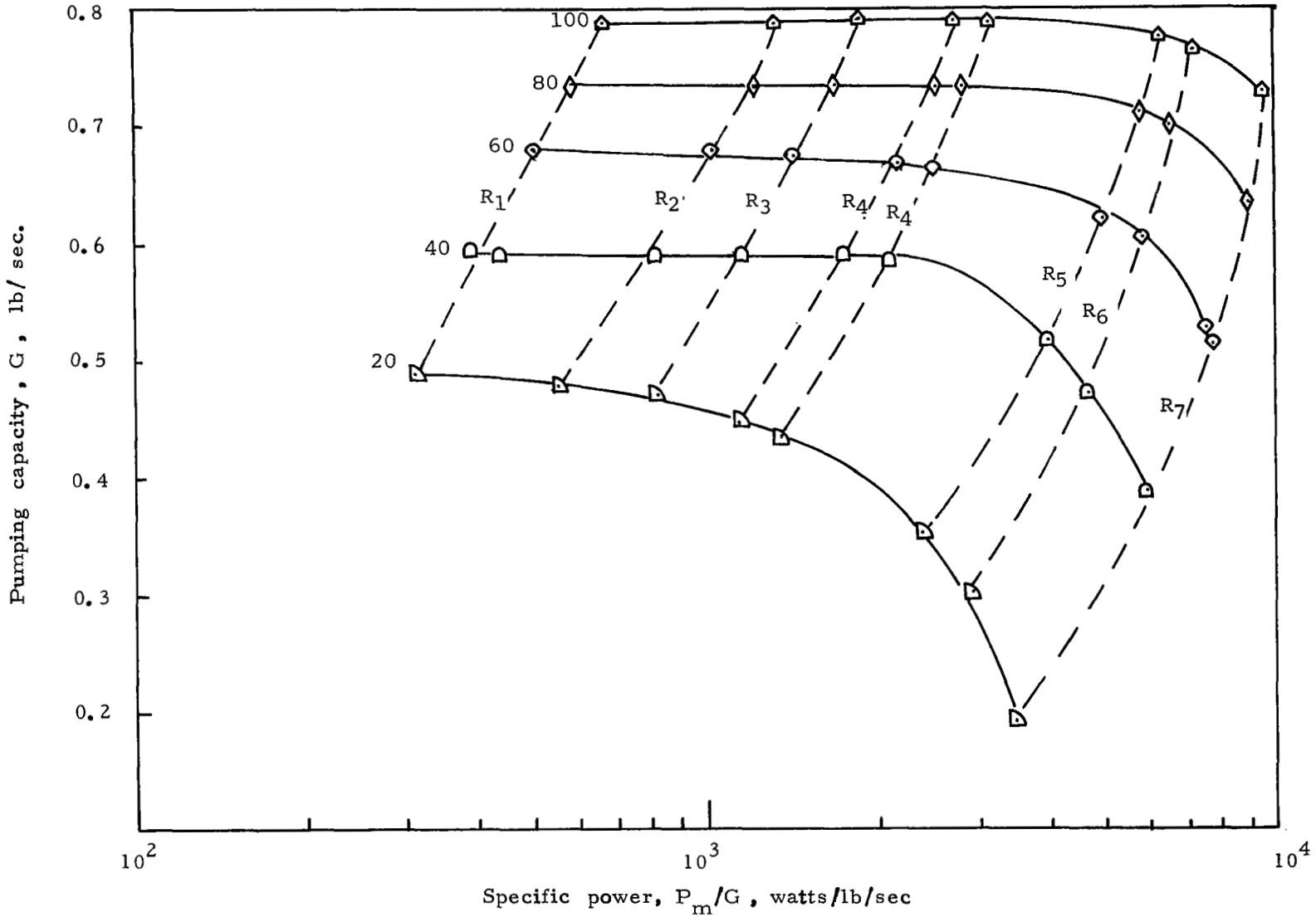

(c) Nozzle Mach number M= 2

Figure 8. - Continued

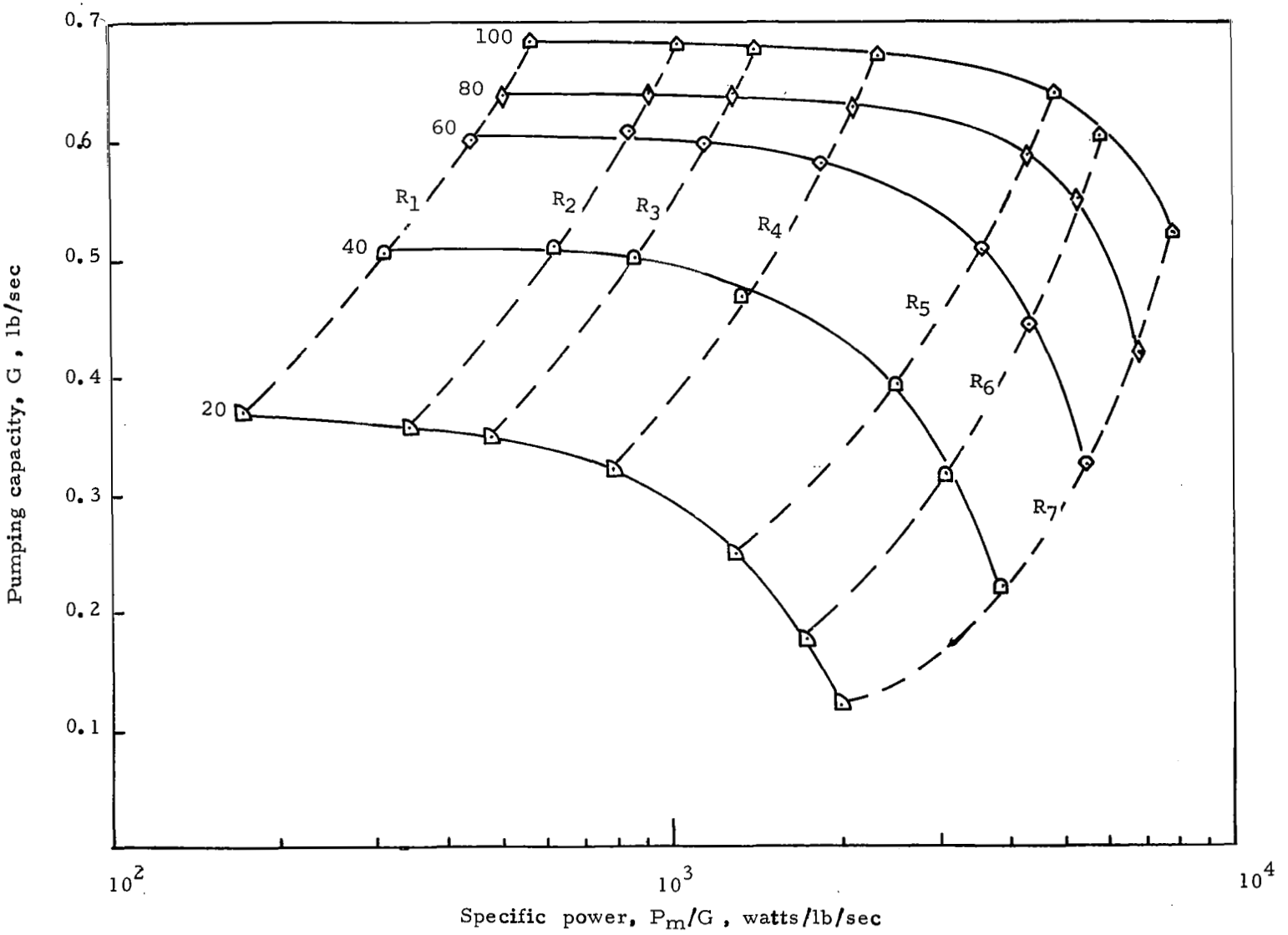

(d) Nozzle Mach number M=2.5

Figure 8. - Continued

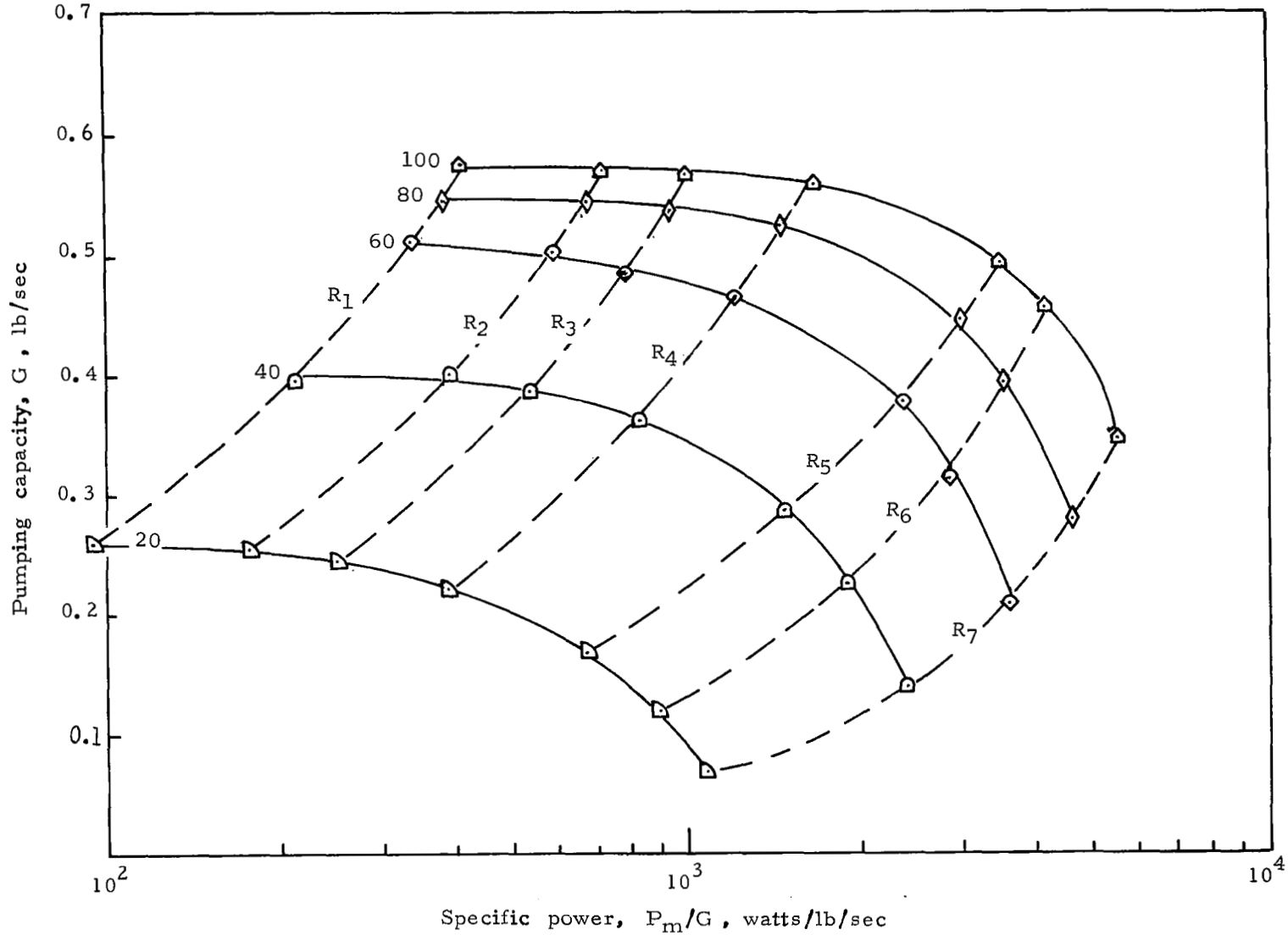

(e) Nozzle Mach number M=3

Figure 8. - Concluded

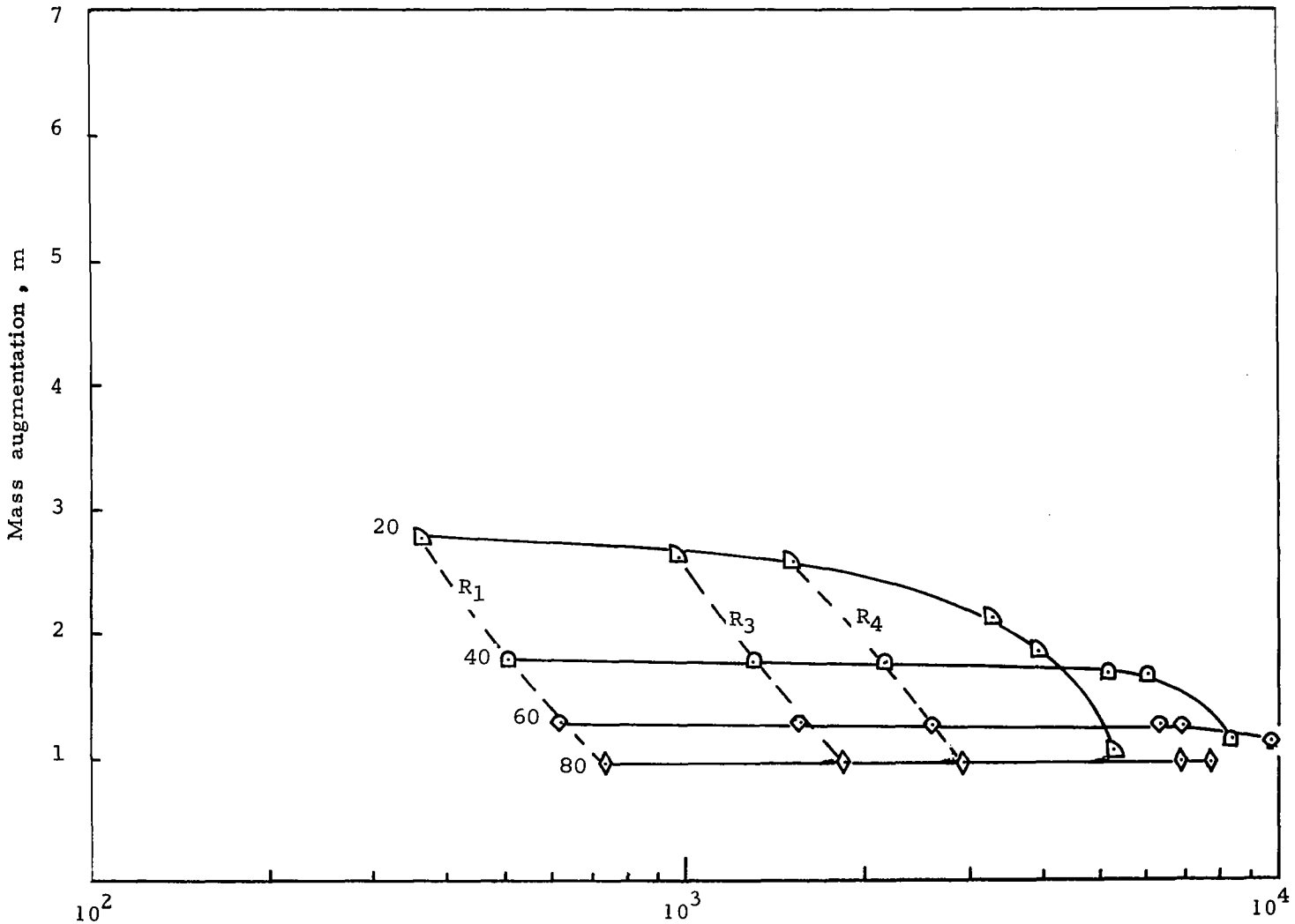

(a) Nozzle Mach number M = 1

Figure 9. Mass augmentation of ejector

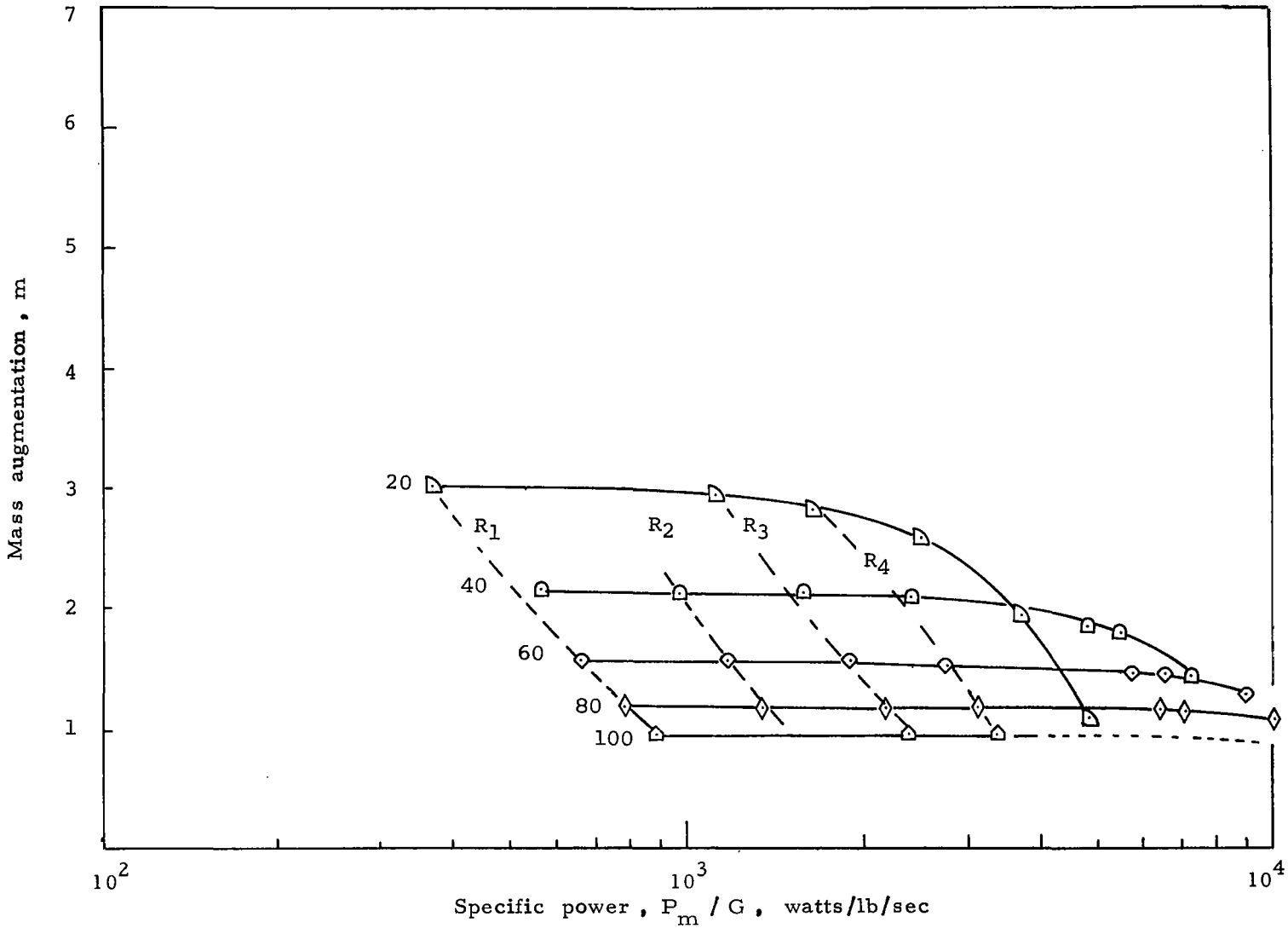

(b) Nozzle Mach number M = 1.5

Figure 9.- Continued

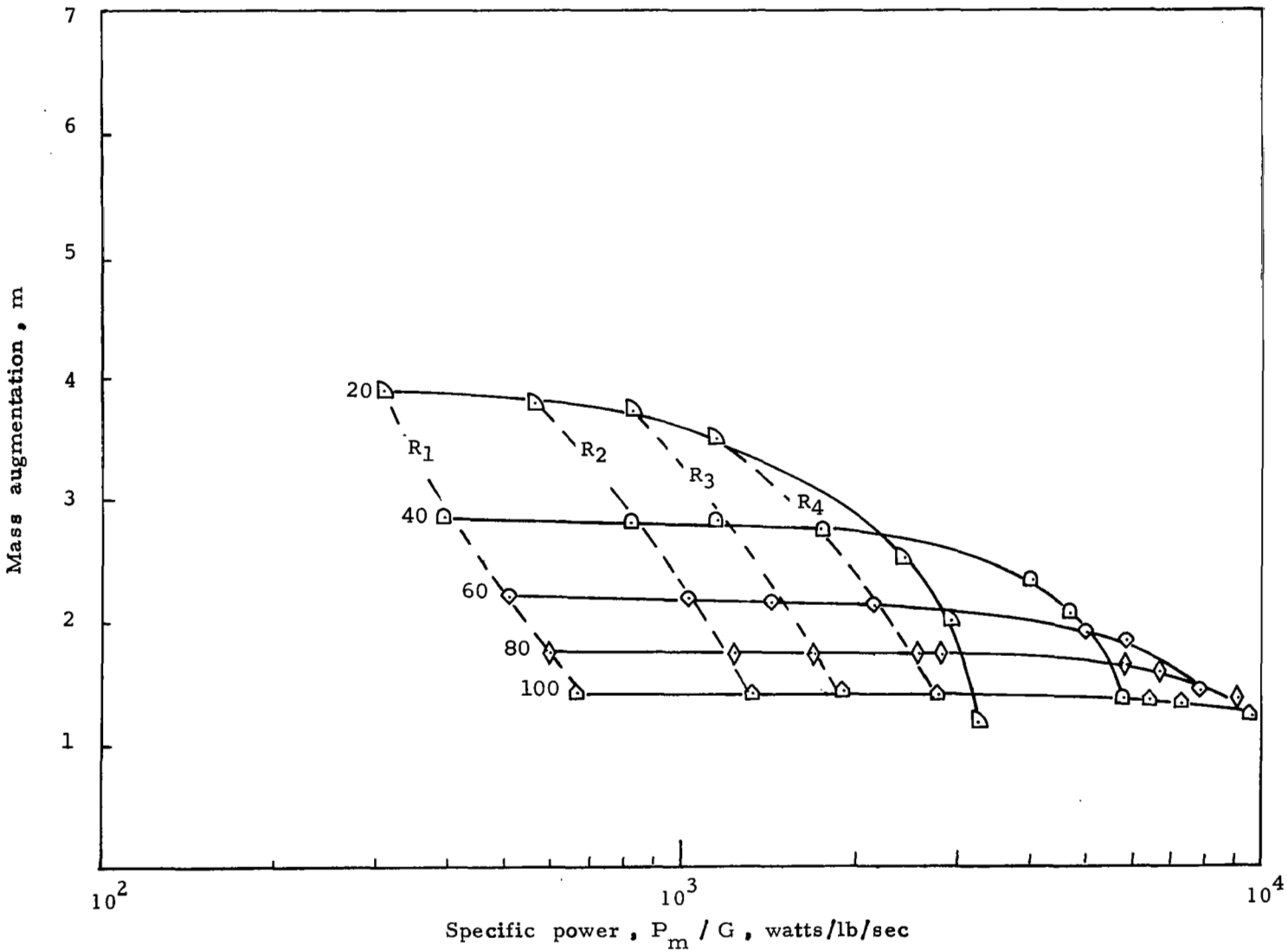

(c) Nozzle Mach number M = 2

Figure 9. - Continued

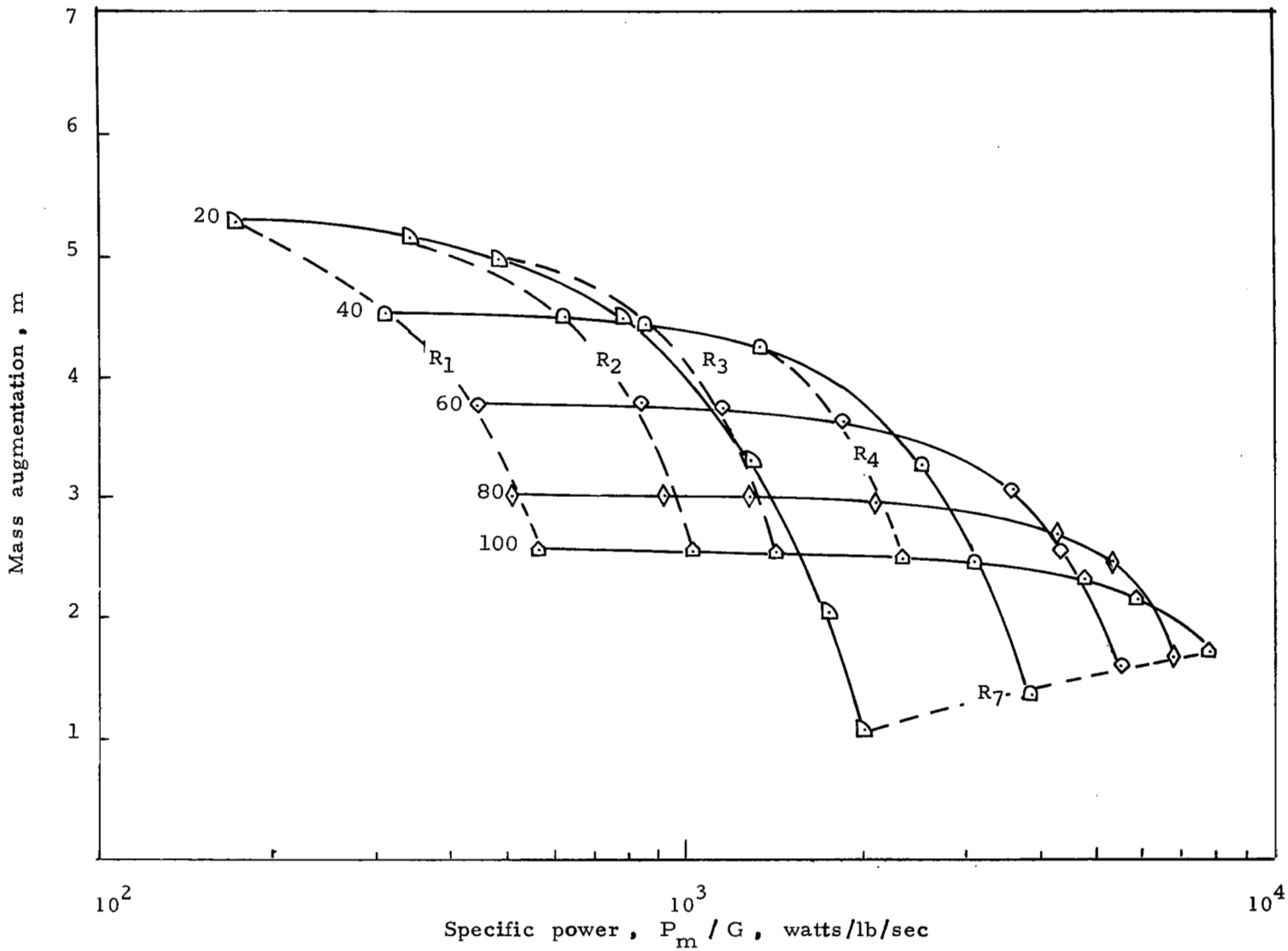

(d) Nozzle Mach number M = 2.5

Figure 9.- Continued

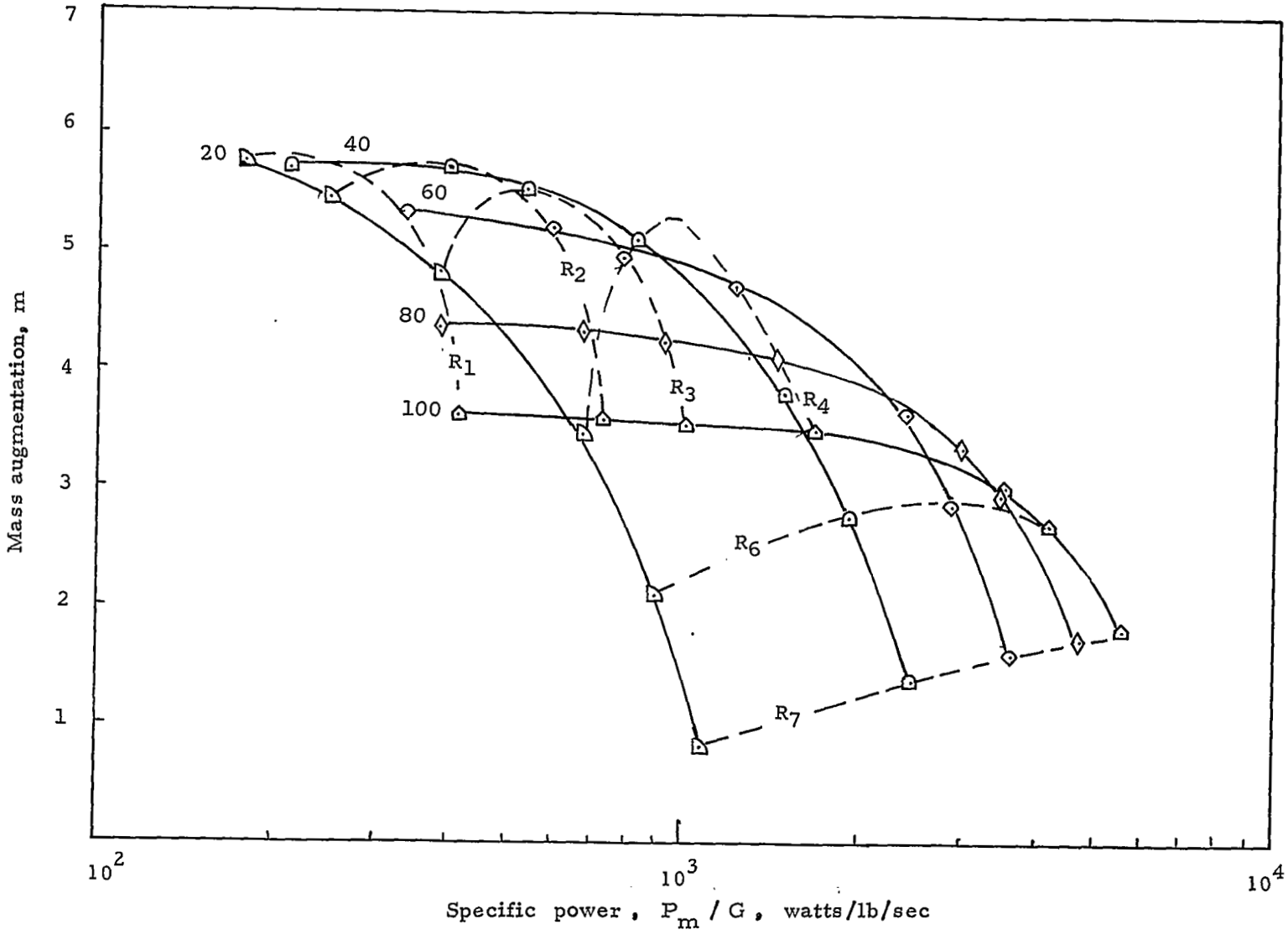

(e) Nozzle Mach number M= 3

Figure 9. - Concluded

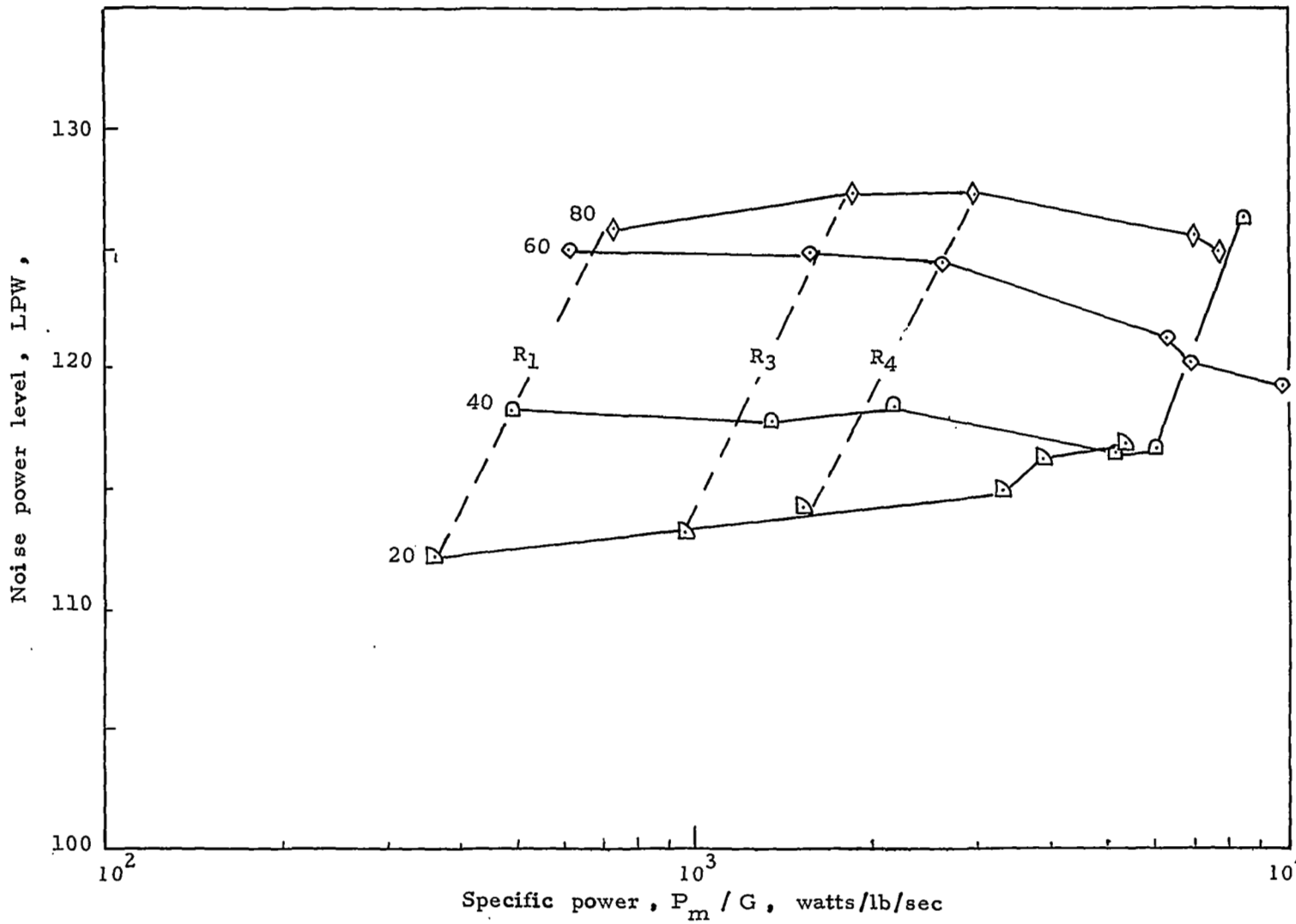

(a) Nozzle Mach number M = 1

Figure 10. Noise generation of ejector

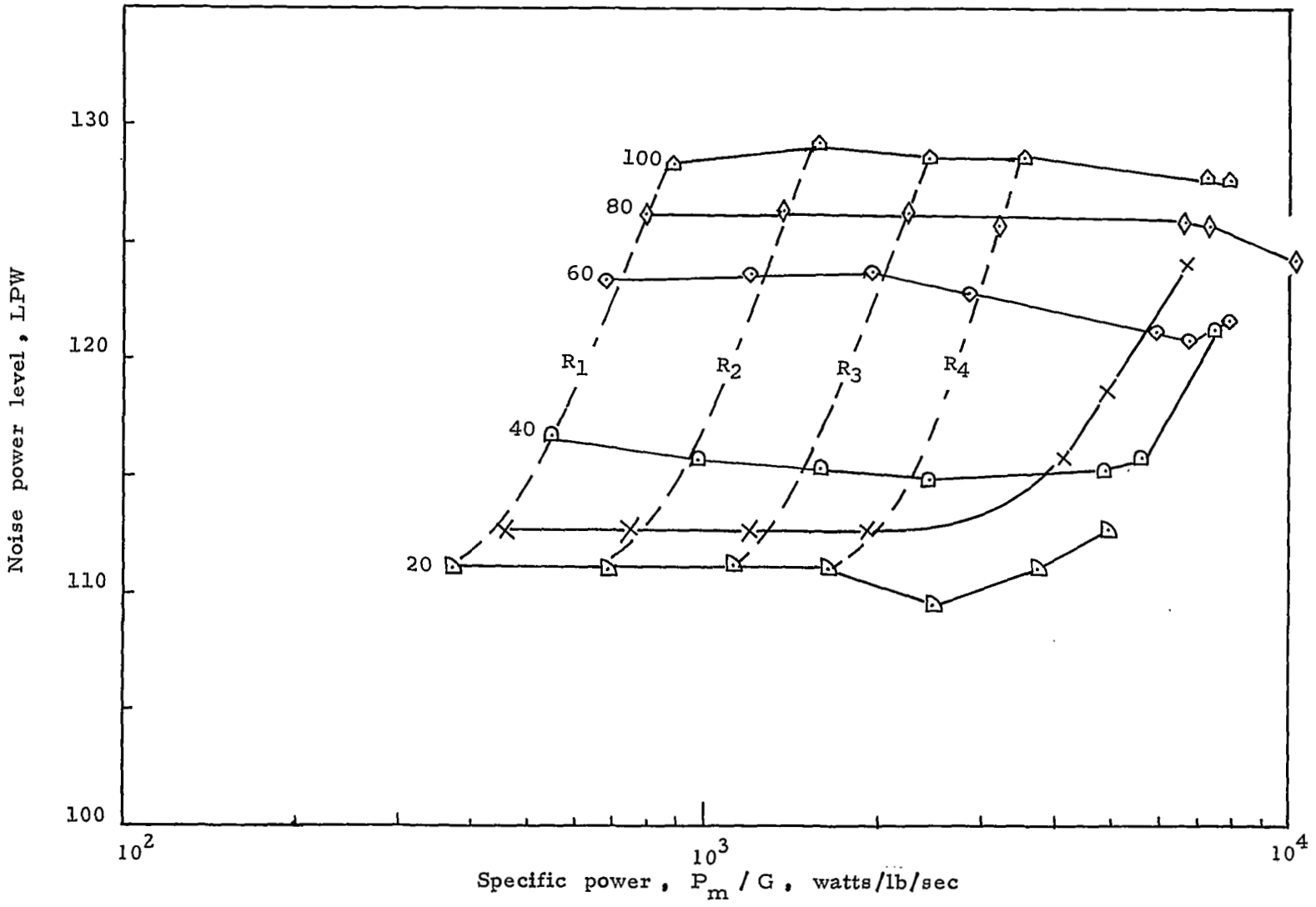

(b) Nozzle Mach number M = 1.5

Figure 10. - Continued

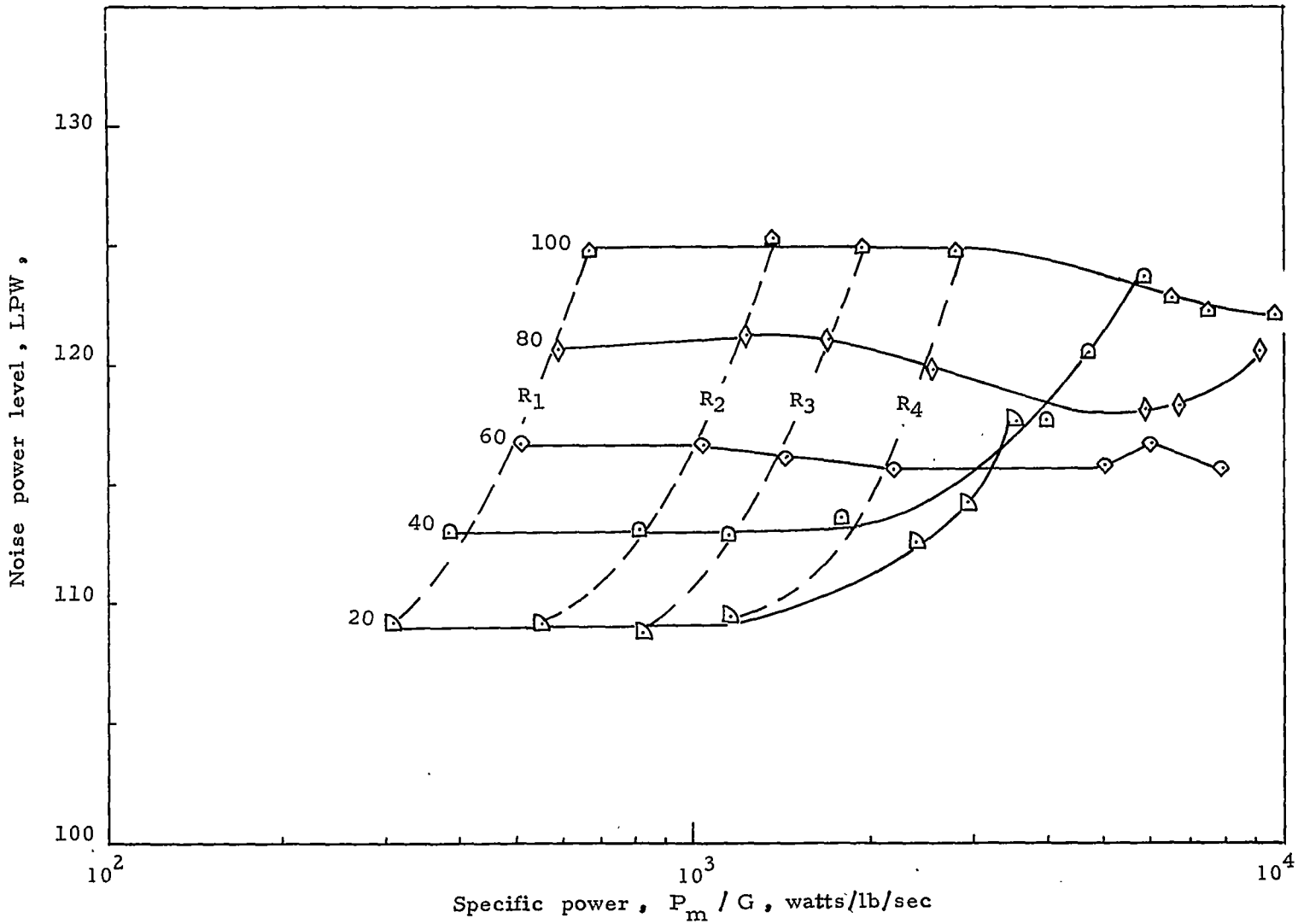

(c) Nozzle Mach number M = 2

Figure 10. - Continued

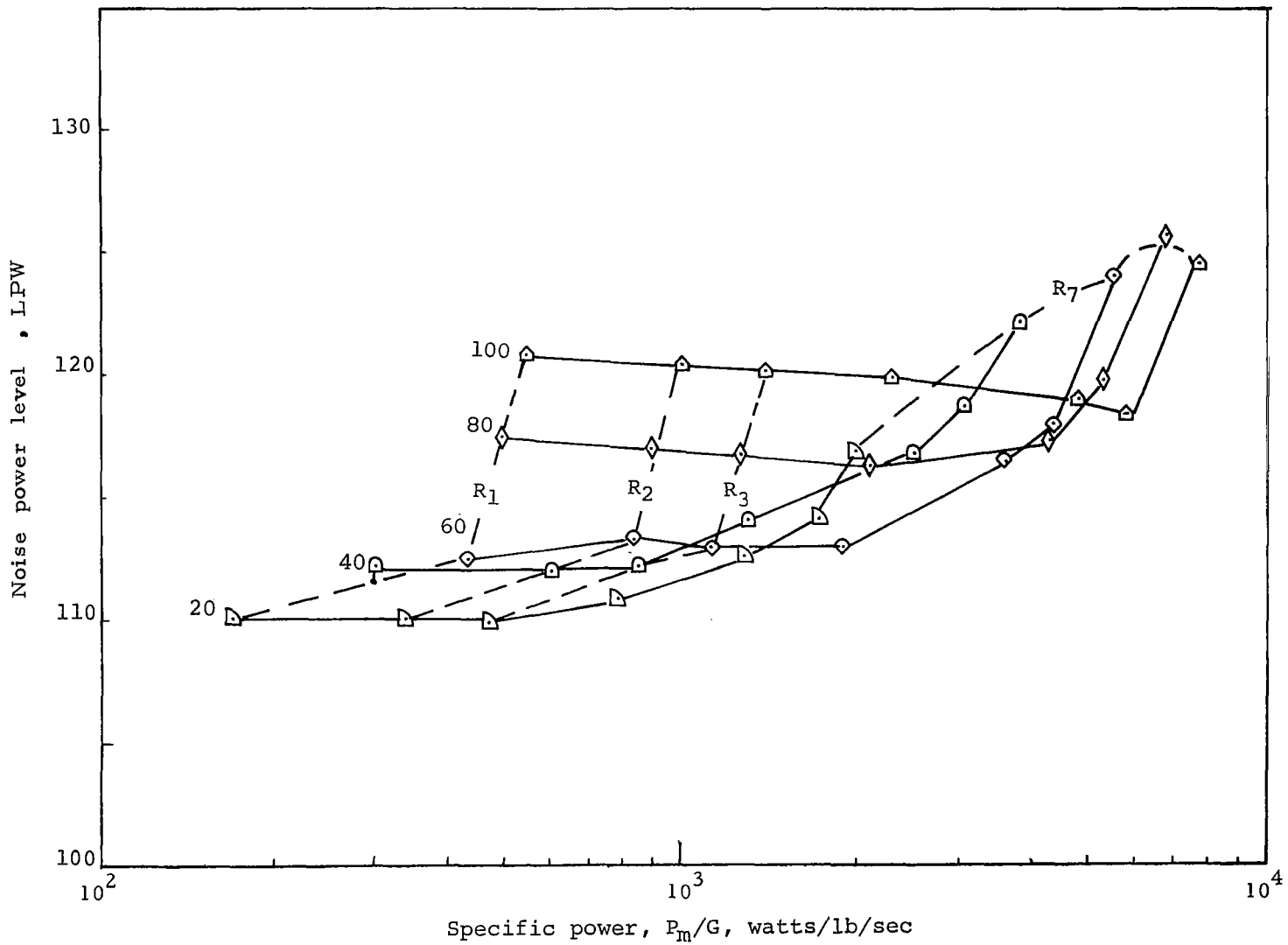

(d) Nozzle Mach number M = 2.5

Figure 10. - Continued

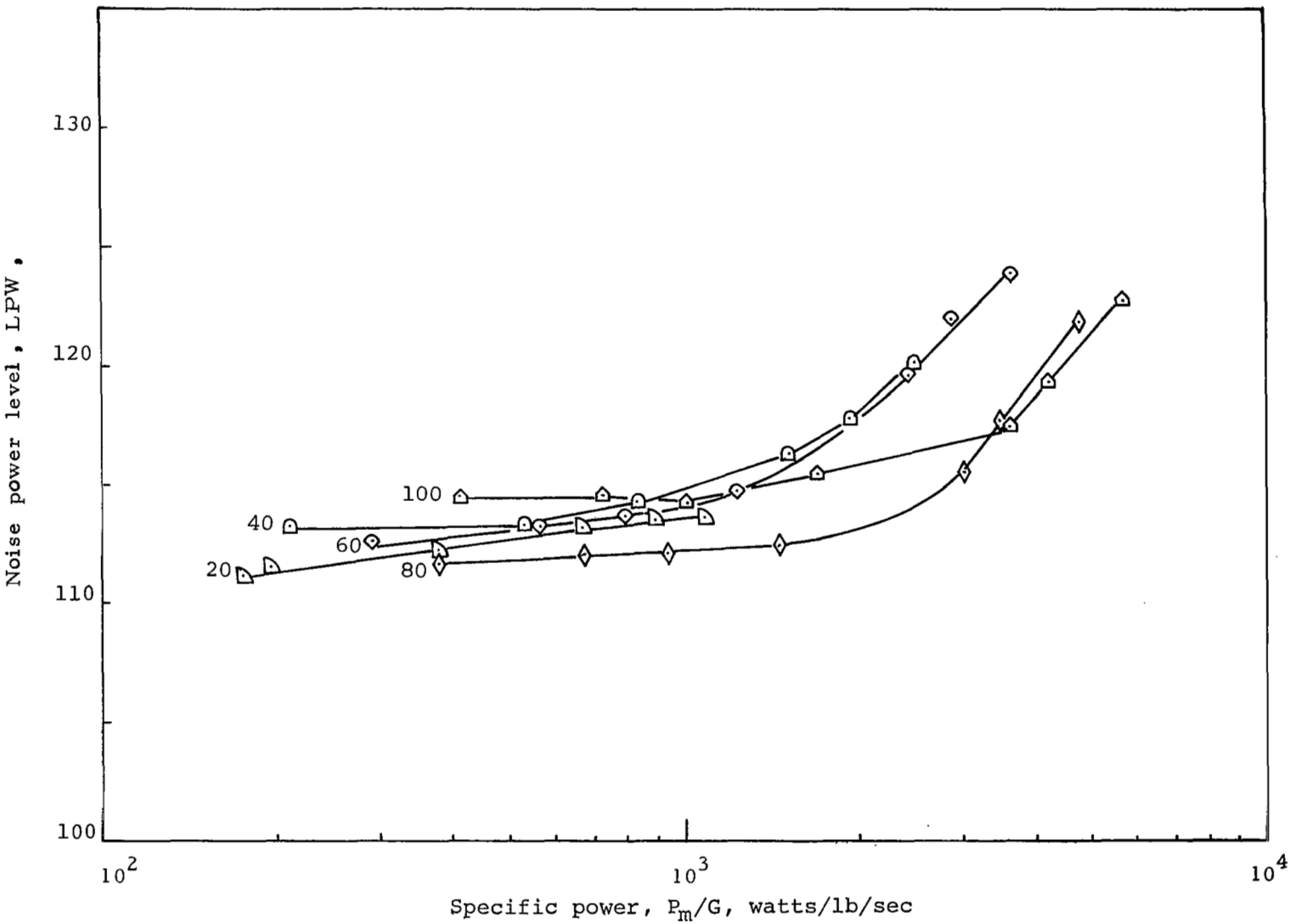

(e) Nozzle Mach number M = 3

Figure 10.- Concluded

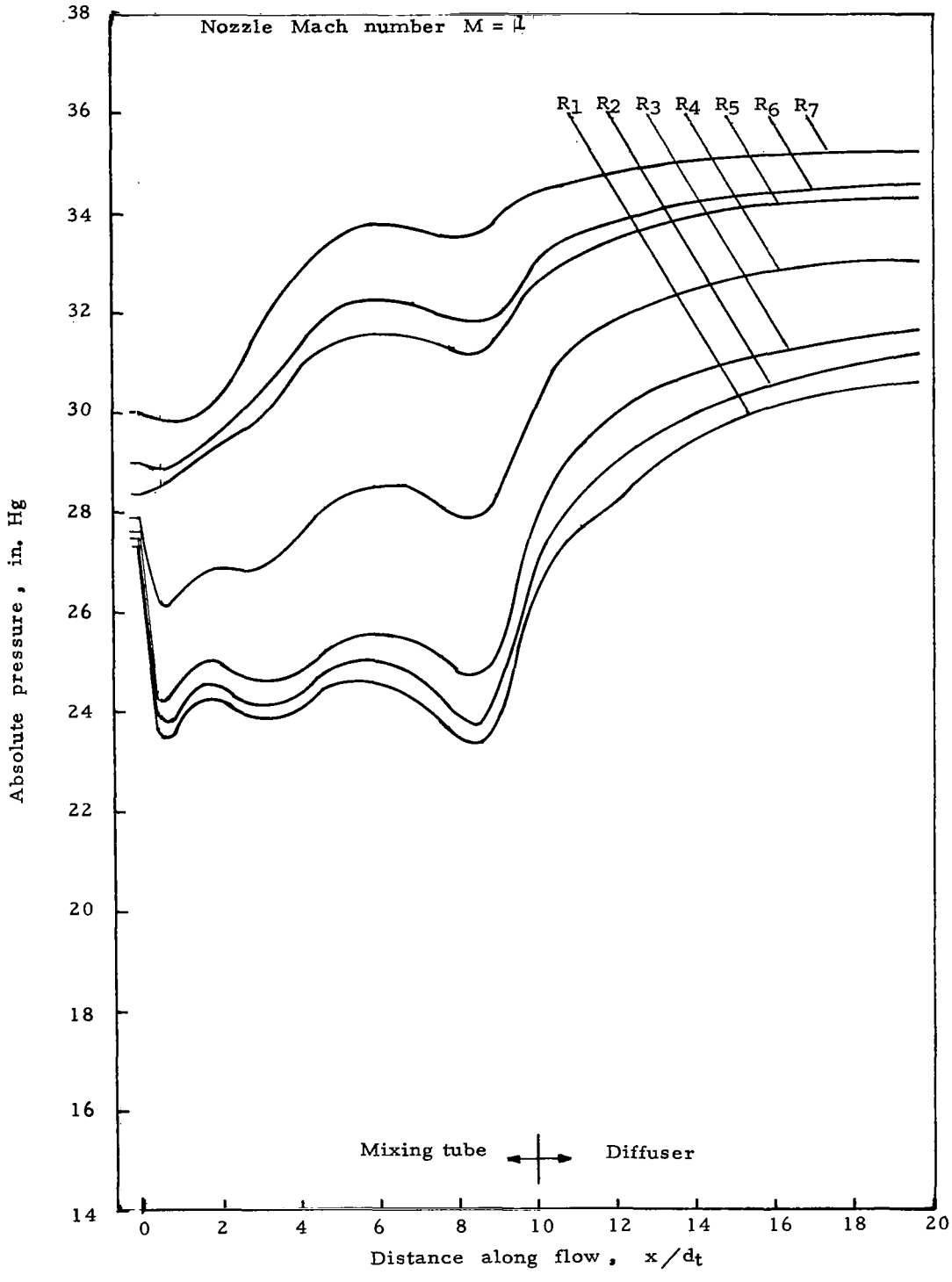

(a) Primary pressure P_1 = 20 psi

Figure 11.- Pressure distribution along mixing tube and diffuser.

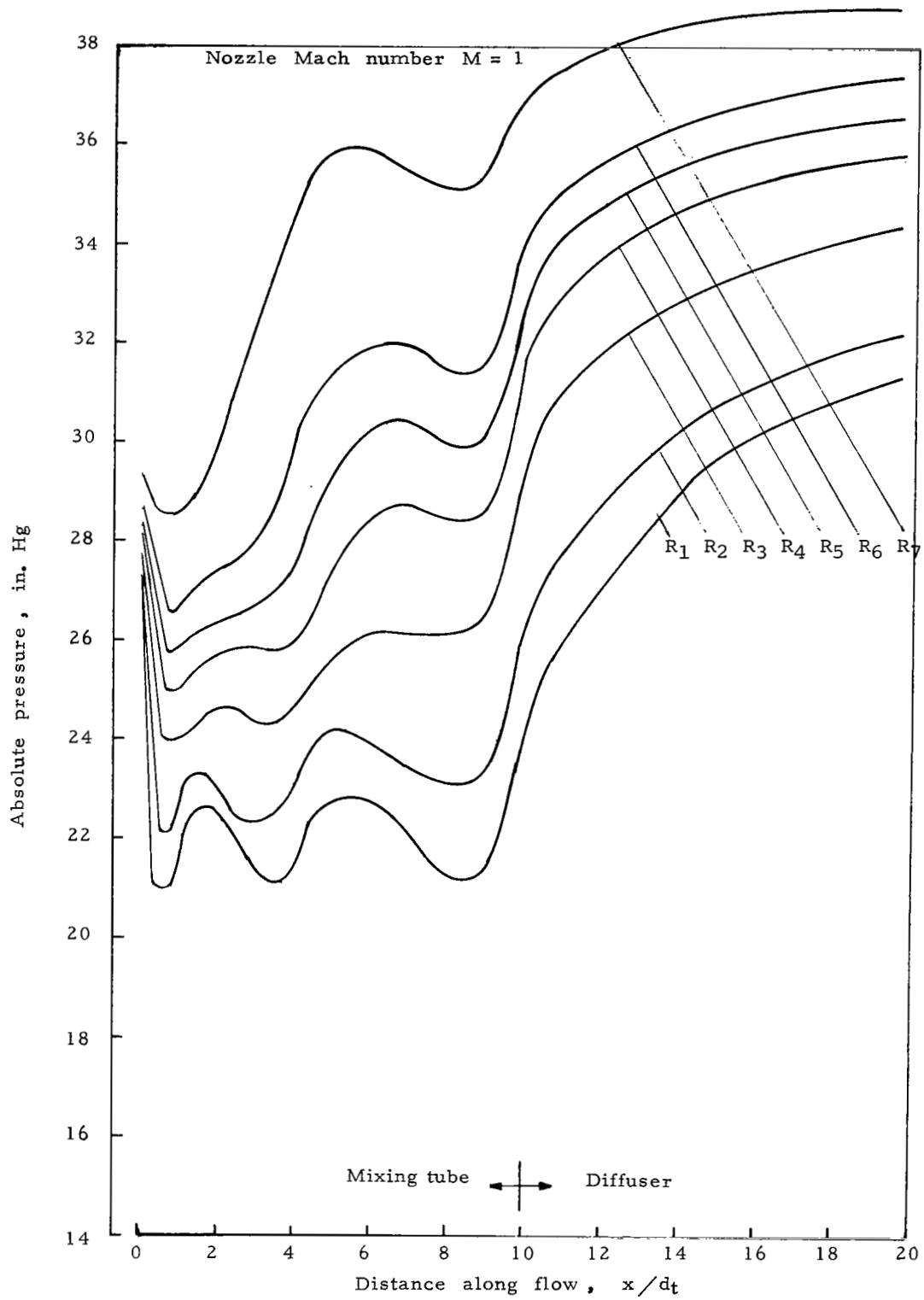

(b) Primary pressure P_1 = 40 psi

Figure 11.- Continued.

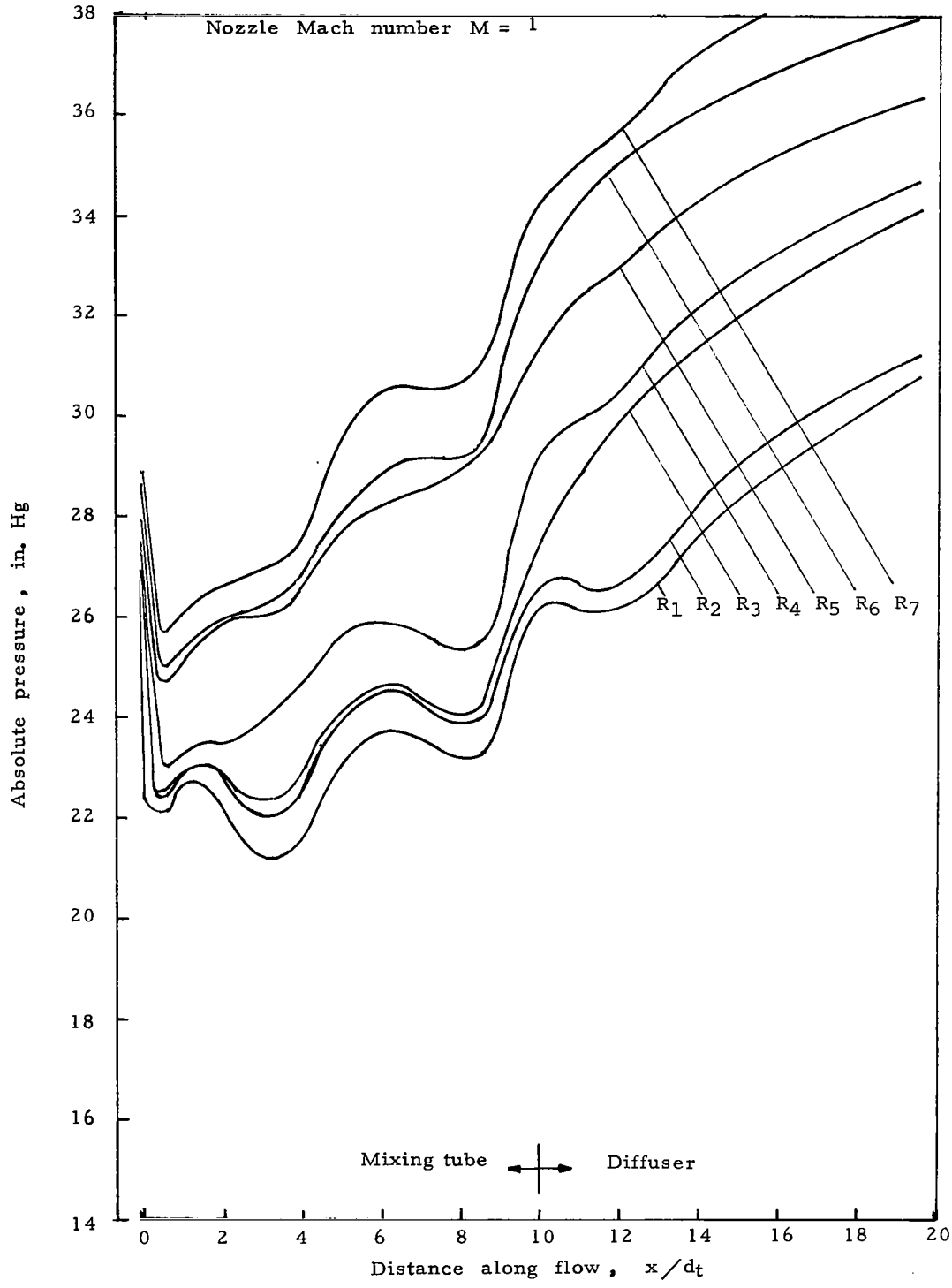

(c) Primary pressure P_1 = 60 psi

Figure 11.- Continued.1

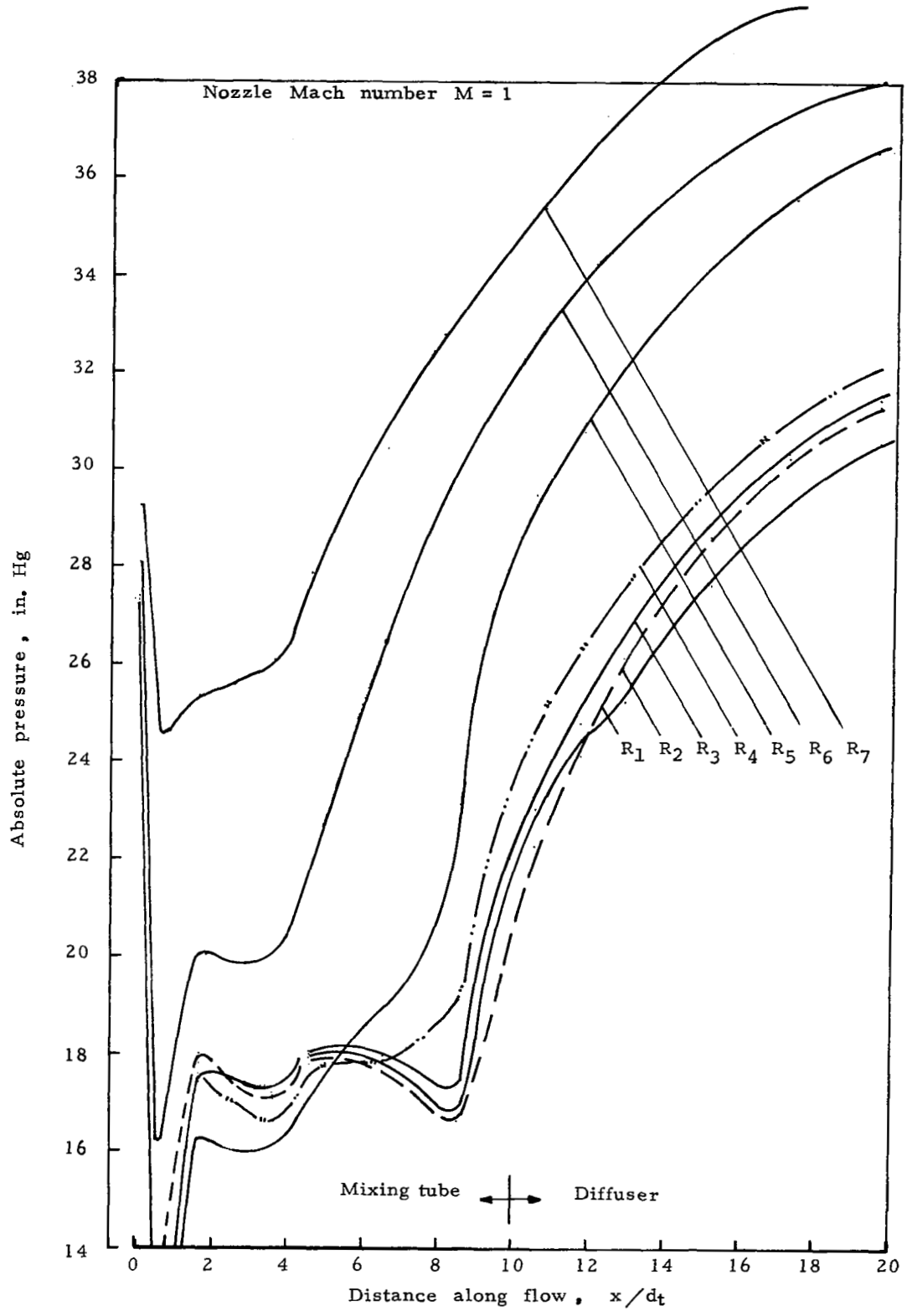

(d) Primary pressure P_1 = 80 psi

Figure 11.- Concluded.

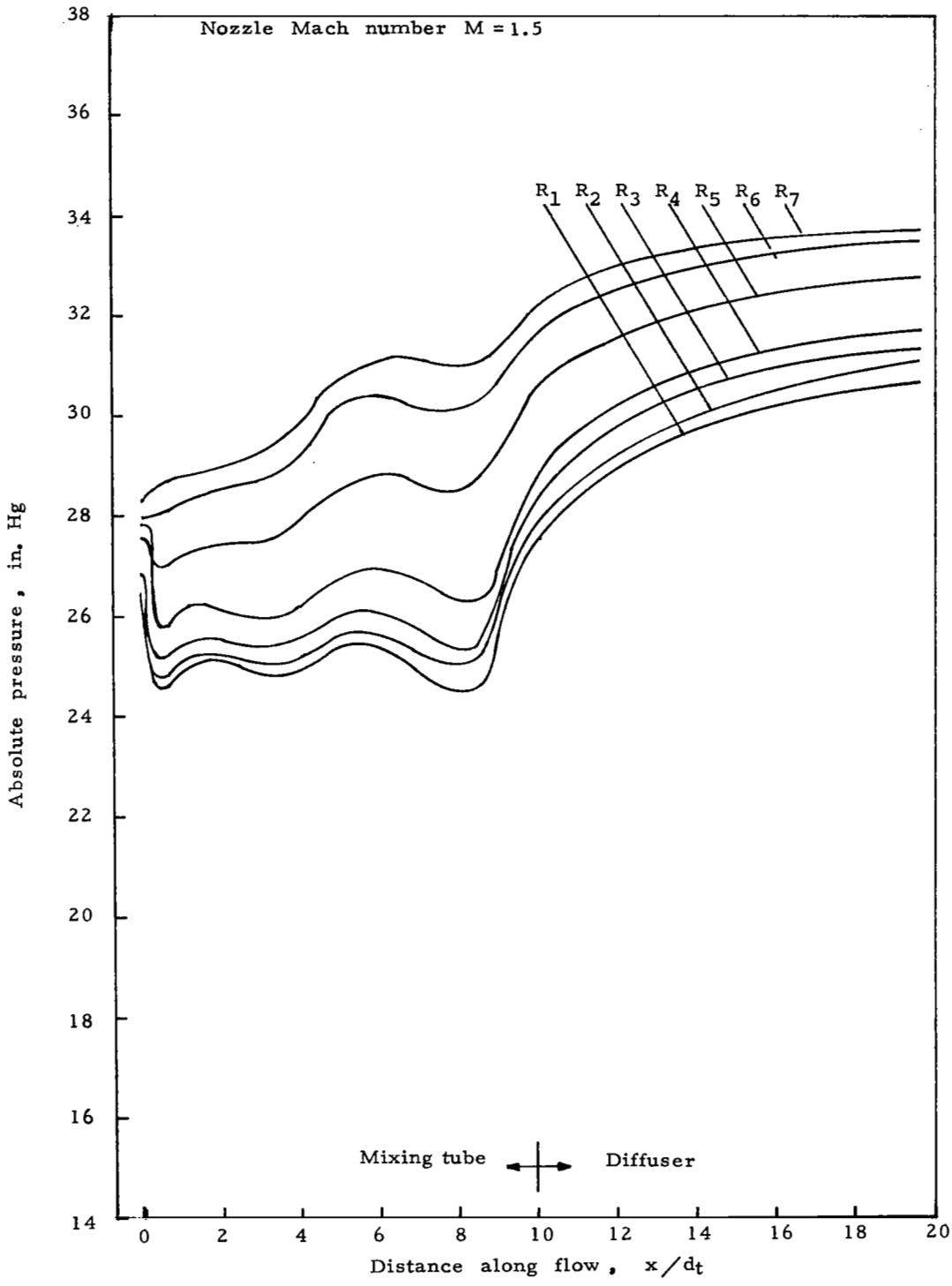

(a) Primary pressure P_1 = 20 psi

Figure 12.- Pressure distribution along mixing tube and diffuser.

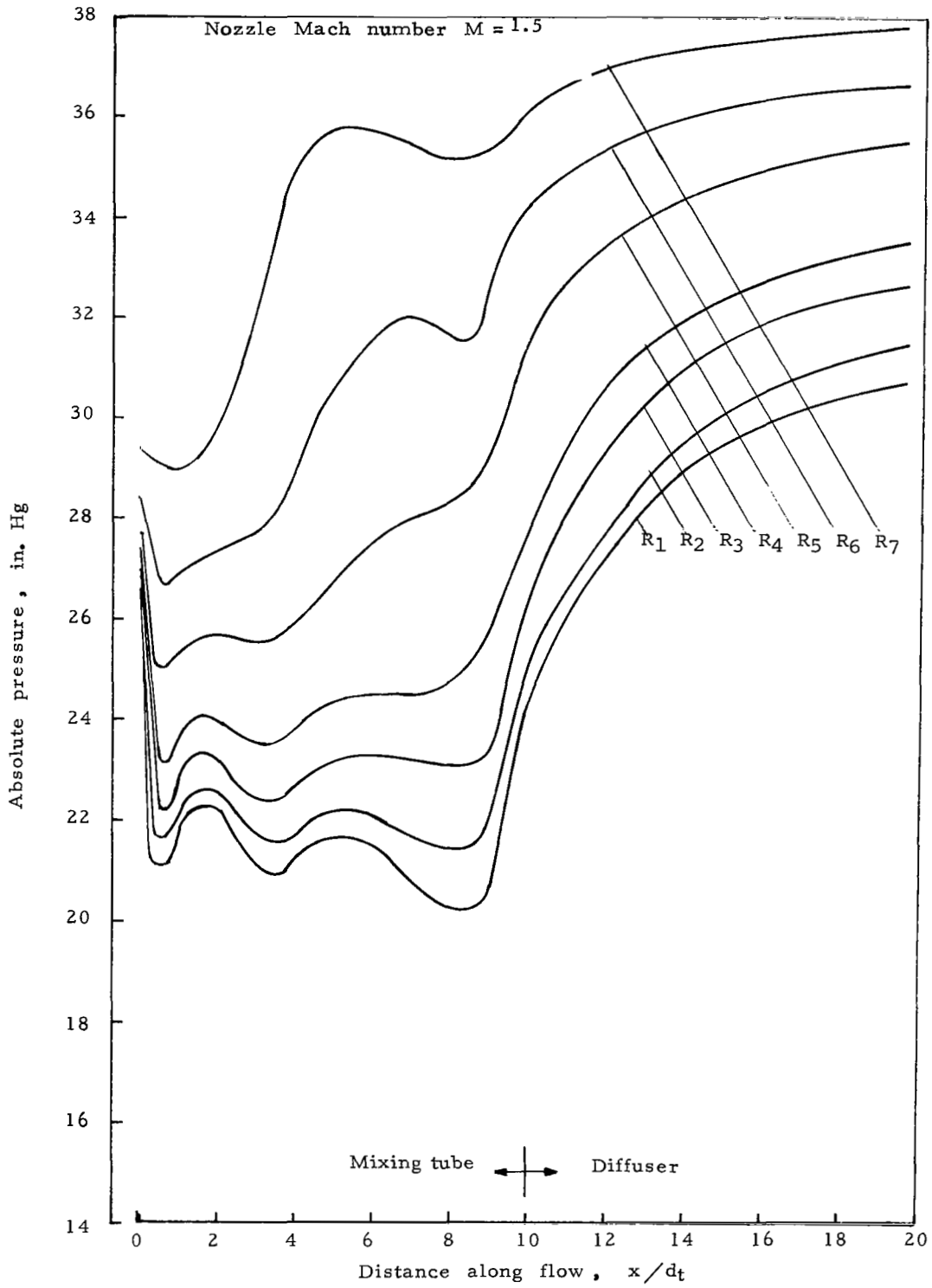

(b) Primary pressure P_1 = 40 psi

Figure 12.- Continued.

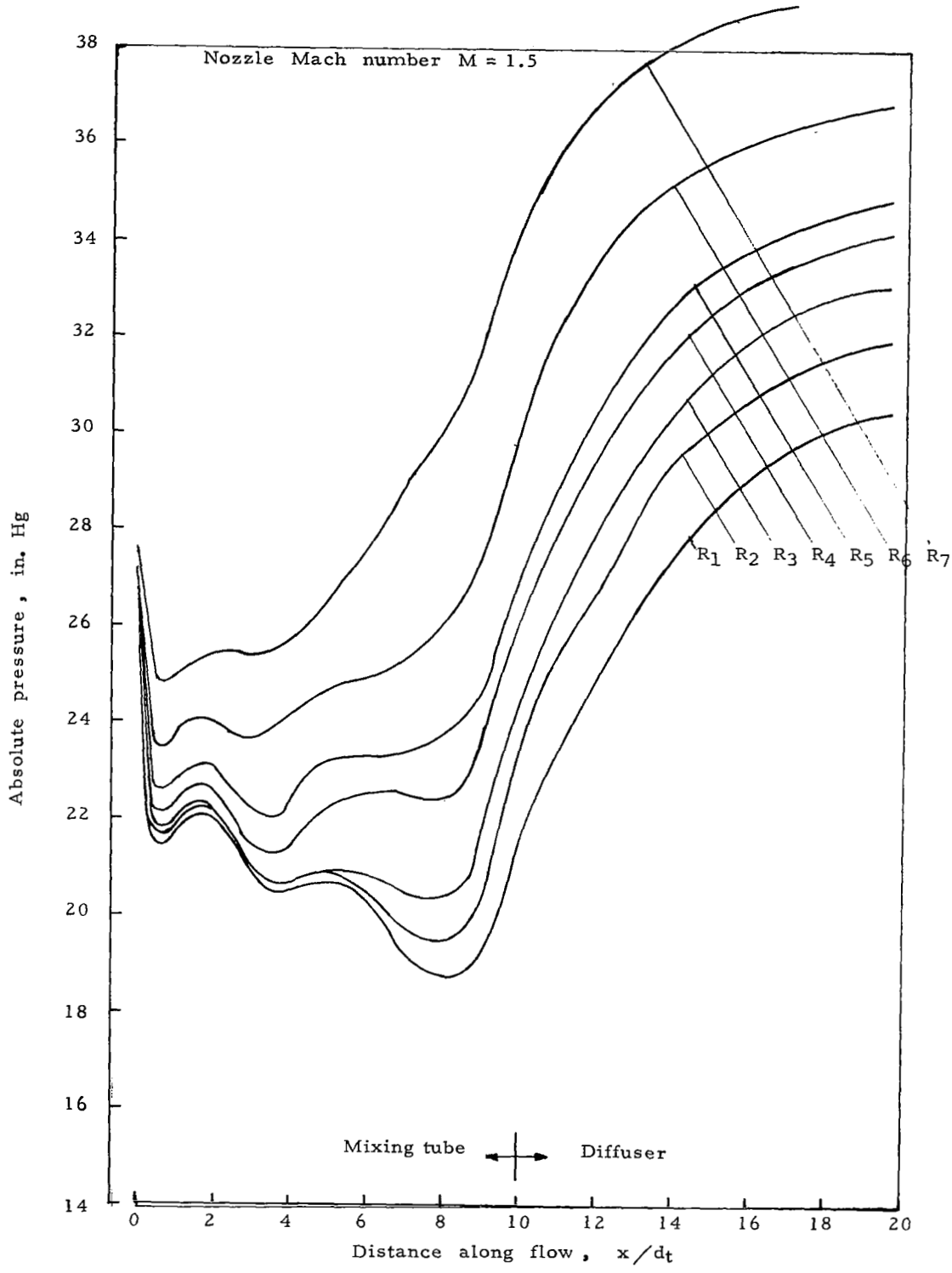

(c) Primary pressure P_1 = 60 psi

Figure 12.- Continued.

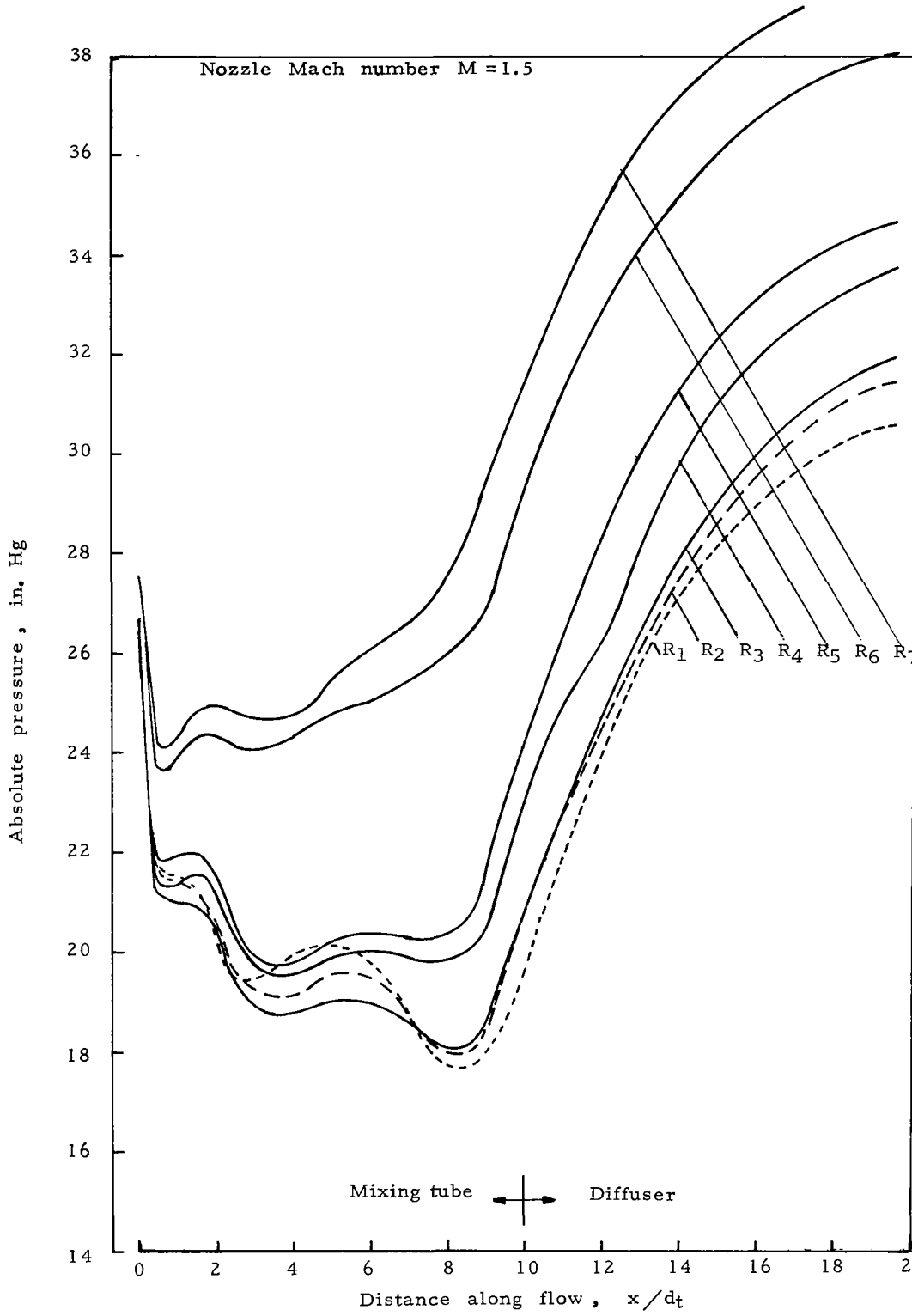

(d) Primary pressure P_1 = 80 psi

Figure 12.- Continued.

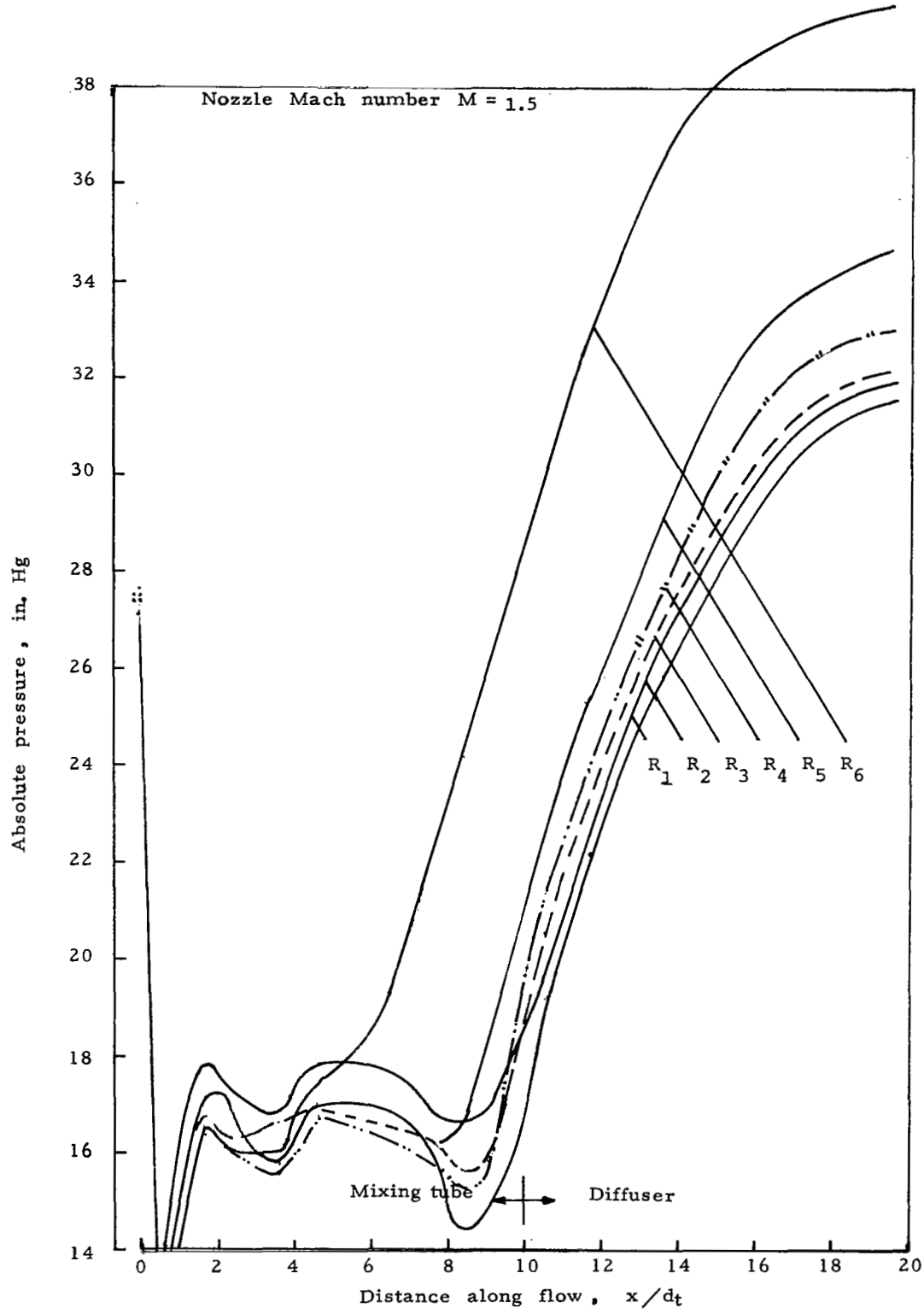

(e) Primary pressure P_1 = 100 psi

Figure 12.-Concluded.

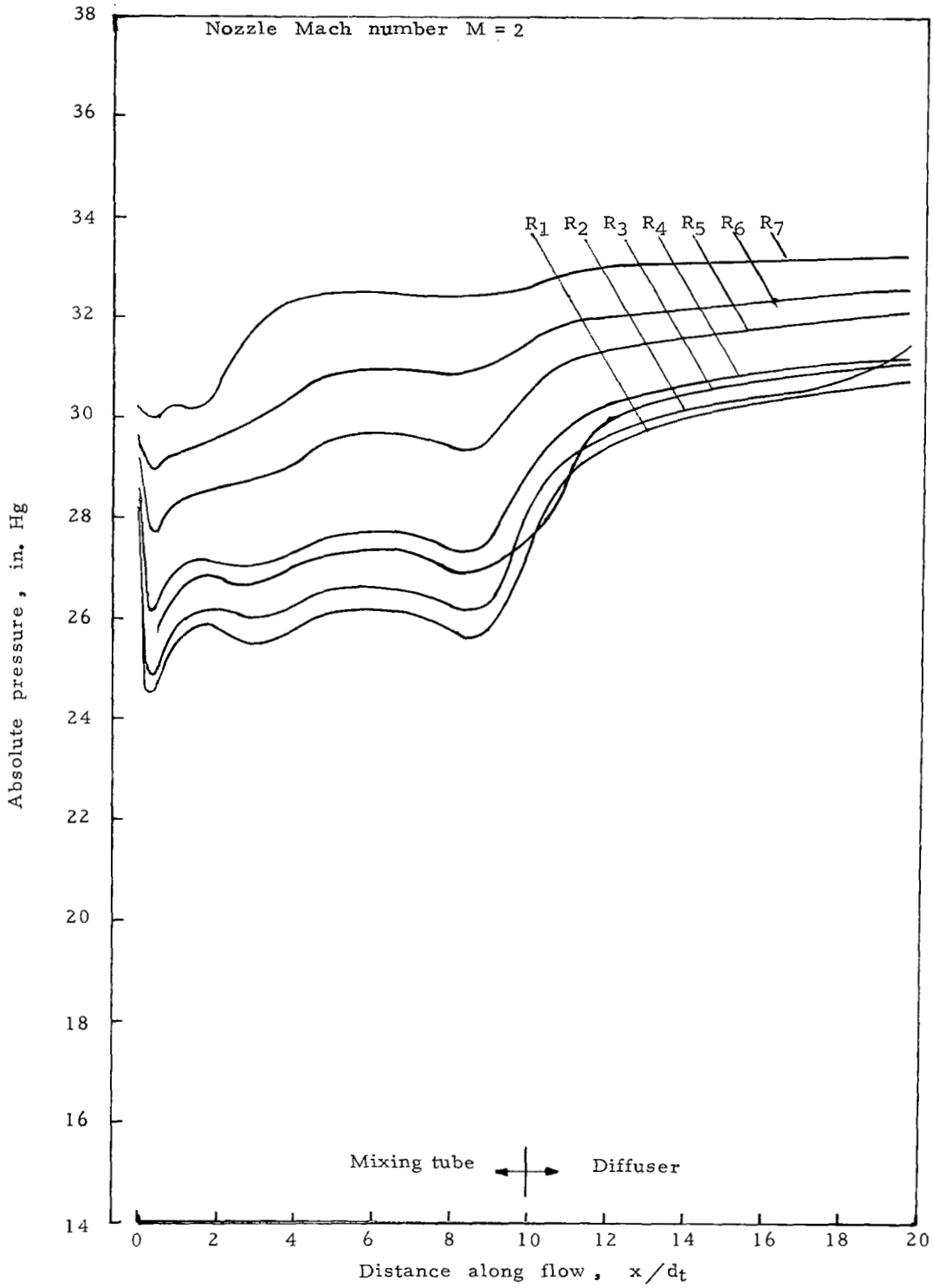

(a) Primary pressure P_1 = 20 psi Figure

13.- Pressure distribution along mixing tube and diffuser.

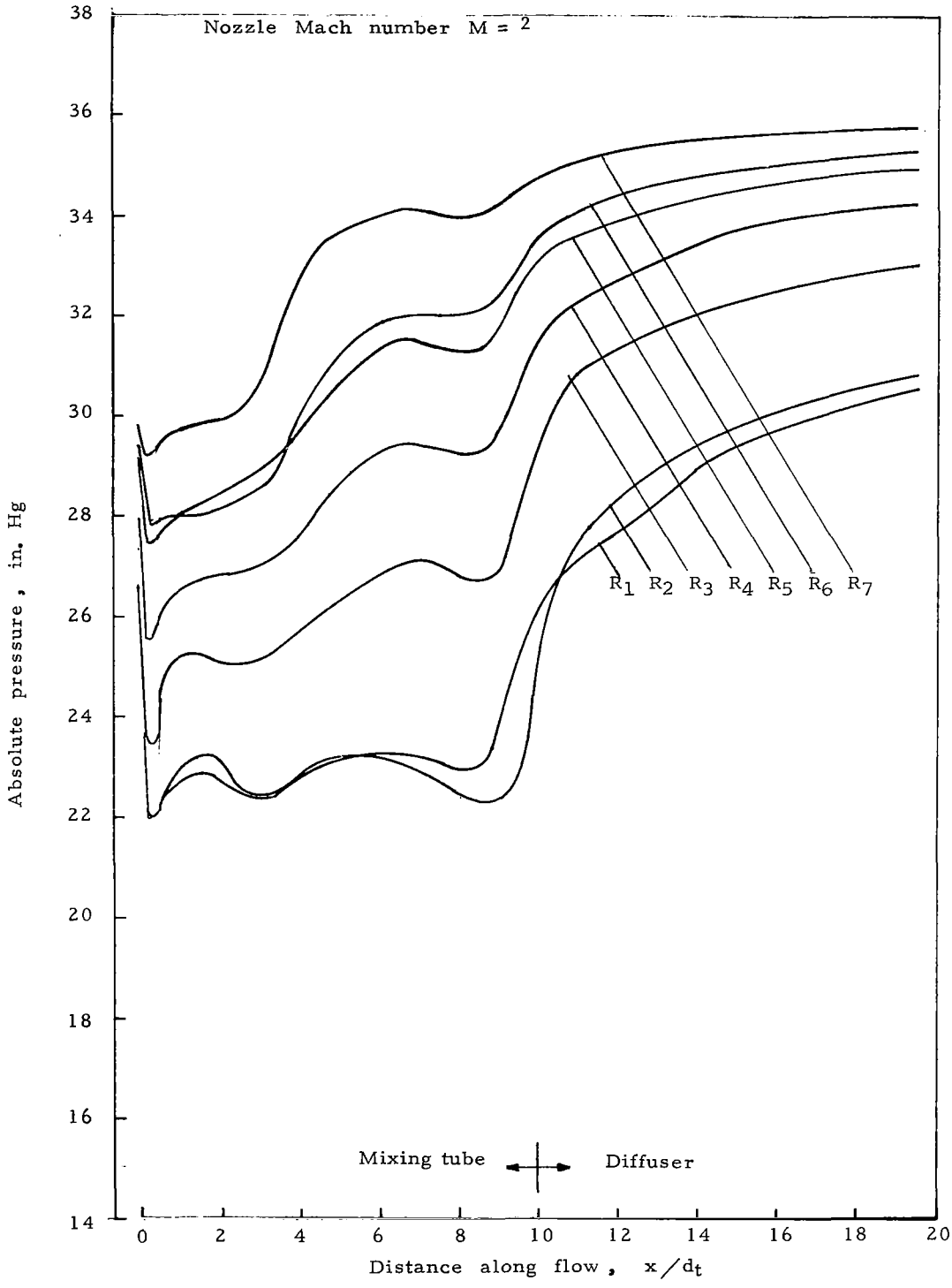

(b) Primary pressure P_1 = 40 psi

Figure 13.- Continued.

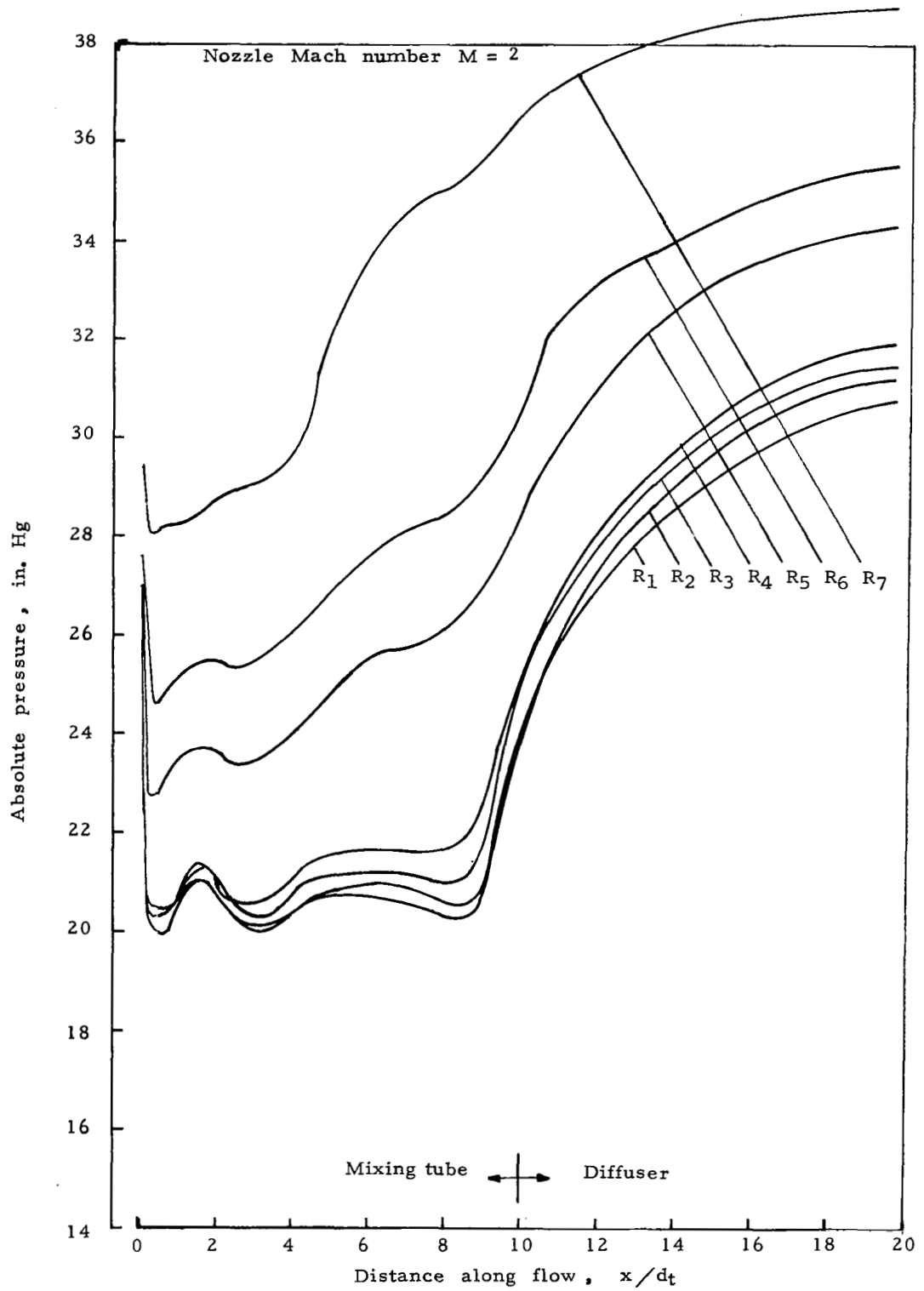

(c) Primary pressure P_1 = 60 psi

Figure 13.- Continued.

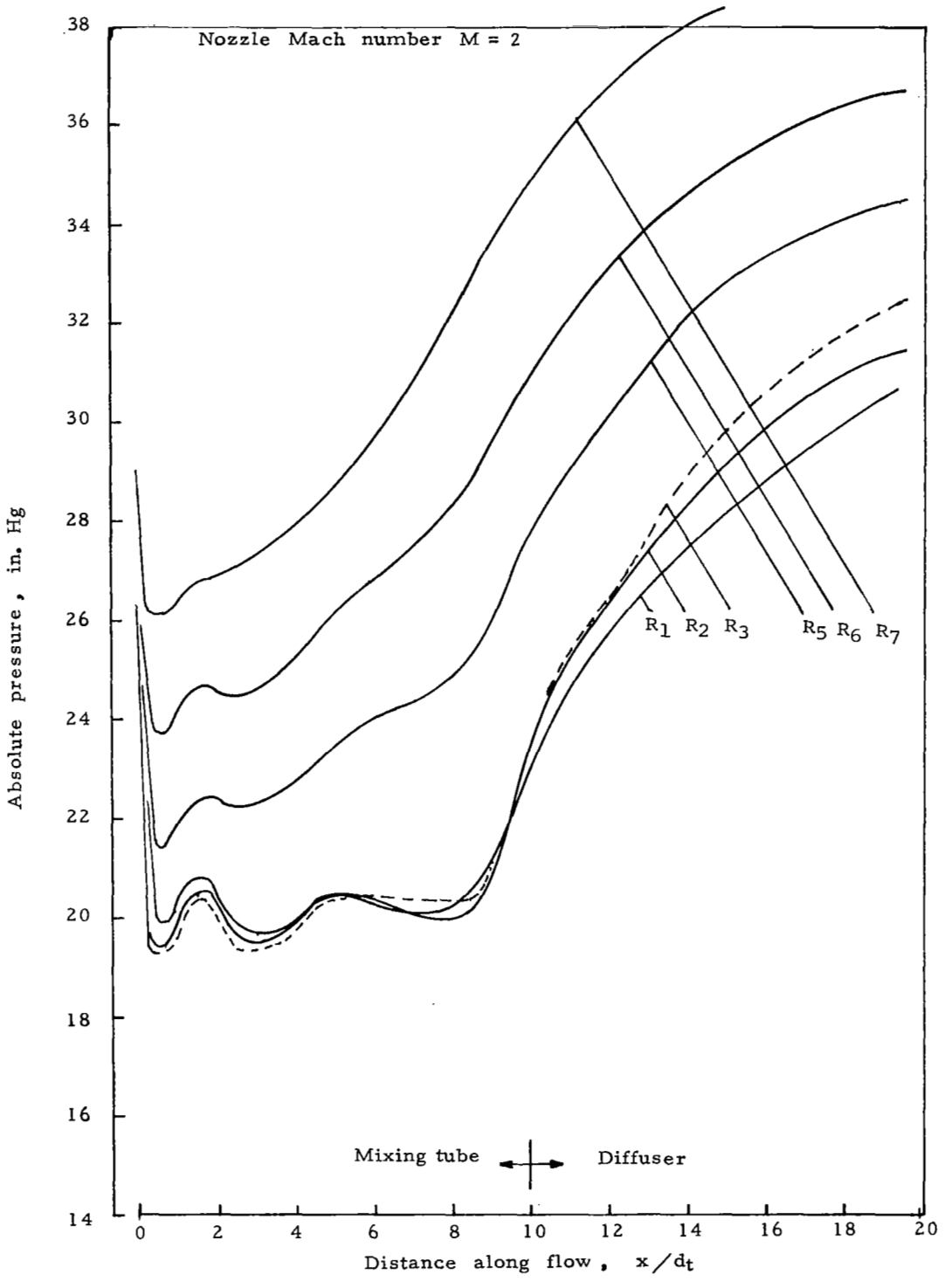

(d) Primary pressure P_1 = 80 psi

Figure 13.- Continued.

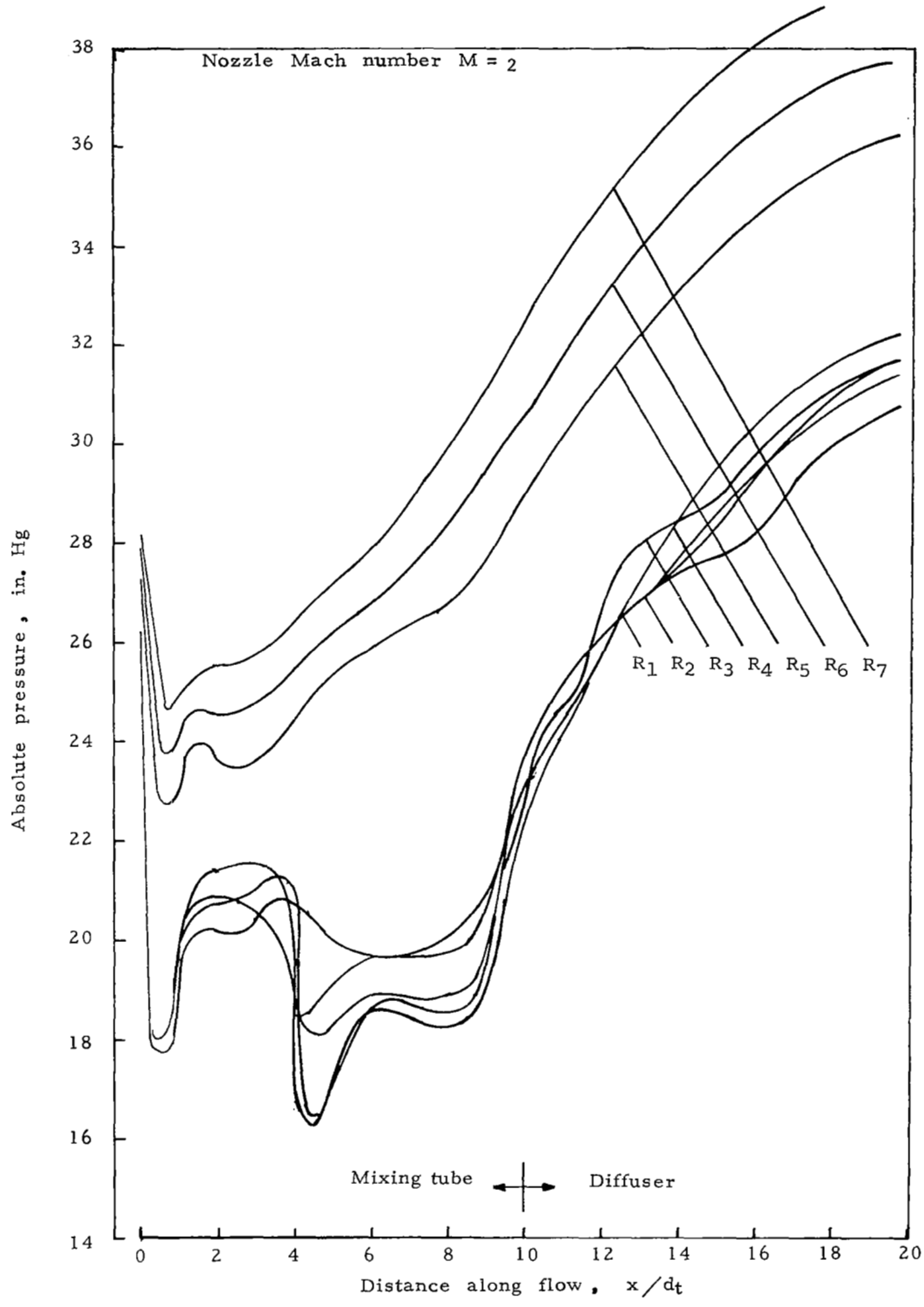

(e) Primary pressure P_1 = 100 psi

Figure 13.- Concluded.

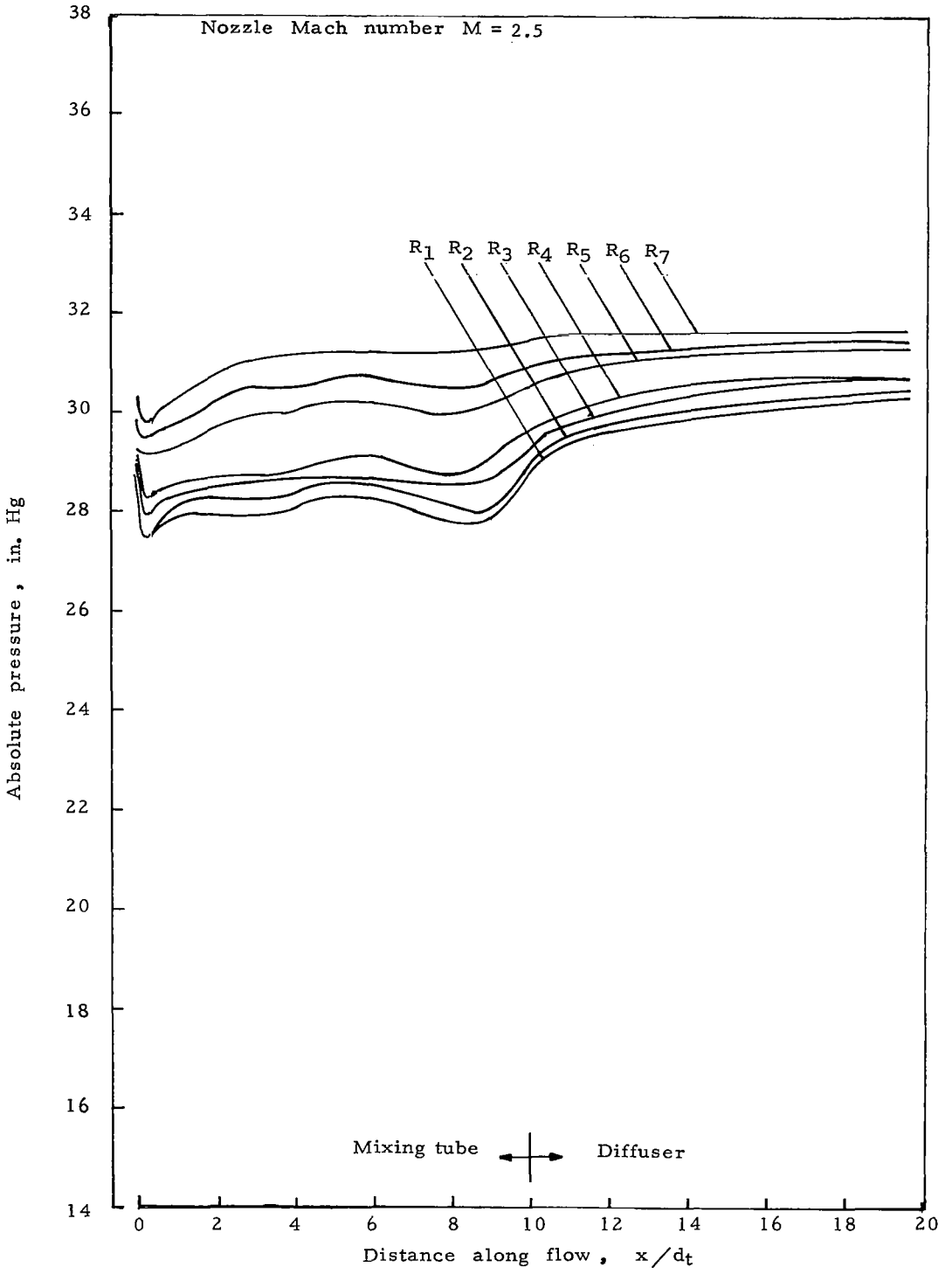

(a) Primary pressure P_1 = 20 psi

Figure 14.- Pressure distribution along mixing tube and diffuser.

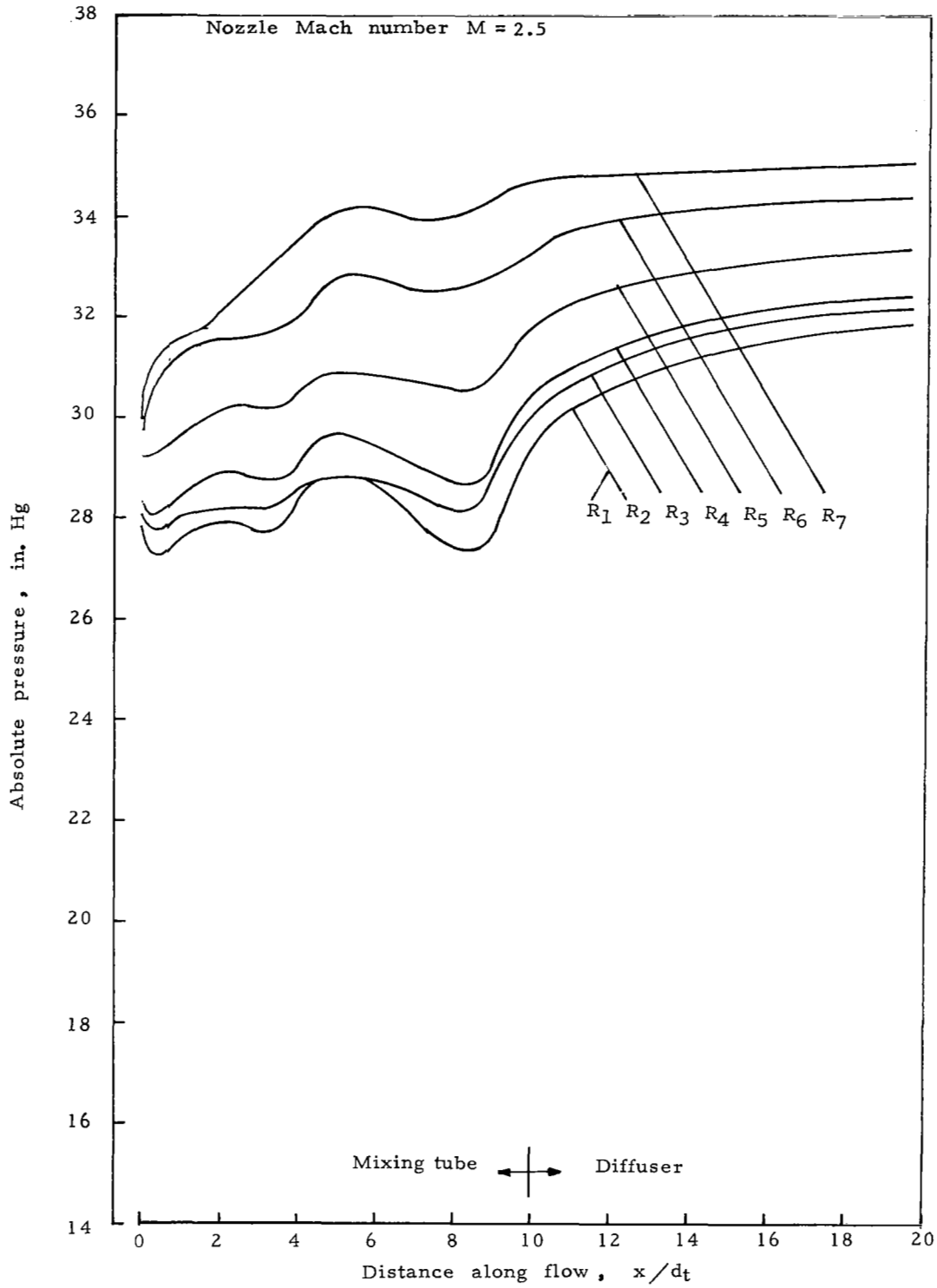

(b) Primary pressure P_1 = 40 psi

Figure 14.- Continued.

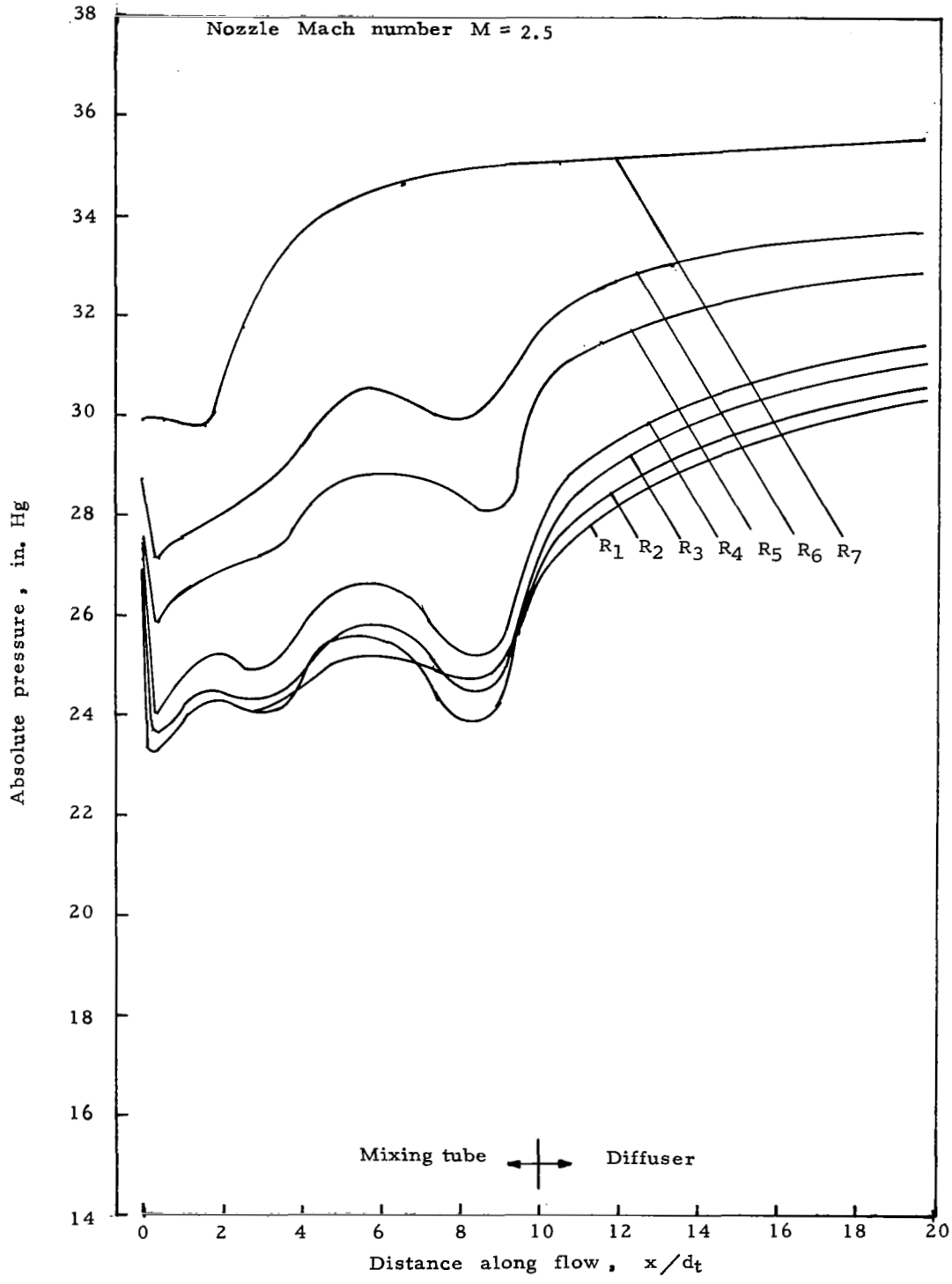

(c) Primary pressure P_1 = 60 psi

Figure 14.- Continued.

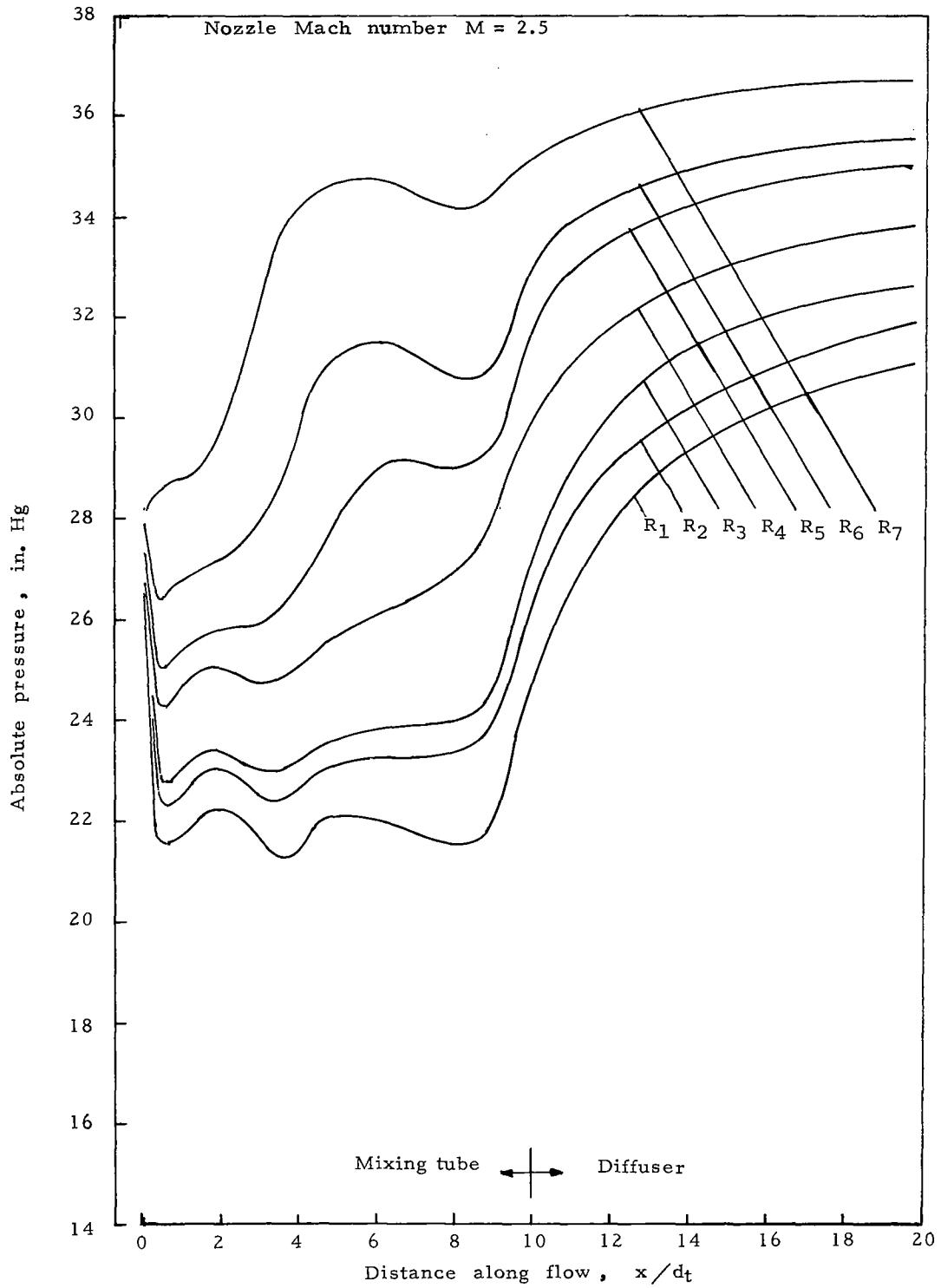

(d) Primary pressure P_1 = 80 psi

Figure 14.- Continued.

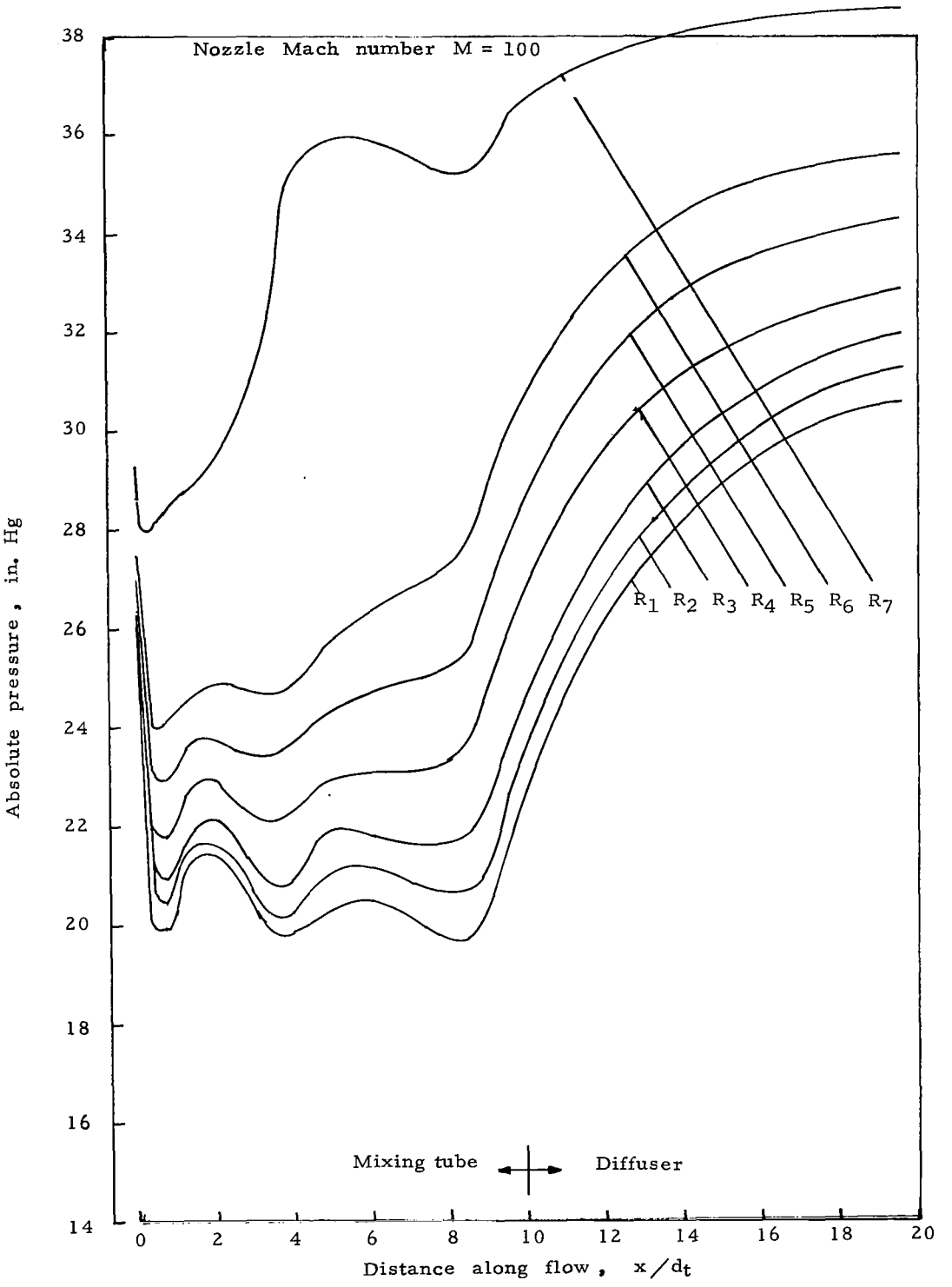

(e) Primary pressure P_1 = 100 psi

Figure 14.- Concluded.

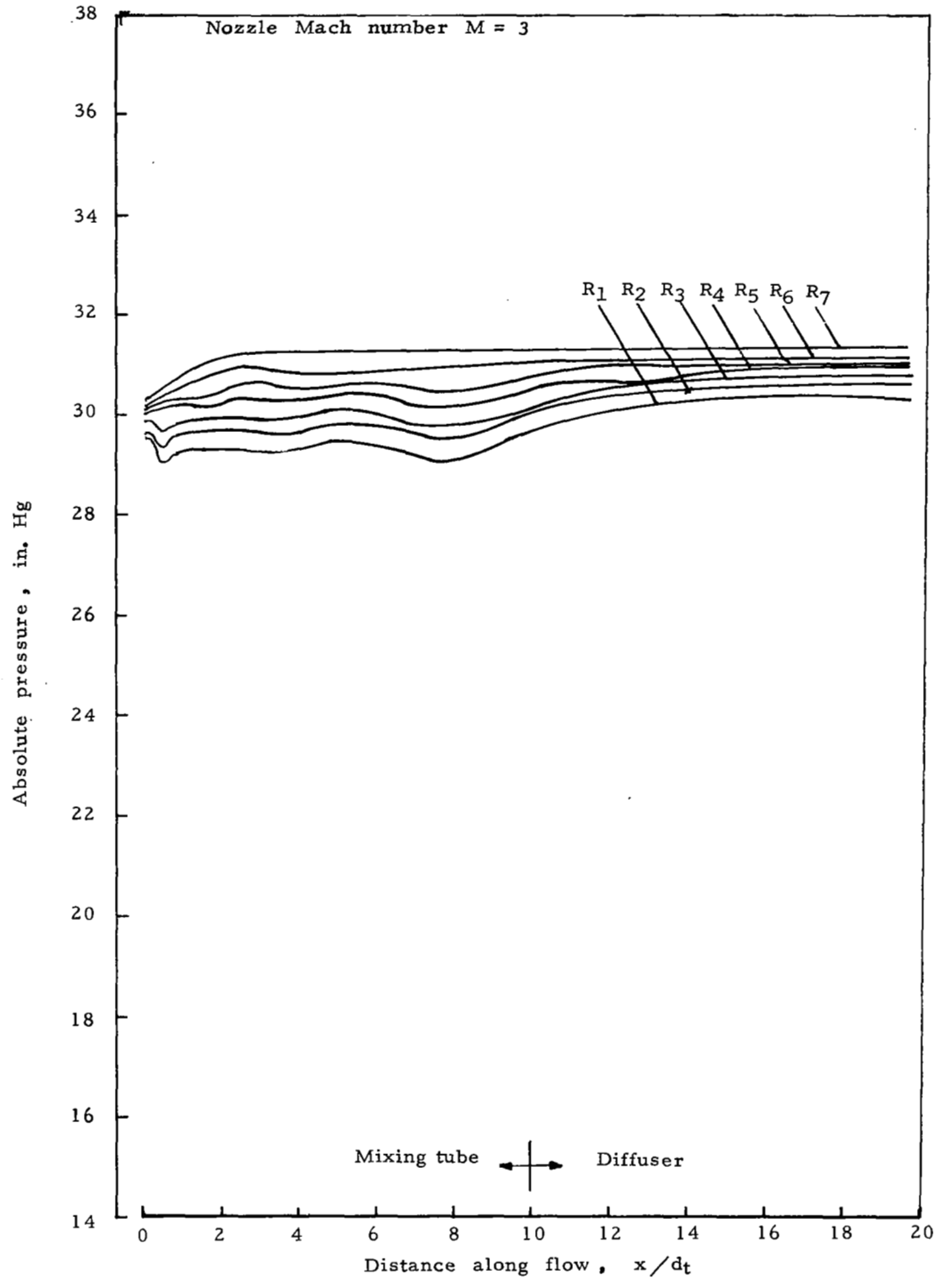

(a) Primary pressure P_1 = 20 psi

Figure 15.- Pressure distribution along mixing tube and diffuser.

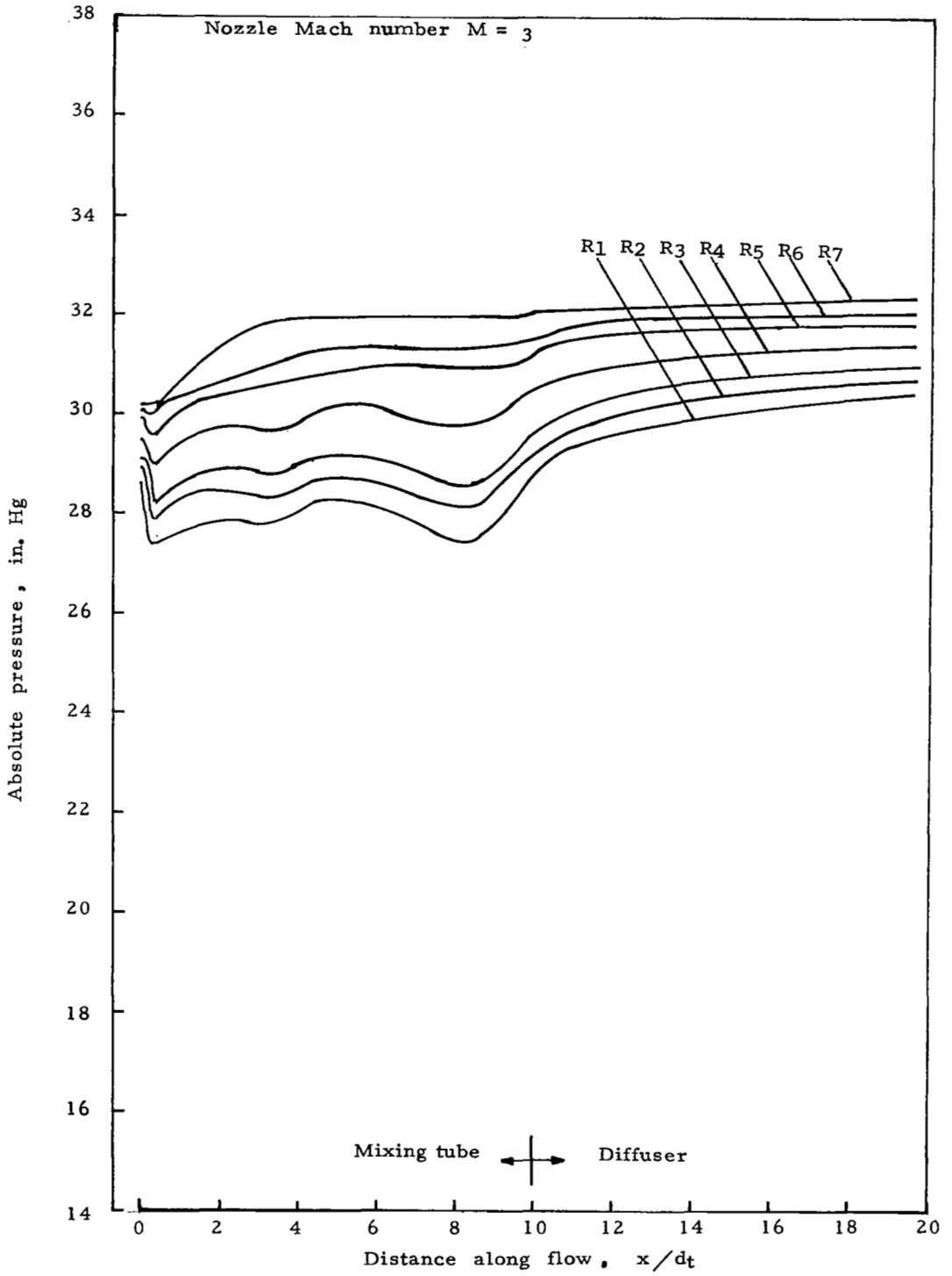

(b) Primary pressure P_1 = 40 psi

Figure 15.- Continued.

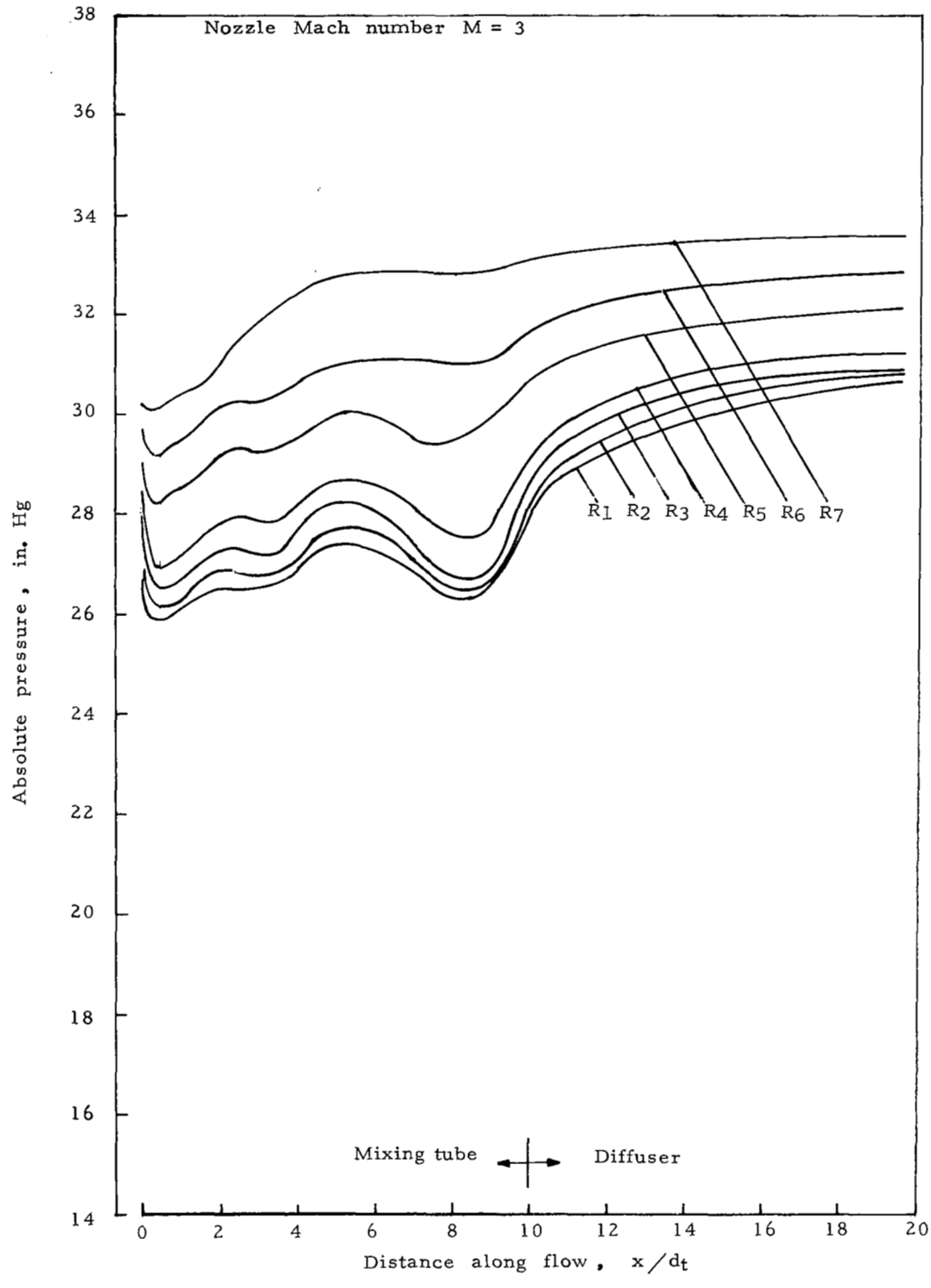

(c) Primary pressure P_1 = 60 psi

Figure 15.- Continued.

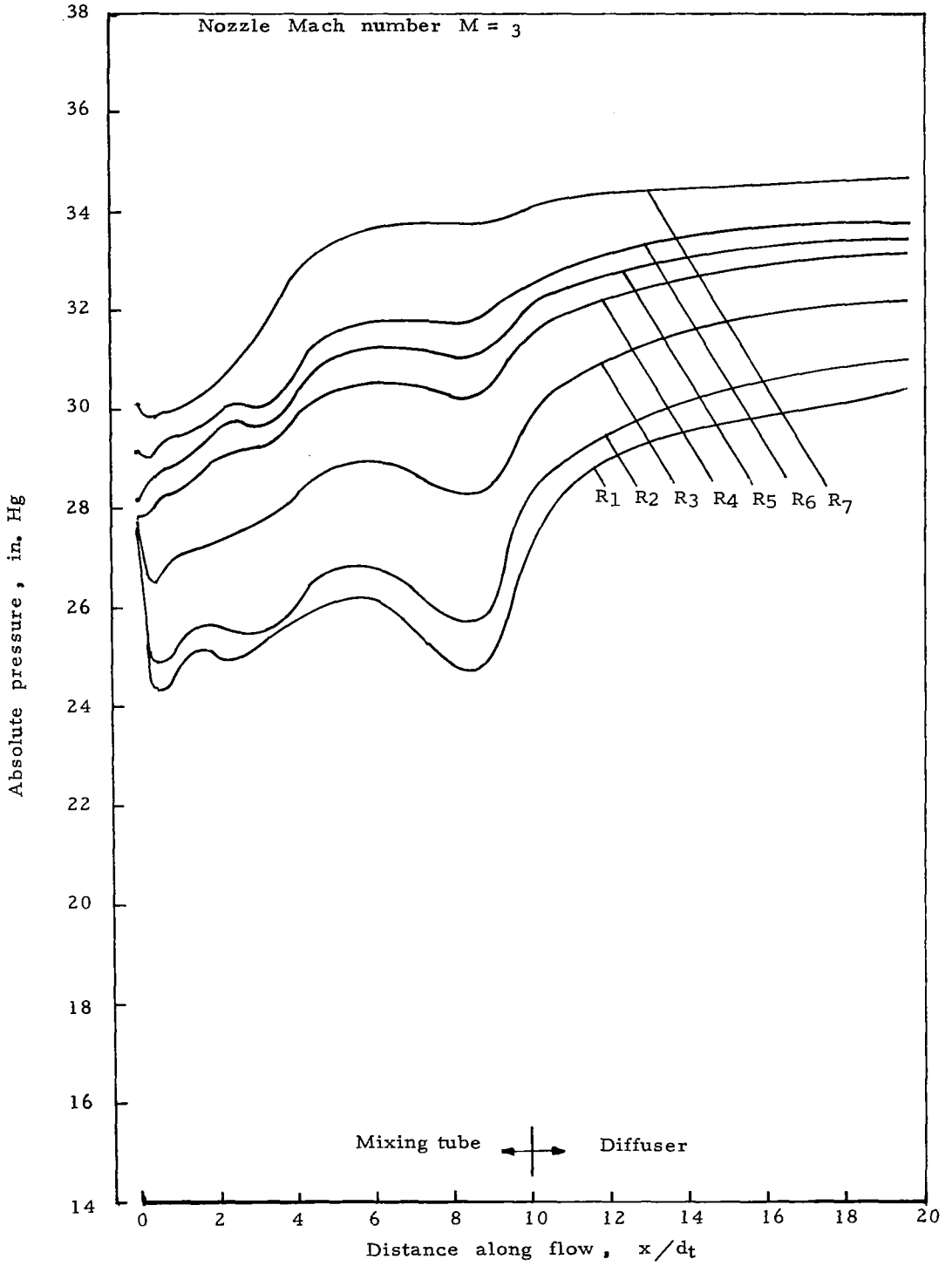

(d) Primary pressure P_1 = 80 psi

Figure 15.- Continued.

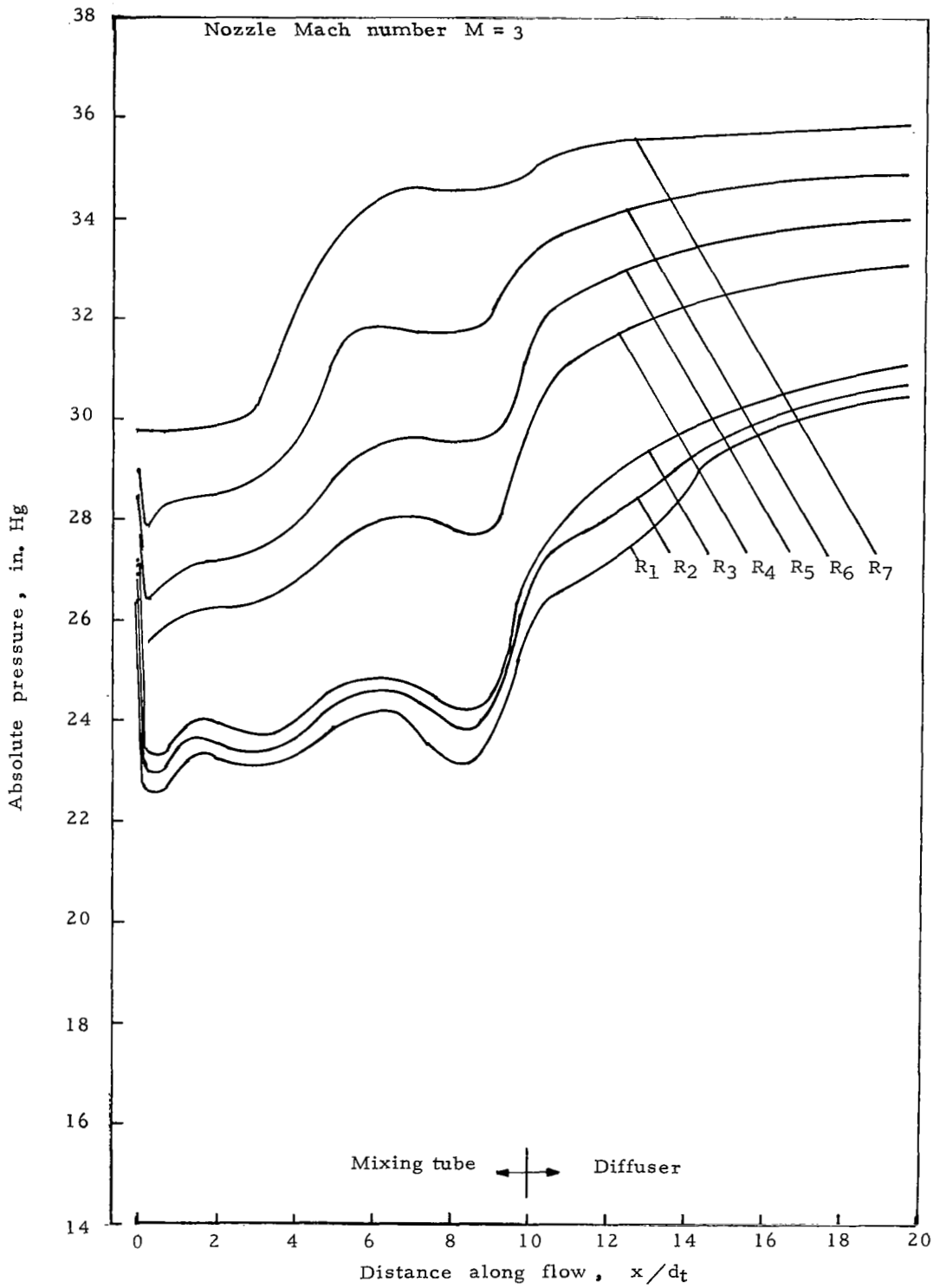

(e) Primary pressure P_1 = 100 psi

Figure 15.- Concluded.

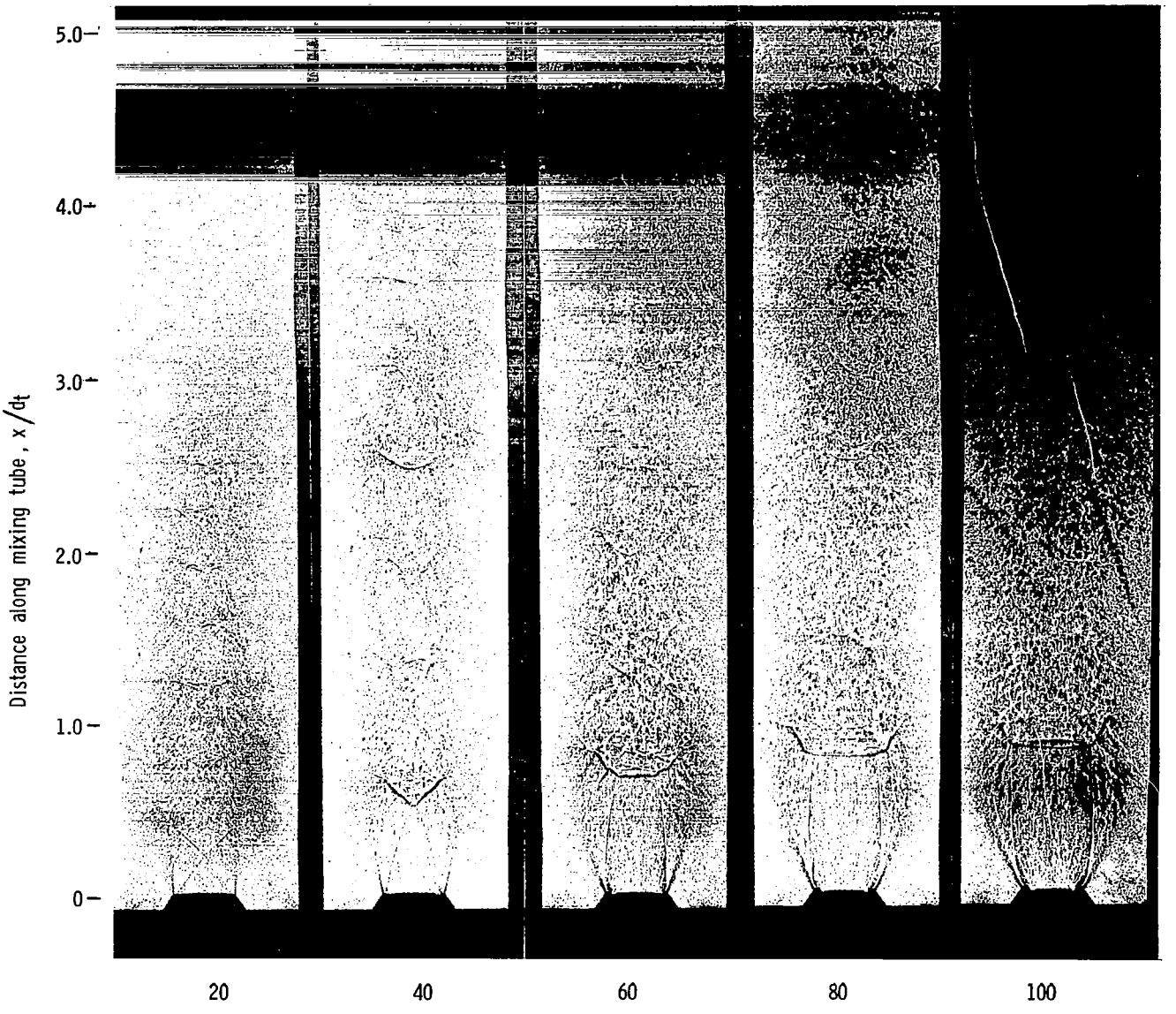

(a) Low resistance (L)

Fig. 16 Shadowgraph pattern of M = 1.0 nozzle

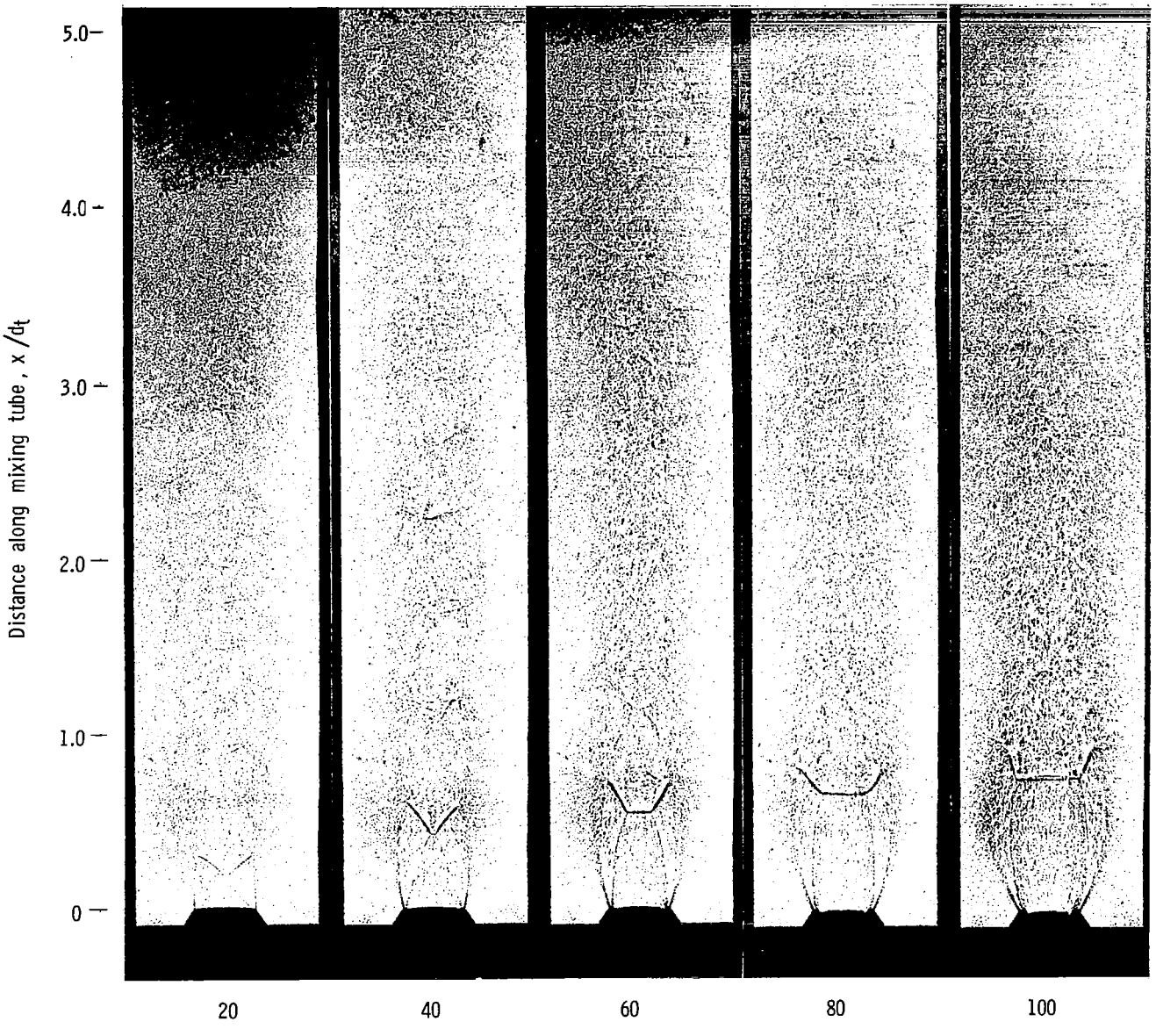

(b) High resistance (H)

Fig. 16 -- Concluded

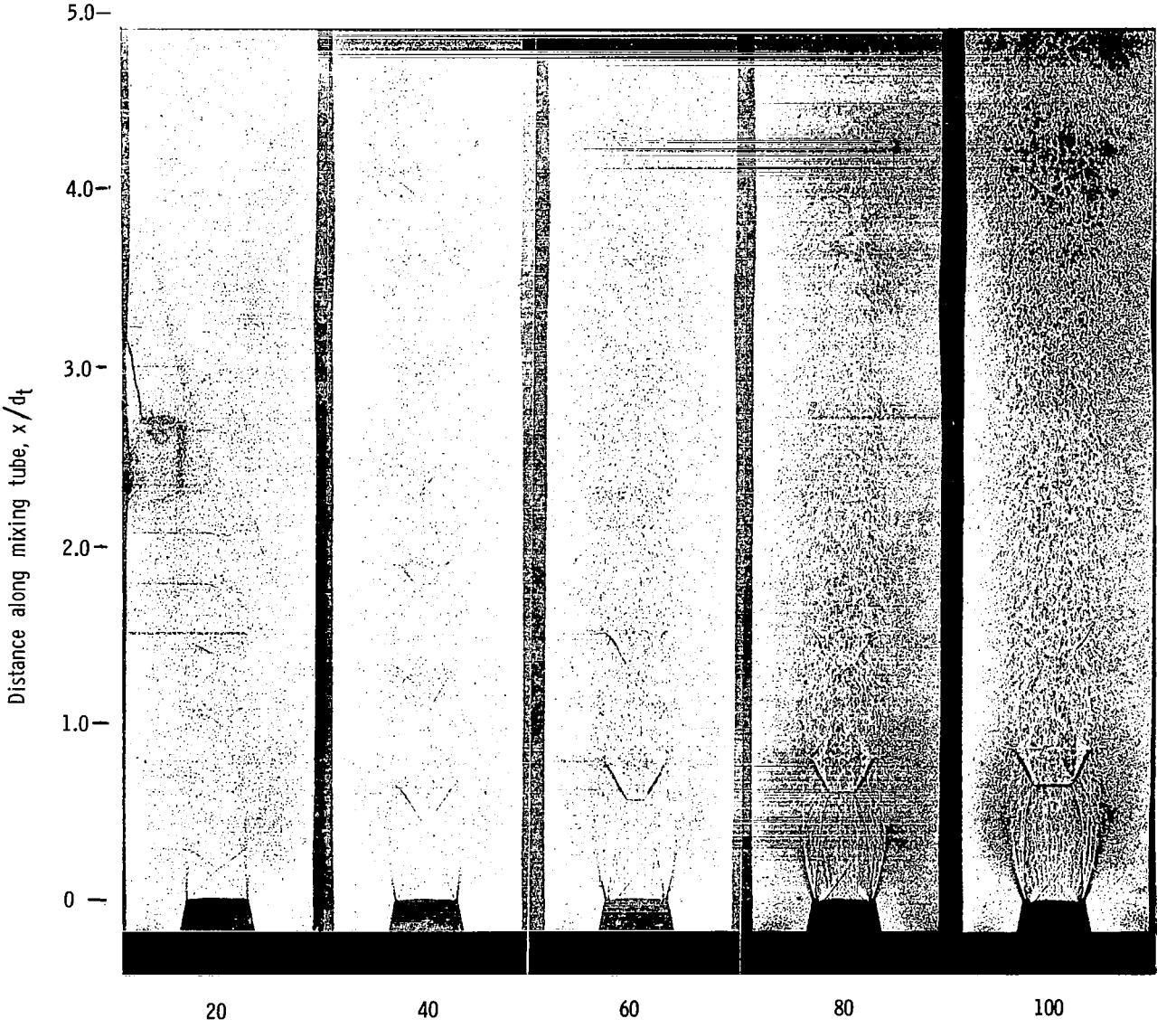

(a) Low resistance (L)

Fig. 17 Shadowgraph pattern of M = 1.5 nozzle

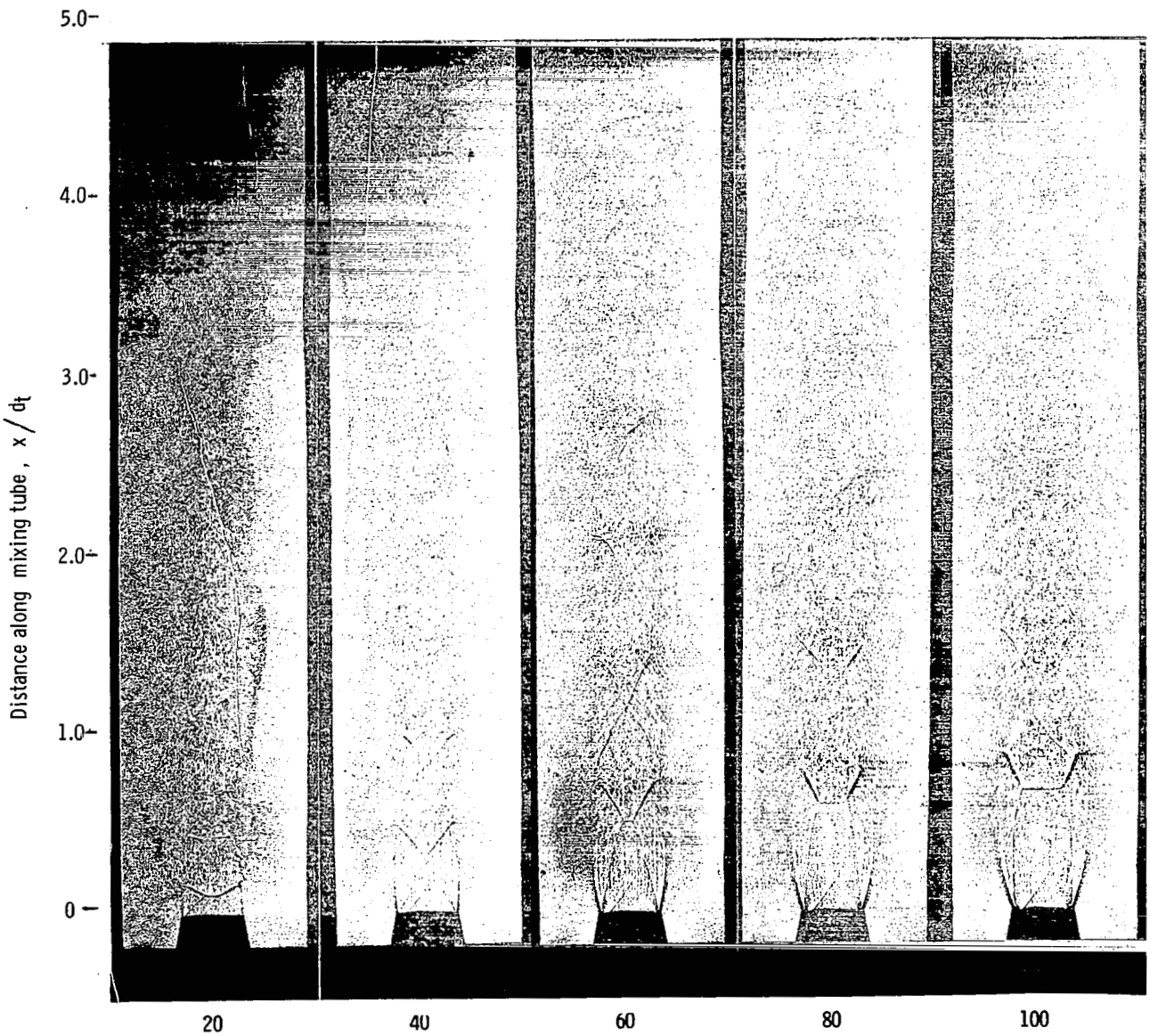

(b) High resistance (H)

Fig. 17 -- Concluded

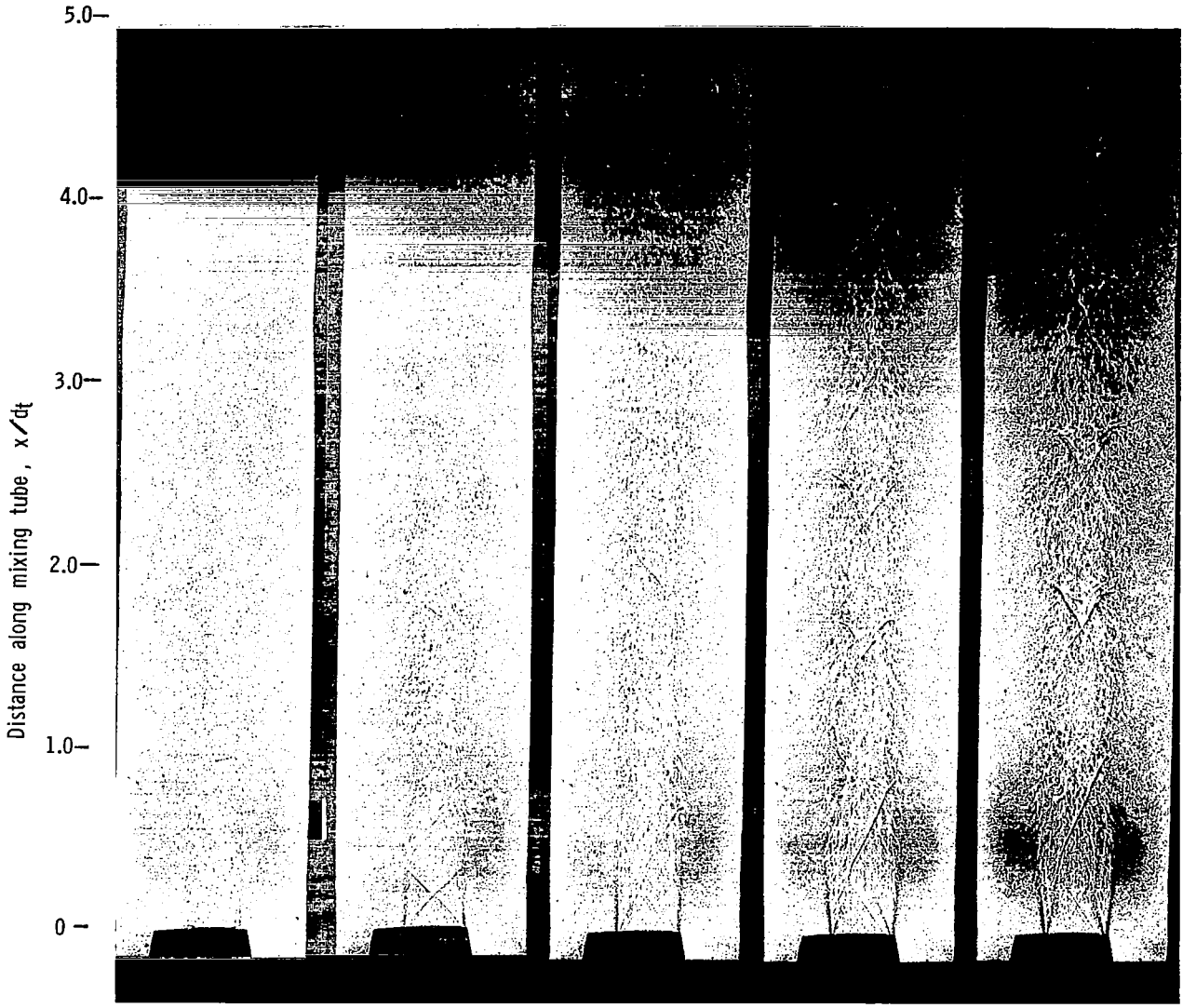

(a) Low resistance (L)

Fig. 18 Shadowgraph pattern of M = 2.0 nozzle

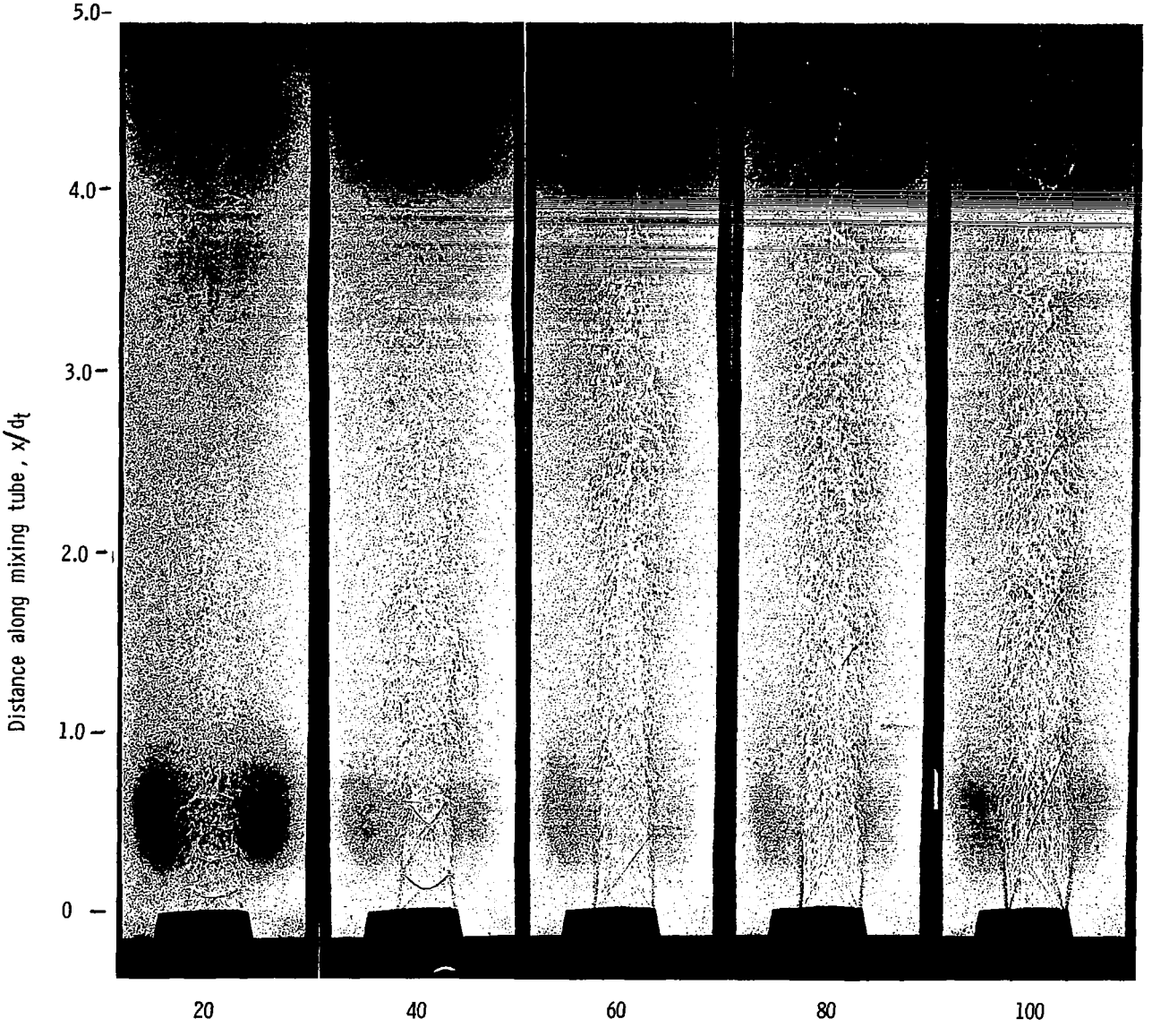

(b) High resistance

Fig. 18 -- Concluded

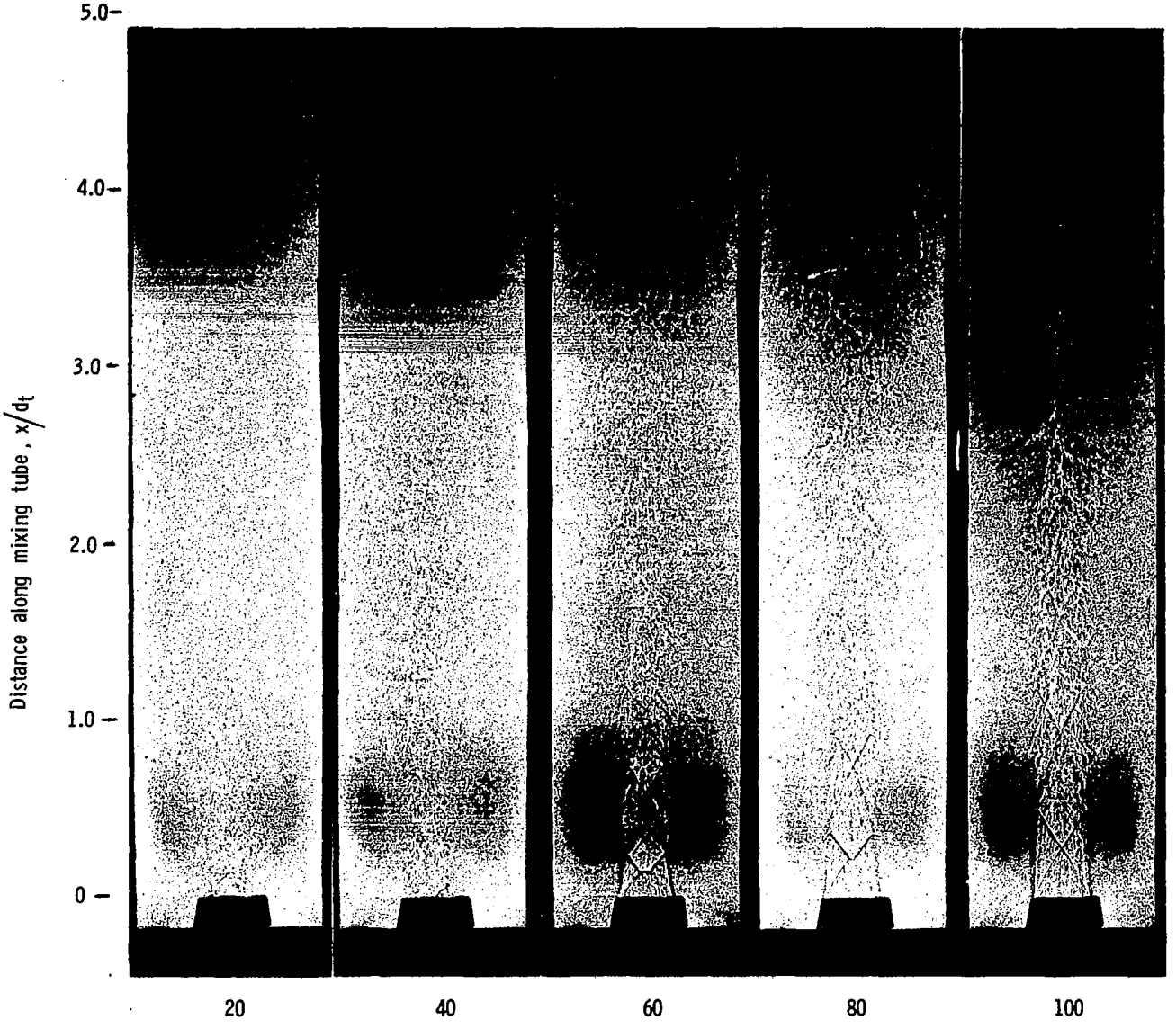

(a) Low resistance (L)

Fig. 19 Shadowgraph pattern of M = 2.5 nozzle

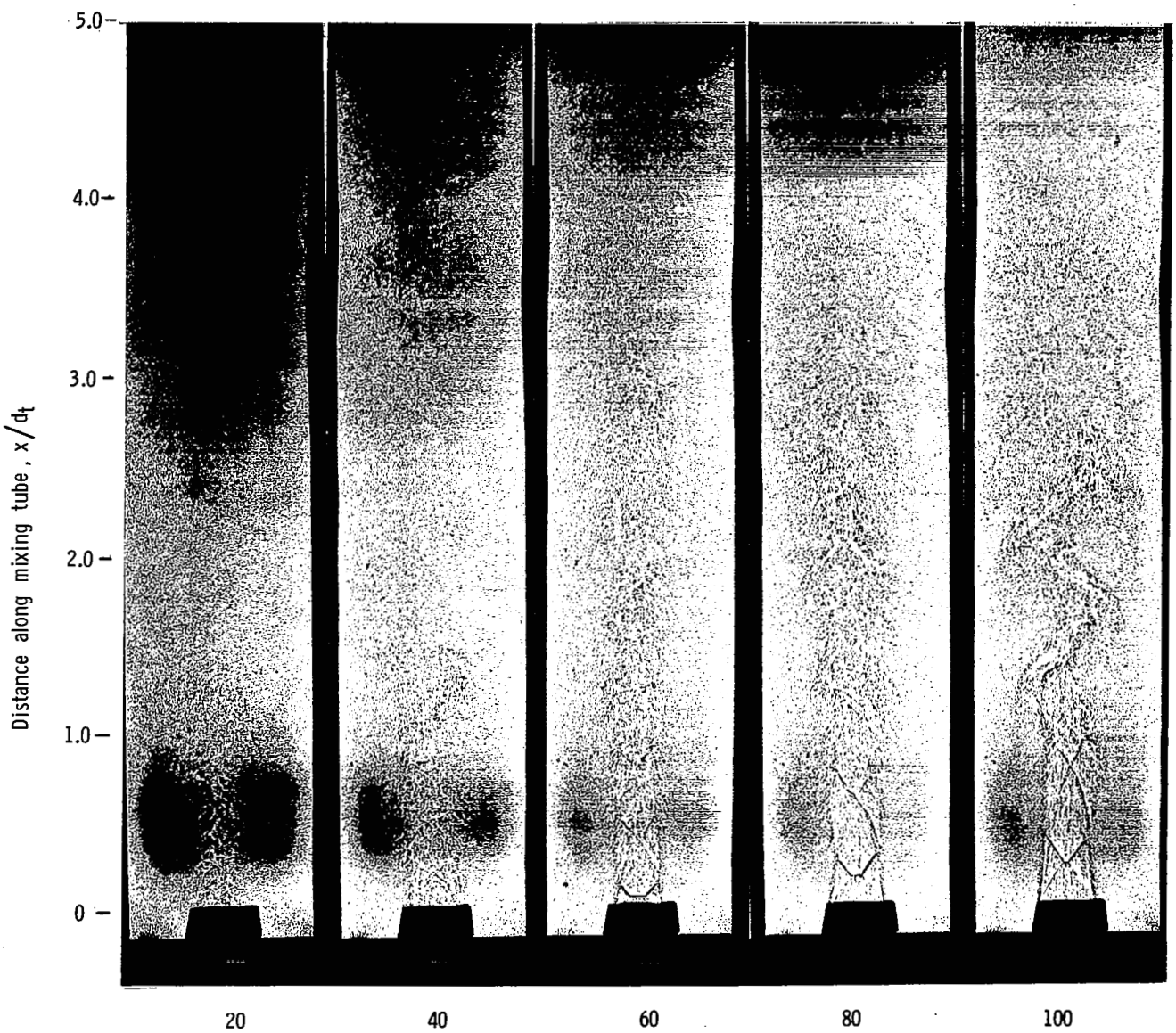

(b) High resistance (H)

Fig. 19 -- Concluded

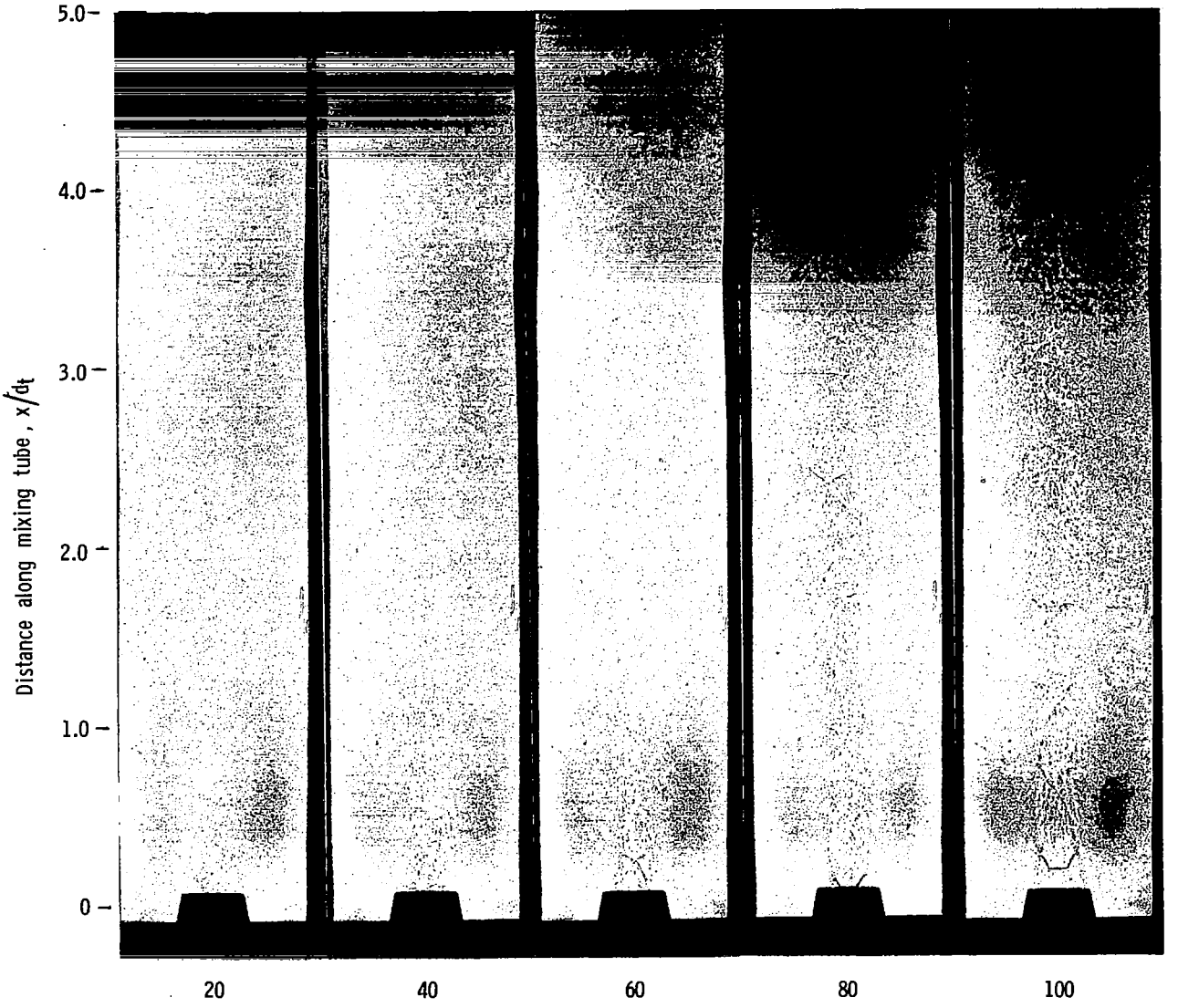

(a) Low resistance (L)

Fig. 20 Shadowgraph pattern of M = 3.0 nozzle

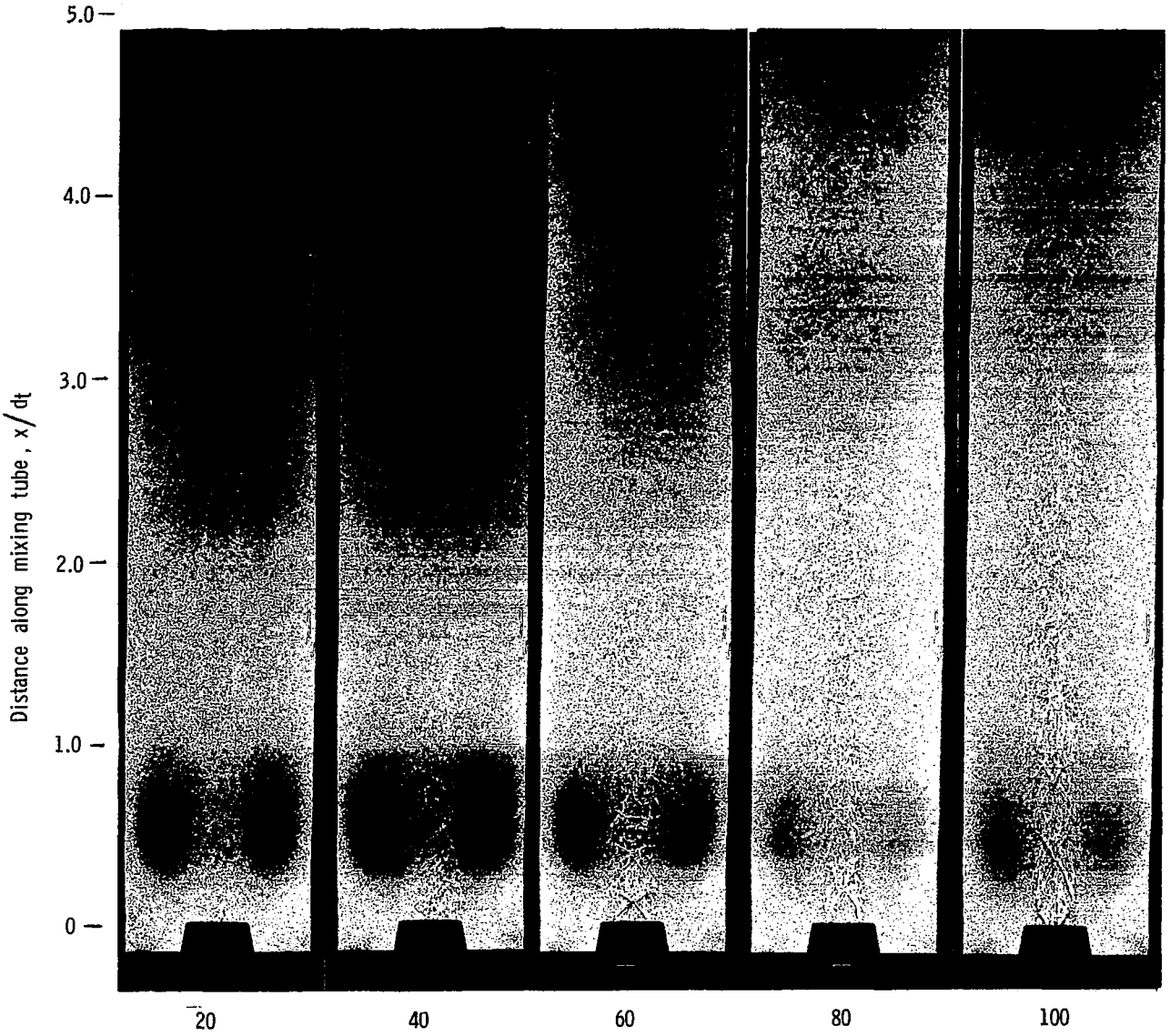

(b) High resistance (H)

Fig. 20 -- Concluded

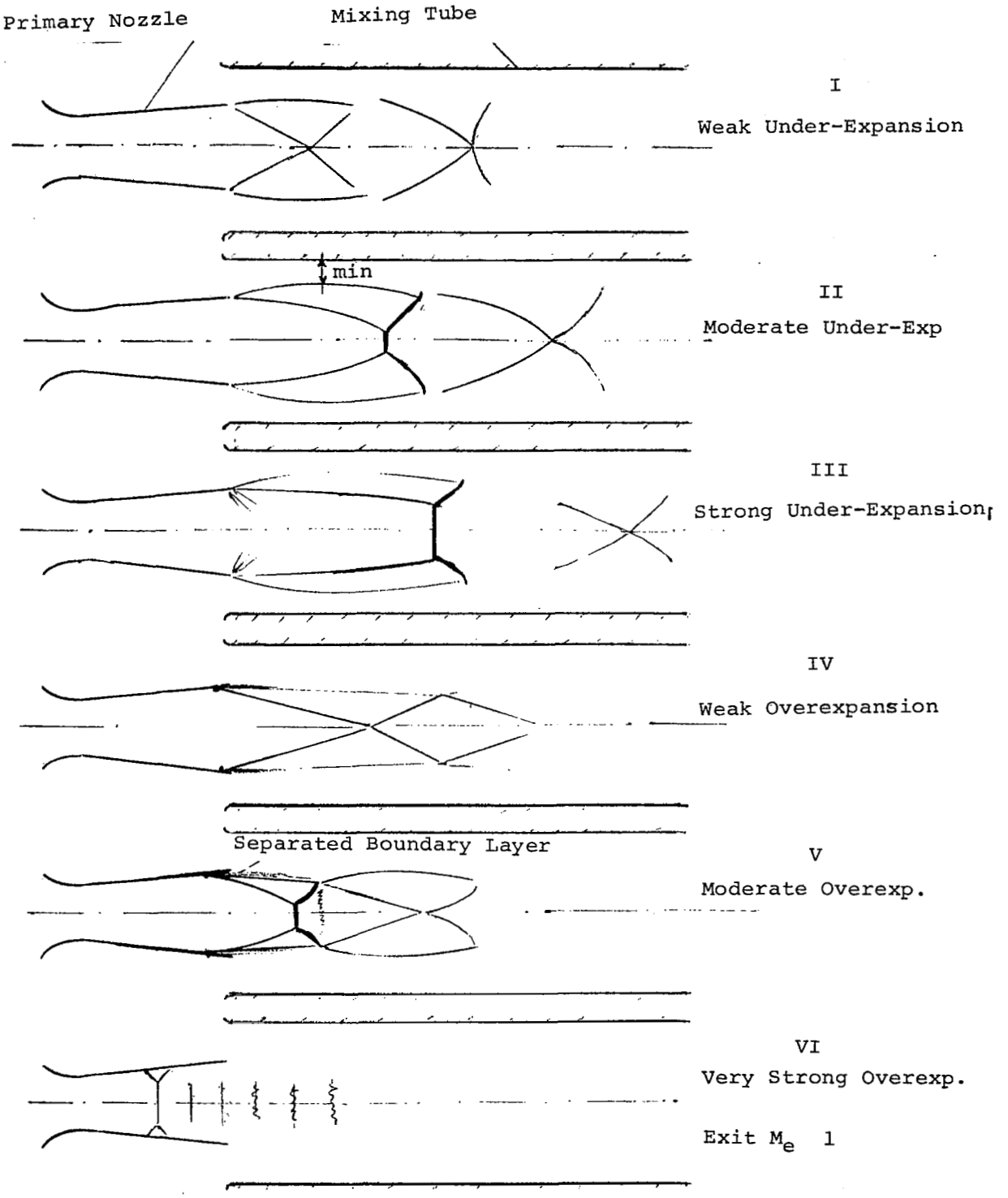

Figure 21.- Flow Patterns in Mixing Tube for Incorrectly Expanded Primary Nozzles.

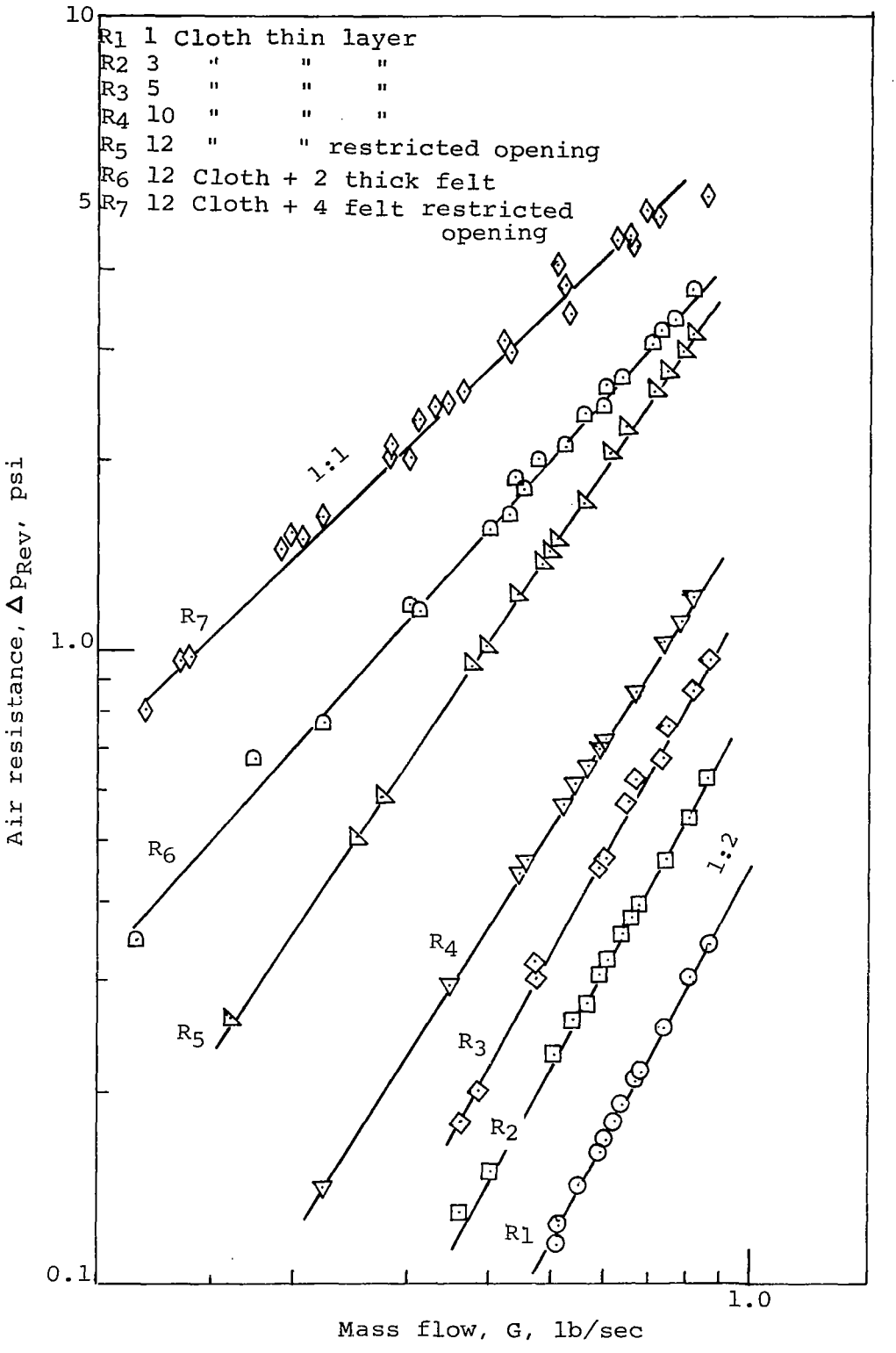

Figure 22.- Resistance characteristics of felt layers.